POLITECNICO DI TORINO

Master's Degree in Aerospace Engineering

Master's Degree Thesis

Conceptual design methodology and tools for the estimation of emissions from SABRE engine in airbreathing mode

Supervisors

Prof. ROBERTA FUSARO

Prof. NICOLE VIOLA

Dott. GUIDO SACCONE

Ing. VALERIA BORIO

Candidate

FABRIZIO BORGNA

APRIL 2024

Summary

Since its establishment, the space sector has pursued the development of technologies required to further expand space exploration activities with an almost complete focus on performance achievement. With the projected increase in the frequency of access to space, it is of utmost importance to evaluate and develop minimization strategies for the environmental impact since the earliest design stages. This work aims at extending the applicability of NOx estimation methods developed for the aviation sector to a Single Stage To Orbit vehicle. This implies an adaptation of already existing formulations to cover propellants (different from Jet-A1 kerosene) and different propulsive technologies and speed regimes, ranging from subsonic to supersonic and hypersonic. In particular, this work discloses a new set of emissions estimation formulations tailored to the Synergetic Air-Breathing Rocket Engine (SABRE) technology, the key element of the future Skylon vehicle. The SABRE engine is designed to power the vehicle, a horizontal take-off and landing single stage to orbit, allowing the transition from air-breathing to rocket mode and employing liquid hydrogen as fuel. A modelling strategy able to capture the complexity of this propulsive system is crucial for the development of a reliable and accurate emissions database, which is, in turn, the foundation for the upgrade of the emissions predictive models. In particular, this work focuses on the analysis and modelling of the air-breathing operating modes. In detail, an already existing propulsive model is upgraded (i) by integrating the effect of the regenerative closed-loop helium cycle on the engine performance, (ii) by enhancing the combustion modelling thanks to the integration of 2-phases thermodynamic combustion simulations, and (iii) by increasing the accuracy of the mixing modelling. Both the mixing and the combustion modelling are performed thanks to the exploitation of an open-source suite i.e., Cantera. In addition, Cantera software is used to generate the emissive database starting from the propulsive database, using 0D chemical kinetic simulations. Eventually, new predictive formulations for NOx emissions are developed using the newly defined emissions database as a dataset and the P3-T3 and the BFFM2 as reference formulations. The original estimation equations are upgraded by tuning the numerical parameters of the formulations as well as by integrating new variables including the Mach number, the water-to-fuel ratio at the inlet of the main combustion chamber, the air-mass flow ratio in the pre-burner and the helium-to-air mass flow ratio. Discussions on the physical characterization of these parameters are reported.

Sommario

Storicamente, il settore spaziale ha sempre perseguito lo sviluppo di nuove tecnologie necessarie per espandere le attività di esplorazione spaziale, con un focus specializzato per la massimizzazione delle prestazioni e per la minimizzazione dei costi. La crescita esponenziale prevista per la richiesta per l'accesso allo spazio rende, quindi, di massima importanza la valutazione dell'impatto ambientale di questo settore e lo sviluppo di nuove strategie per minimizzarlo sin dalle prime fasi di progettazione. In questo contesto, il presente lavoro ha come obiettivo quello di estendere l'applicabilità dei metodi di stima delle emissioni di NO_x sviluppati nell'ambito dell'aviazione a un veicolo Single Stage To Orbit. Ciò implica un adattamento delle formulazioni analitiche esistenti al caso di propellenti diversi dal cherosene Jet-A1 e al caso di diverse architetture propulsive e regimi di velocità, dal subsonico fino ad arrivare all'ipersonico. In particolare, nella presente tesi viene derivato un nuovo insieme di formulazioni di stima delle emissioni adattate per il Synergetic Air-Breathing Rocket Engine (SABRE), l'elemento chiave del veicolo spaziale Skylon. Il motore SABRE è progettato per alimentare Single Stage To Orbit Skylon, un velivolo monostadio riutilizzabile a decollo e atterraggio orizzontale. Il SABRE consente la transizione dalla modalità air-breathing alla modalità razzo e impiega idrogeno liquido come combustibile durante tutta la missione. Una strategia di modellizzazione in grado di catturare la complessità di questo sistema propulsivo è cruciale per lo sviluppo di due database, propulsivo e emissivo, affidabili e accurati. Tali database costituiscono a loro volta la base per l'aggiornamento dei metodi analitici di stima delle emissioni. In particolare, questo lavoro si concentra sull'analisi e sulla modellizzazione della fase air-breathing del motore SABRE. A tale proposito, un modello propulsivo precedentemente sviluppato per il motore viene aggiornato (i) integrando l'effetto sulle prestazioni del motore del ciclo chiuso rigenerativo all'elio, (ii) migliorando la modellizzazione della combustione grazie all'integrazione di software specifici per la simulazione dell'equilibrio in camera di combustione e (iii) aumentando l'accuratezza della modellizzazione dei processi di Mixing che precedono i due stadi di combustione. Sia la modellizzazione dei mixer che quella della combustione vengono eseguite mediante l'utilizzo del software Cantera. Inoltre, lo stesso software viene utilizzato per generare il database emissivo mediante simulazioni cinetico-chimiche 0D a partire dai dati di input derivanti dal database propulsivo. Infine, vengono sviluppate nuove formulazioni predittive per le emissioni di NO_x utilizzando come input i dati dei due database, e i metodi di stima P3-T3 e BFFM2 come formulazioni di riferimento. Le formulazioni matematiche originali dei metodi di stima vengono aggiornate integrando nuove variabili, tra cui il numero di Mach, il rapporto tra le frazioni in massa di H_2O e H_2 all'ingresso della camera di combustione principale, il rapporto tra la portata d'aria inviata al PreBurner e quella inviata direttamente alla camera di combustione principale, e il rapporto tra la portata di aria in ingresso al motore e quella di elio utilizzata per gestire rigenerativamente il carico termico del motore. La caratterizzazione fisico-chimica di questi parametri viene discussa, unitamente al loro ruolo matematico all'interno delle formulazioni.

Table of Contents

List of Figures

List of Tables

Chapter 1 - Introduction

1.1 Research context

Taking place between 30th November and 12th December 2023 in Dubai, United Arab Emirates, the 28th Conference of the Parties (COP28) produced the first global assessment of progress toward achieving the climate objectives outlined in the Paris Agreement. During the COP28 UN Climate Change Conference (UNCC), participating institutions have established the necessity to reach the peak of global greenhouse gas emissions by 2025, followed by a 43% reduction by 2030 and a 60% reduction by 2035 compared to 2019 levels. These measures are crucial to limit global warming to 1.5 ºC in accordance with the Paris Agreement [1]. In this scenario of attention towards emissions reduction, the aerospace sector has proven to be one of the most hard-to-abate. Global aviation activities have been identified as substantial contributors to climate change, generating an intricate network of processes that collectively culminate in a noteworthy warming effect on the Earth's surface. In addition to this, the global rocket engine sector has experienced significant growth in recent years, driven by increasing commercial, governmental, and scientific interest in space exploration. This growth has led to a substantial increase in the number of space launches annually, thereby contributing to a significant rise in emissions. The need to estimate the Aerospace Sector Emission Index (ASEI) has become increasingly imperative to assess the magnitude of the environmental impact and develop targeted strategies to curb emissions. According to recent studies [2], the emissions from the aerospace sector have experienced exponential growth, raising concerns about their potential impact on anthropogenic climate forcing. Over the past twenty years, the rate of increase in the number of launches has reached unprecedented levels, clearly highlighted in the graphs presented in Figure 1.1, consistent with the data presented in reference [3].

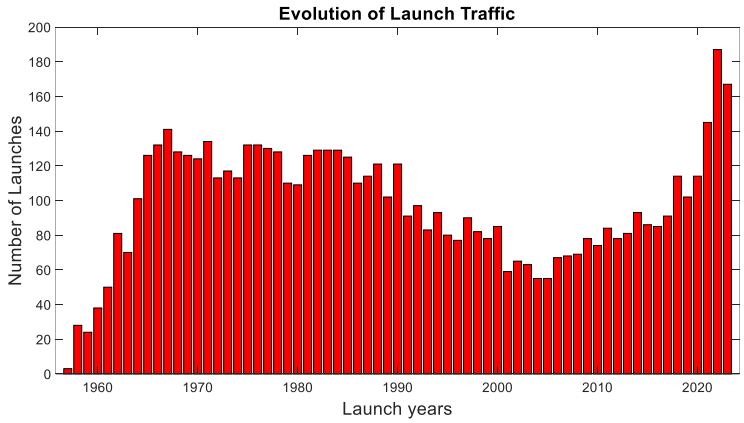

Figure 1.1 - Evolution of annual space launches from 1957 to 2023 [3]

The widespread adoption of expendable launch systems has played a major role in the buildup of on-orbit space debris, encompassing inactive satellites, discarded rocket stages, and residual fragments from various space missions The perpetual presence of this debris poses an imminent threat to operational spacecraft and satellites, increasing the likelihood of collisions and subsequent cascading effects, known as the Kessler syndrome [3]. The challenge of accumulating space debris in orbit has been addressed through various approaches. The introduction of dedicated graveyard orbits to accommodate such debris has proven beneficial, although the scientific community is unanimous in asserting that the ultimate solution to this problem lies in transitioning from expendable systems to reusable ones. Alongside the concerns regarding space debris, the rapid expansion of space-related activities has led to increased emissions in the upper atmosphere, where the residence times of emitted species vary, and the environmental impact of emissions, particularly NO_x, proves to be critical. The issue of high-altitude emissions raises concerns not only in the domain of space access but also within the aviation industry, especially regarding high-speed flights. In the aviation domain, CO_2 emissions have historically been a primary focus of interest for the scientific community, as the aviation sector contributes to 2.5% of global CO_2 emissions [4]. To reduce these emissions and meet the objectives outlined in the most recent climate agreements, a first approach proposed by the aviation industry has been the introduction of green alternatives to traditional fuels. Recently, several alternatives to the traditional kerosene-based fuel have been proposed, including Sustainable Aviation Fuels and hydrogen, which have proven to be the most promising. According to [5], hydrogen emerges as the optimal candidate for minimizing the carbon footprint within the sector. Indeed, the use of hydrogen as fuel eliminates both particulate matter and carbon dioxide (CO_2) emissions, while generally limiting emissions to water vapor (H_2O) and nitrogen oxides (NO_x). In the context of high-speed flights, the advantage of using liquid hydrogen (LH_2) as fuel stems from its relatively high energy density per unit volume, which allows for the storage of more energy compared to conventional fuels. This characteristic is the same one historically responsible for the adoption of hydrogen as a liquid propellant, in combination with liquid oxygen, for launch vehicles used for access to space. In this regard, recent research in the field of reusable Single Stage To Orbit (SSTO) vehicles, whose propulsion systems are capable of functioning in both air-breathing mode and rocket mode, confirms the close link between high-speed flight and the aerospace domain. The benchmark engine for this category is the Synergetic Air-Breathing Rocket Engine (SABRE) developed by Reaction Engines Limited (REL) and designed for the reusable SSTO vehicle Skylon. This engine operates in air-breathing mode up to an altitude of 25 km, reaching a Mach value of 5 before transitioning to rocket mode to achieve the target orbit. Skylon re-enters the atmosphere and lands without generating space debris during operations. The utilization of hydrogen as fuel during both the air-breathing and rocket phases of the mission, in combination with air and Liquid Oxygen (LO_X) respectively, ensures continuity between the two operational modes of the SABRE. The hypersonic flight phase of the SABRE, like all high-speed flights in general, occurs at significantly higher altitudes compared to subsonic flights. Therefore, the non-CO_2 emissions resulting from hydrogen combustion take place in the stratosphere where they exhibit longer atmospheric lifetimes compared to emissions from subsonic aircraft, which predominantly operate within the troposphere. The consequences of these emissions, particularly those of NO_x, can be critical for the ozone layer, which serves as a shield for the Earth and influences global warming. Indeed, NO_x emissions during high-speed flights at high altitudes can lead to both an increase and decrease in ozone levels, depending on flight conditions, thereby increasing the complexity of environmental implications [6,7,8]. The ongoing research on reusable SSTO vehicles in the aerospace sector, and that on high-speed flight in the aviation sector, are characterized by a significant gap in established methodologies for accurately estimating emissions before they occur. This gap presents a notable challenge for the respective industries as they aim to transition towards a greener future. While the adoption of hydrogen as an alternative fuel represents a key strategy to mitigate environmental impact, it is imperative to recognize that challenges persist in assessing and addressing this impact comprehensively. The present thesis aligns with this scenario of aircraft emissions assessment by deriving and applying new analytical formulations for estimating the NO_x Emission Index ($EINO_x$) during the conceptual design of a reference hydrogen-fuelled aircraft. These new formulations are derived from the traditional methods

originally devised for assessing the Emission Index of greenhouse gases and pollutants produced by engines powered by traditional fuels and used for subsonic flight. The original mathematical formulations of these methods need to be modified and adapted to (i) advanced air-breathing propulsion systems for high-speed flights and (ii) environmentally friendly fuels, such as hydrogen. The engine selected as the case study for this work is the Synergetic Air-Breathing Rocket Engine (SABRE), which is analysed during its air-breathing phase until it reaches hypersonic speed regime. This engine, besides being designed for a reusable launcher, incorporates the innovative use of hydrogen as fuel during its air-breathing phase, making it the perfect candidate for researching a methodology to update emissions estimation methods that are applicable in both high-speed flight and space applications domains. Through propulsion and kinetic-chemical modelling of the SABRE system in its air-breathing phase, conducted in collaboration with the Italian Aerospace Research Centre (CIRA), new strategies have been developed to estimate the $EINO_x$ of this unique engine concept, which is currently still under study by REL.

1.2 Study guidelines and objectives

The increasing scientific, logistical, and even tourist interest in space has propelled the space industry to become one of the world fastest-growing sectors in recent years. Therefore, it is imperative to assess the impact of already operational launch assets and to adopt design-to-sustainability strategies for both under-development and future launchers. Simultaneously, the aviation industry's interest in the field of high-speed travel has experienced a significant boost due to the growing demand for faster air transportation. Consequently, the research sector is actively engaged in assessing the environmental impact of potential fleets of supersonic and hypersonic aircraft, starting from the estimation of their emission indices. The utilization of hydrogen as an alternative aviation fuel has alleviated concerns associated with the carbon footprint of aviation sector. Nonetheless, a thorough investigation into non-CO_2 emissions occurring in the upper layers of the atmosphere and their consequential impact on climate change is mandatory. Such emissions, particularly NO_x, exert a substantial influence on the ozone layer and, consequently, on global warming. This issue pertains to both aviation and aerospace sector, concerning emissions resulting from activities that occur beyond the troposphere, at altitudes significantly higher than those characterizing subsonic flight. In this complex and very challenging scenario, the present thesis proposes a strategy to anticipate pollutant and Greenhouse Gas (GHG) emissions prediction for high-speed flight vehicles since the conceptual design phase, specifically focusing on nitrogen oxide emissions. NO_x emissions are indeed of particular importance in the context of hydrogen combustion, which finds application both in the aeronautical and space domains. Furthermore, the impact of such emissions is critical when they occur in the upper layers of the atmosphere. The specialization of this study for system and technologies enabling high-speed flight is carried out having in mind the potential dual applicability of the proposed estimation methodologies: the aviation domain on one side and the access to space on the other. To this end, the SABRE engine is selected as the case study for the adaptation of traditional emission estimation methods due to its dual propulsion architecture, encompassing both air-breathing and rocket modes. In this thesis, the air-breathing phase of this engine is studied, which allows the SSTO Skylon to reach a hypersonic speed regime before switching to rocket mode. To generalize the proposed methodology to the entire category of high-speed flight using hydrogen as fuel, this thesis begins with an in-depth documentation regarding the state of the art in green aviation. In this regard, Chapter 2 explores the aviation sector emissions, the constraints imposed by international climate agreements, and the proposed intervention solutions for climate change mitigation. The role of hydrogen as an eco-friendly alternative fuel emerges from the study of H_2-Air combustion. However, it is essential to study the emissions resulting from this combustion, particularly NO_x, and their formation processes. Then, Chapter 3 provides readers with useful insights into the case study. The Skylon single stage to orbit is introduced, and its propulsive (SABRE) technology described. In Chapter 4, the propulsive and emissive databases of this engine available in the literature are

discussed, identifying possible improvements to be made to the engine propulsion and emissions models that generated them. In this chapter, a comprehensive review of emissions estimation techniques and their applicability beyond traditional subsonic aeroengines and fuels is also provided. Among all the available methods, the Fuel Flow and the P3T3 methods are selected to be modified and adapted to the characteristics of the case study to estimate its NO_x emissions, considering their applicability since the early design phases. For the selected estimation methods of $EINO_x$, Chapter 5 proposes a strategy for upgrading the mathematical formulations to ensure their applicability in high-speed flight and hydrogen fuel conditions. This strategy involves updating the propulsion modelling of the engine, recalculating the propulsive and emissive databases, and analysing the correlations that exist between the chemical-propulsive parameters of the engine and its NO_x production. The modifications made to the reference models aim at ensuring the coherence of the generation process of the two databases, thereby improving their reliability. Chapter 6 provides a detailed description of the new formulations of the Fuel Flow Method and the P3T3 method for high-speed aircraft using hydrogen, based on the results reported in the previous chapter. Once the two databases are updated, the method enhancement involves introducing additional parameters compared to the original formulation. These parameters are selected using a correlation-based approach and integrated into the original formulations of the methods through mathematical interpolation based on solving nonlinear least-squares curve fitting problems. The updated mathematical formulations applied to the case study are presented in Chapter 7. Additionally, a discussion regarding the chemical-physical justifications for the mathematical contributions to the formulations for $EINO_x$ of the newly introduced parameters is provided. Finally, the results of the new formulations are compared with the NO_x Emission Indices evaluated from the engine emissions modelling to verify their estimation effectiveness.

Chapter 2 - Sustainable Solutions for Aviation

2.1 Aviation emissions

Aircraft release radiatively and chemically active substances directly into the Upper Troposphere (UT) and Lower Stratosphere (LS), particularly over the Northern Hemisphere, where aviation activities are predominantly concentrated. These gases and particulate matter (PM) impact the levels of atmospheric greenhouse gases, such as carbon dioxide (CO_2), water vapor (H_2O), ozone (O_3), and methane (CH_4), inducing a net global warming effect that constitutes 3.5% of the overall global climate change due to anthropogenic emissions. The combustion products can be classified into two distinct categories based on their environmental impact. Substances such as CO_2 and H_2O are termed as climate-altering since they directly contribute to the phenomenon of global warming by acting as greenhouse gases. Conversely, substances like NO_x are recognized as pollutants as they degrade local air quality and pose a direct threat to human health. Additionally, the impact of these substances varies depending on the spatial coordinates of the emission point. Global aviation has significant climate impacts, with one-third of radiative forcing associated with CO_2 emissions, while the remaining two-thirds are primarily linked to nitrous oxides (NO_x) and water vapor emissions, manifested as contrail cirrus clouds and particulate matter (PM). The influence of aviation on climate exhibits spatio-temporal sensitivity. Due to the reactive nature of non-CO_2 aircraft emissions, the climatic response varies depending on the chemical composition of the atmosphere, meteorological characteristics at the emission point, and the specific time of day and year when emissions occur. Moreover, the dispersion of aircraft emissions extends over extensive distances and timeframes, introducing complexity to the evaluation of their impact. In today's aviation, kerosene and its derivatives still stand as the most widely used jet fuels. This is owing to their exceptionally high energy density and wide operating temperature range compared to alternative fuel types. These characteristics, coupled with their low cost, ensure that this type of fuel meets the stringent power-to-weight and safety requirements demanded by commercial aircraft. Emissions from aircraft jet engines using kerosene-based fuel encompass a range of pollutants, with carbon dioxide (CO_2) making up approximately 70% of the total. Water vapor (H_2O) accounts for just under 30%, while other pollutant species, such as nitrogen oxides (NO_X), carbon monoxide (CO), sulphur oxides (SO_X), unburned hydrocarbons (HC) or volatile organic compounds (VOCs), particulate matter (PM), and other trace compounds, collectively contribute to less than 1% each of the overall emissions [9]. These emissions can be categorized into two classes based on the profile of their emission indices during flight. The Emission Index (EI) of a substance emitted during the combustion process is defined as the ratio of the mass of the emitted substance, expressed in grams, to the mass of the fuel used during the combustion process, expressed in kilograms. Specifically, CO_2, H_2O, and SO_2 are classified as primary jet fuel combustion products, as their emission indices remain relatively constant throughout all flight phases. This stability arises because these products are directly generated as a result of the combustion reaction, and their emission indices depend on the carbon-hydrogen-sulphur composition of the fuel. NO_x, CO, HC, PM, and trace levels of volatile organic compounds (VOCs), on the other hand,

are classified as secondary jet fuel combustion products. This classification is due to the variability in their production levels, which depends on the nature of the combustion process and the engine load condition. Consequently, their emission indices (EIs) exhibit variability throughout the flight, influenced by factors such as aircraft engine type, engine operating conditions, and atmospheric conditions in the surrounding environment [10]. The Emission Index is a parameter that quantifies emissions, allowing for their categorization. However, there are other strategies for classifying emissions, and of particular interest are those that refer to their actual environmental impact. In this regard, it is useful to introduce the Radiative Forcing parameter. Radiative Forcing (RF) is defined as a metric that quantifies the impact of a factor on the balance between incoming and outgoing energy within the Earth–atmosphere system. A positive RF signifies a warming effect, indicating that the factor enhances the Earth's ability to retain heat. Conversely, a negative RF suggests a cooling effect, signifying that the factor amplifies the Earth's capacity to release heat to space. As mentioned earlier, the aviation sector accounts for 3.5% of the total global net anthropogenic Effective Radiative Forcing (ERF). However, it is essential to qualitatively refine this data for the emissions with the most significant impact. Different emissions, whether directly or indirectly, alter the planetary radiation balance through effects that vary in terms of the involved time and spatial scales. Starting from CO_2 emissions, they contribute positively to the Earth's radiative forcing budget, leading to a warming effect. These emissions have residence times on the order of centuries and exhibit excellent atmospheric miscibility, resulting in a spatially homogeneous environmental impact globally. Since CO_2 itself is a greenhouse gas (GHG), its emissions directly alter the concentrations of gases in the atmosphere. For the same reason, water vapor emissions also have a direct effect on the percentages of greenhouse gases present in the atmosphere, resulting in a positive warming effect. Additionally, H_2O emissions play a role in two processes that indirectly contribute to warming: the reduction of the ozone layer and the formation of contrails and aviation-induced cirrus both of which impart a positive contribution to radiative forcing. Due to their much shorter residence times compared to CO_2 emissions, these emissions do not have a significant impact when released in the troposphere. However, as their residence time increases when released in the stratosphere, water vapor emissions become relevant in the domain of high-speed aircraft whose flight altitudes are much higher than those of subsonic aircraft, and their impact will be discussed in a dedicated subsection. As for NO_x emissions, they do not directly affect the alteration of atmospheric gas concentrations. However, they exhibit two indirect effects that result in an overall positive contribution to warming. Concerning the troposphere, NO_x emissions lead to the formation of ozone (O_3) and the destruction of methane (CH_4). The first effect enhances warming and is characterized by monthly timescales, resulting in a hemispheric-scale impact resolution. Conversely, the long-term effect associated with methane destruction translates into a reduction in ozone due to a series of chain reactions, thereby leading to cooling on a global scale. Given that both described effects are indirect and depend on the reaction triggered between NO_x emitted by the engine and the surrounding atmosphere, the impact of NO_x emissions is particularly sensitive to the concentration of species in the atmosphere at the emission point. As a result, it can exhibit significant spatial variations [9]. The discussion regarding the impact of NO_x emissions becomes more complex when extending the scope to supersonic and hypersonic speed regimes and, consequently, to the stratosphere. Concluding this overview of aviation emissions characterized by the most critical impact, it is essential to mention the key points for minimizing these emissions. The distinction into two classes of primary and secondary jet fuel combustion products suggests the need for differentiated optimal minimization strategies for the two categories. Primary jet fuel combustion products are indeed highly dependent on the chemical composition of the fuel used in combustion. To minimize this type of emissions, it is therefore necessary to intervene directly in the fuel selection and optimize the efficiency of the combustion process. Regarding NO_x emissions, which are the most significant secondary jet fuel combustion products, their formation is due to the high percentage of nitrogen (N_2) present in the air, which is inevitably utilized in the combustion process of an air-breathing engine. To minimize these emissions, it is necessary to intervene in the conditions established in the combustion chamber, focusing on parameters such as pressure, temperature, fuel-to-air ratio (FAR), and the chemical composition of the mixture undergoing combustion. As demonstrated in the subsequent chapters, the production of NO_x emissions is

favoured by high values of temperature, and pressure in the combustion chamber, while it is hindered by the presence of water vapor. Based on these guidelines, the most significant international agreements in the aviation sector for emission minimization have been formulated, with Fly Net Zero representing the forefront. This agreement solidifies the commitment of the signing institutions to the sector's decarbonization by 2050, and it is precisely within this framework that the interest of the current work lies in the field of hydrogen-fuelled aircraft, as highlighted in the following sections.

2.2 Fly Net Zero

The 21st century has been marked by a global mobilization to assess the magnitude of climate change, its causes, and its effects. The aviation sector has been actively involved in mapping emissions and developing methodologies to mitigate their environmental impact. Recently, various governments and governmental organizations have independently formulated short and long-term plans to meet the goals of the Paris Agreement. Examples include the United States' Aviation Climate Action Plan (ACAP), drafted in 2021 by the Federal Aviation Administration (FAA), and its European counterpart, the European Plan for Aviation Safety (EPAS), regularly updated to adjust its content based on annual sector emission reports and new technological and research findings. The challenges associated with climate change and global warming are not limited to individual countries but extend to the entire world, requiring a cohesive international effort. In this context, a significant step was taken in 2016 when 192 countries, under the International Civil Aviation Organization (ICAO), endorsed the Carbon Offsetting and Reduction Scheme for International Aviation (CORSIA). This scheme aimed to achieve carbon neutrality for international aviation post-2020, either through fuel switching or by offsetting emissions. Following this, in 2021, the International Air Transport Association (IATA) reinforced this commitment at the 77th IATA Annual General Meeting in Boston, USA. The resolution for Net Zero Carbon by 2050, adopted by IATA member airlines, mandates them to achieve net-zero carbon emissions from their operations by 2050, aligning the sector with the goals of restricting global warming to scenarios below 2.0°C. Furthermore, governments worldwide collectively endorsed a Long-Term Aspirational Goal (LTAG) on climate during the 41st Assembly of the International Civil Aviation Organization (ICAO) in 2022. This shared goal reflects a commitment to decarbonize the aviation industry in alignment with global efforts to address climate change. The common strategy proposed by the mentioned agreements aims to reduce as much CO_2 as possible using in-sector solutions. These solutions encompass four major areas of application: transitioning from traditional fuels to sustainable aviation fuels, introducing new aircraft technology, updating operational planning while implementing more climate-efficient infrastructure, and the development of zero-emissions energy sources, with particular attention to electric and hydrogen power. In addition to these, out-of-sector solutions are being considered for emissions that cannot be eliminated at the source. In this regard, strategies involving carbon capture and storage, as well as innovative offsetting schemes, are being developed [11]. According to the ICAO 2022 Environmental Report, the adoption of Sustainable Aviation Fuels (SAFs) is at the forefront of innovative solutions proposed for the green transition, as illustrated in the graph below, with an impact percentage of 53%.

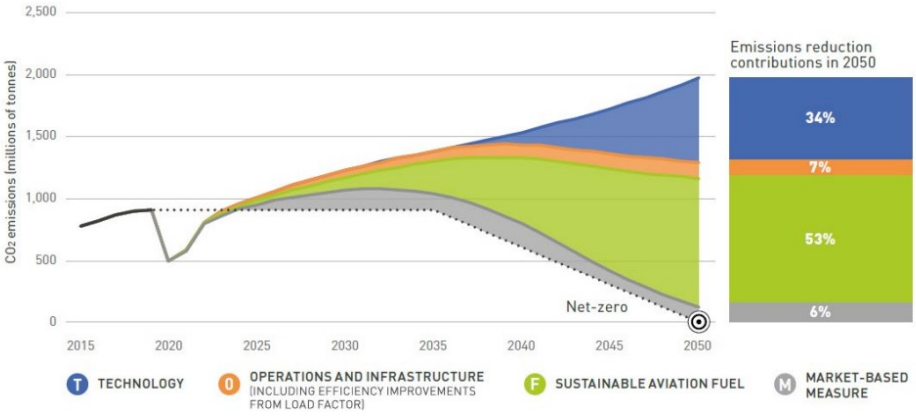

Figure 2.1 - Impact of decarbonisation strategies by 2050 [12]

The Air Transport Action Group (ATAG) Waypoint 2050 study examines forecast scenarios in the evolution of the aviation industry in the coming years and analyses the potential options for almost complete decarbonization of air transport. The industry, at a global level, is projected to achieve net-zero carbon emissions a decade or so after 2050. ATAG concludes that the single largest opportunity to meet and surpass the industry's 2050 goal lies in the transition to sustainable aviation fuel (SAF) and other new energy sources, such as Hydrogen. In this regard, the Waypoint 2050 report [13] provides a thorough analysis of the entire lifecycle of SAFs and Hydrogen, from production and storage to utilization, highlighting their advantages and challenges. Regarding SAF, the study suggests their widespread adoption to meet international agreement targets, with an estimated annual consumption of around 330-445 million tonnes of SAF per annum by 2050. Hydrogen, on the other hand, is mentioned in the report with a dual role in aircraft energy production. Firstly, it could serve as a viable fuel alternative by replacing conventional kerosene in most large aircraft. Besides being associated with a lower GWP compared to traditional fuels and SAFs, hydrogen also meets all the chemical-physical requirements of aviation fuels, exhibiting excellent atomization characteristics and the highest energy per unit mass of any chemical fuel. Secondly, hydrogen is utilized for power generation through fuel cells, a high-potential technology that offers significant energy efficiency and decarbonization benefits. Focusing on the use of hydrogen as an alternative fuel, Vertatene D. [14] have demonstrated how its utilization has the potential to reduce the energy utilization of long-range transport aircraft by approximately 11%. The environmental, structural, and propulsion benefits arising from the use of hydrogen must contend with its very low energy density per unit volume, posing a challenge in utilizing it as an energy vector. To make hydrogen commercially viable for the aviation market, its volumetric density needs to be vastly increased, adopting innovative storage strategies, including the slushed form. In addition to optimizing this parameter, the research sector is recently focusing on studying the effects of adopting hydrogen as fuel for high-speed aircraft, certifying its significant potential for these flight regimes. The following two subchapters delve into the topics of SAFs and hydrogen propulsion introduced here.

2.3 Sustainable Aviation Fuel

Alternative aviation fuel are non-fossil derived fuels currently utilized in commercial aviation. The Sustainable Aviation Fuel (SAF) falls into this category as they present an alternative feedstock to crude oil and enable a reduction in CO_2 emissions by up to 80% [11]. Their sustainability lies in the ability to produce them continually and repeatedly while preserving ecological balance by avoiding depletion of natural

resources. Sustainable feedstock can derive from both biomass and solid and gaseous waste. Besides not causing the depletion of raw materials for their production, SAFs also make a significant contribution to the aviation industry decarbonisation roadmap. A Sustainable Aviation Fuel is a sustainable, non-conventional alternative to fossil-based jet fuel. Several definitions and terminologies may apply, depending on regulatory context, feedstock basis, and production technology [15]. SAF recognized fuels can be divided into two categories based on this definition: (1) drop-in fuels and (2) non-drop-in fuels. Drop-in fuels (1) have physical and chemical characteristics that are almost identical to conventional fossil-based jet fuel and can therefore be safely mixed at various blend ratios. Additionally, drop-in fuels use the same fuel supply infrastructure as traditional jet fuels and do not require system and architecture adaptation. Synfuels and biofuels fall into this category. (2) Non-drop-in fuels, on the other hand, are characterized by new fuel grades, new fuel specifications, and their approval process is not yet addressed in detail. These fuels are intended only for new aircraft and require separate and different infrastructure from traditional fuels [15]. Among non-drop-in fuels, the most recently focused on is hydrogen fuel (H_2). This section is dedicated to drop-in fuels, referred to by the generic term SAFs, while hydrogen, recognized as non-drop-in fuels, will be addressed in the subsequent section. In this regard, it is important to underline how the molecules in drop-in SAF are identical to those in conventional jet fuel, thus SAFs present physical and chemical characteristics that are almost identical to conventional fossil-based jet fuel. This implies that the combustion of SAF emits comparable quantities of CO_2 and other GHGs to conventional fuels. However, SAF still offers an environmental advantage when considering all stages in a life cycle assessment, resulting in reduced emissions compared to the baseline life cycle value of 89gCO_2e/MJ for jet fuel [16]. The benefit arises from using biomass to produce SAF: plants absorb CO_2 during photosynthesis, which is subsequently emitted back into the atmosphere during combustion, ideally forming a carbon-neutral closed loop. When other substances are used to derive the sustainable feedstock, such as municipal solid wastes, agricultural wastes or industrial waste gases, emissions reductions stem from the multiple uses of fossil carbon. Assessing the lifecycle reductions of CO_2 emissions in SAF is complex due to the multitude of factors influencing this decrease, but all stem from the basic premise of using a fuel based on feedstocks that absorb CO_2 during production, either recycling CO_2 emissions from waste sources or directly capturing CO_2 from the air. At present, a SAF is classified as a drop-in fuel, meaning a synthetic and completely interchangeable substitute for conventional petroleum-derived hydrocarbons that does not require adaptation of the engine, the fuel system to be used or the fuel supply infrastructure. SAFs are used in fuel blends with traditional fuels, forming drop-in fuel blends with a maximum SAF percentage in currently approved drop-in fuel blends of about 50%. With these percentages, it is possible to achieve a maximum decrease of 40% in CO_2 emissions from aircraft using these blends. Considering the current perspective of total decarbonization of the sector, the percentage of SAF within the blends is expected to increase to 100% in the coming years [17]. The goal of achieving net zero carbon emissions is made possible through a shift to SAF, and it can be pursued through two methods: by increasing the volumes of SAF deployed, meaning increasing the fraction of SAF blended with traditional fuel, and by enhancing the emissions reduction factor associated with SAF compared to traditional fuels. Despite the excellent results in terms of CO_2 reduction and other emissions, such as NO_x and particulate matter, the adoption of SAF by the aviation industry is currently stalled at a percentage of 2% compared to the globally used fuel annually. The main challenges limiting the widespread use of these drop-in fuel blends can be attributed to the difficulty in ensuring sustainability and meeting technical requirements, the fragmentation of the policy landscape, as well as cost issues, which are still high but expected to decrease in the coming years [13]. At the end of 2023, EU lawmakers signed the ReFuelEU Aviation Regulation, a part of the 'fit for 55' package aimed at implementing policies on climate, energy, land use, transport, and taxation to reduce net greenhouse gas emissions by at least 55% by 2030, compared with 1990 levels. Within the aviation context, this legislative package, as imposed by the ReFuelEU Aviation Regulation, mandates fuel suppliers to distribute sustainable aviation fuels (SAF) and facilitate their uptake among airlines to reduce emissions from aviation. The proposed plan includes achieving binding five-year targets to gradually increase the share of sustainable aviation fuels in the fuel supply chain and hence at European airports. The Commission proposed setting the minimum percentage

of SAF supplied at each EU airport relative to the total fuel supplied at 2% in 2025 and 5% in 2030, increasing to 20% in 2035, 32% in 2040, 38% in 2045, and 63% in 2050 [18]. The regulations concerning the expansion of SAFs aim to meet the primary goal of complete decarbonization by 2050. However, these regulations also underscore an additional challenge related to the sustainability of these fuels when considering large-scale production. The following figure presents an estimate of SAF production capability, adapted by Khandelwal et al. from ICAO and IATA.

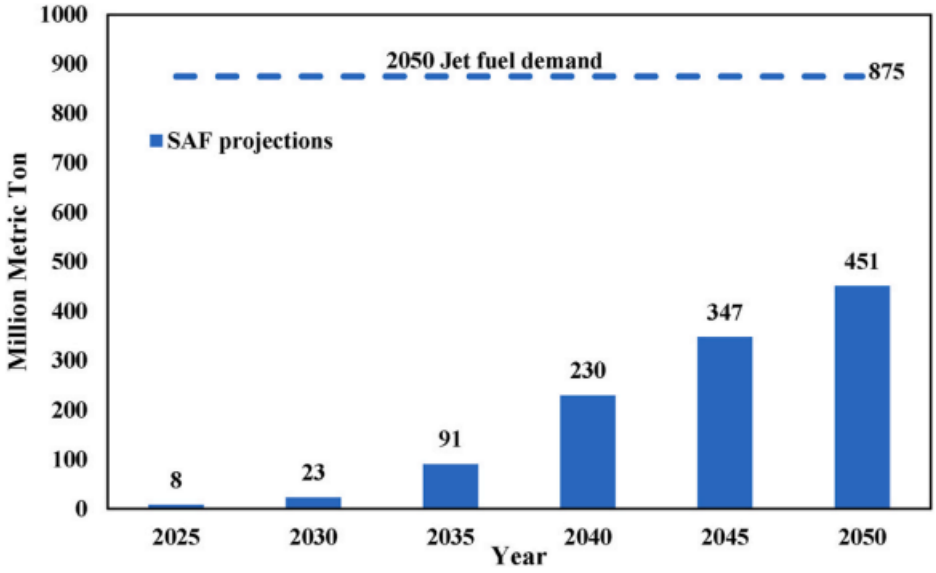

Figure 2.2 - Estimate of SAF production capability, adapted from ICAO and IATA [17]

As evident from the graph, over the next 25 years, SAF production will need to increase by nearly 500 times compared to current levels. This raises concerns regarding the resources that will need to be utilized to achieve this objective, particularly concerning biomass and land use. Today, SAFs are produced using various feedstocks, but there is a pressing need for further diversification and approval of new production pathways to ensure the long-term sustainability of the production of these environmentally friendly fuels. To address this issue and enhance cost competitiveness, governments and policymakers should establish a clear strategy to attract investments into SAF production and provide incentives for their consumption, while monitoring the sustainability of the projects proposed by the ReFuelEU Aviation Regulation on an annual basis. Based on these considerations, it can be concluded that in the near future SAFs alone cannot fully meet aviation demands and climate objectives due to their high costs, limited feedstock availability, and land constraints for feedstock cultivation. Therefore, it is necessary to consider other alternative fuels that are inherently carbon-free, such as hydrogen, to achieve the goal of total decarbonization of the aviation sector.

2.4 Hydrogen as an eco-alternative fuel

The use of hydrogen as fuel eliminates both particulate and carbon dioxide (CO_2) emissions, making it the optimal candidate for minimizing the carbon footprint within the sector. In this regard, the study by Y. Bicer and I. Dincer focuses on evaluating the overall life cycle emissions of aircraft running on various conventional and alternative fuels. The resulting emissions from various alternative fuels are compared

with those of conventional kerosene-based jet fuel for various impact categories. The assessment demonstrates that a hydrogen-fuelled aircraft route releases the lowest greenhouse gas (GHG) emissions among the considered cases, amounting to 0.014 kg CO_2 per tonne-kilometre. In contrast, a kerosene-fuelled aircraft releases 1.05 kg CO_2 per tonne-kilometre when considering the complete cycle [5]. The beneficial effects of hydrogen usage are also evident in the assessment of Global Warming Potential (GWP), as shown by the research findings presented in the figure below.

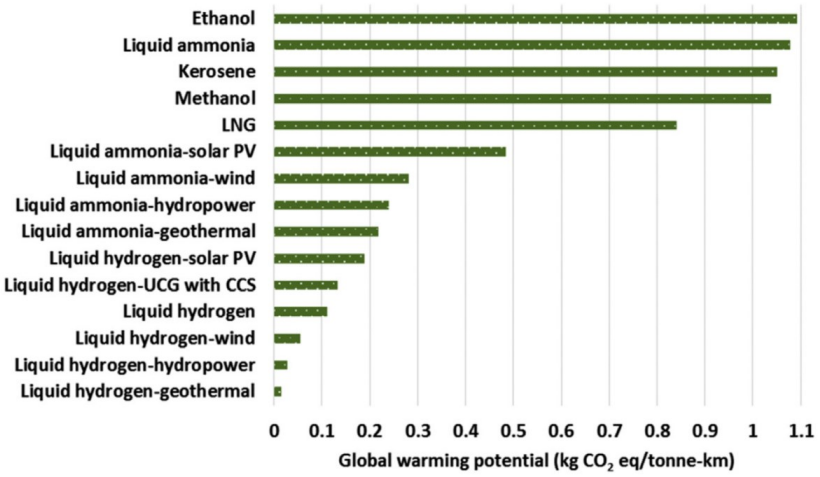

Figure 2.3 - Global Warming Potential of various fuelled aircrafts per travelled tonne-km [5]

Although the use of hydrogen as a fuel represents an avant-garde approach in green aviation, aiming to reduce greenhouse gas (GHG) emissions and mitigate the effects of aviation on global warming, the overall impact of aviation on climate change extends beyond the scope of CO_2 emissions alone. This conclusion is supported by Lee et al.'s study, which assessed the environmental impact of the aviation sector. According to the research conducted by Lee et al., aviation is responsible for approximately 3.5% of the total global net anthropogenic Effective Radiative Forcing (ERF), indicating a 3.5% contribution to the Earth warming phenomenon. Approximately one-third of this contribution is attributable to CO_2 emissions, while the remaining 66% is attributed to non-CO_2 terms, specifically contrail cirrus, water vapor (H_2O) and Nitrogen Oxides (NO_x) emissions. Furthermore, emissions containing nitrogen dioxide (NO_2) and nitrogen monoxide (NO) play a substantial role in altering concentrations of greenhouse gases in the stratosphere. These emissions cause a short-term formation of ozone (O_3), contributing to warming. However, these emissions also contribute to the cooling phenomenon, as they cause the depletion of methane (CH_4) and stratospheric water vapor, along with a long-term decrease in ozone [19]. In light of this, despite the numerous benefits associated with the use of hydrogen as fuel, it is imperative to quantify non-CO_2 emissions from aviation, particularly NO_x emissions, to assess the actual environmental impact of this sector. The impact of aviation NO_x emissions becomes even more concerning when considering the recent aviation industry's expansion into the field of high-speed aircraft.

2.4.1 Hydrogen combustion process

Liquid hydrogen (LH_2) historically constitutes one of the most utilized energy sources in aerospace applications. Liquid Propellant Engines employed in launch vehicles, for instance, involve its utilization in conjunction with liquid oxygen (LO_x) due to the significant energy release per unit mass during their

combustion. Recently, hydrogen has also assumed the role of an alternative fuel for high-speed, air-breathing, trans-atmospheric, and long-term passenger transportation aircraft [20]. The characteristics of hydrogen that make it a promising eco-friendly alternative to traditional fuels are manifold. The combustion of hydrogen is particularly efficient, as the energy contained in this fuel is more than double that of traditional fossil-based fuels, on a mass-equivalent basis [21]. Compared to these fuels, when burned in combination with air, H_2 allows for the elimination of carbon emissions and a significant reduction in NO_x emissions, up to 90% as reported in [21]. Due to its high mass-specific energy density, it exhibits the highest heat release with the shortest kinetic time among all commonly used aviation fuels. Additionally, it has a wide flammability range, extending from 4% by volume with dry air up to 75% [20]. This allows ignition of the hydrogen-air mixture even under fuel-rich conditions, as in the case of the SABRE engine. Ignition and combustion under conditions beyond stoichiometry result in a reduction in flame temperature and consequently a decrease in NO_x emissions produced. Regarding the auto-ignition of the hydrogen-air mixture, the temperature at which it occurs is higher than that observed for traditional fossil fuels. This allows for greater compression of the flow and consequently greater combustion efficiency but may necessitate the use of an igniter if the mixture is not sufficiently hot. Additionally, this fuel exhibits excellent cooling properties and can thus be employed for regenerative thermal management of the engine load. Furthermore, H_2 can be treated physically and chemically as an ideal gas over a wide temperature range even at elevated pressures, and due to its excellent volatility and diffusivity characteristics, its mixing time can generally be neglected [20]. Despite the positive properties of hydrogen, it also presents significant limitations. Its cryogenic nature entails important challenges in its handling and onboard storage, which must occur at particularly low temperatures. Moreover, despite its high mass-specific energy density, it has a very low volumetric density, requiring tanks of significant size for storage, as well as very cold temperatures. Finally, the processes for producing hydrogen in liquid form are particularly energy-intensive and can thus have a non-negligible environmental impact.

For the combustion modelling of the air-hydrogen process in the SABRE engine, the software Cantera is utilized in this thesis. Cantera is open-source software for 0D/1D kinetic-chemical modelling. This software is used in this work both in its Python interface and in its Matlab interface to evaluate the chemical equilibrium conditions in the combustion chamber and to perform 0D time-dependent simulations of homogeneous, isochoric, and adiabatic batch reactors with premixed gaseous reacting hydrogen/oxygen mixtures. To model the kinetic and thermodynamic evolution of the mixture, the software solves the mass and energy balance equations utilizing the *z24_nox20* kinetic mechanism developed by the Swedish Defence Research Agency FOI modelling group. This mechanism is specifically designed for air-hydrogen combustion and is the optimal candidate for estimating NO_x emissions resulting from such combustion. In combustion engines, the oxidation of H_2 by means of the O_2 contained in the air occurs very quickly and allows for the conversion of the chemical energy stored in the fuel into thermal energy through a series of complex radical reactions. In particular, the *z24_nox20* kinetic mechanism, in addition to containing the fundamental physicochemical parameters of the elements and species involved in the air-hydrogen combustion process, defines 24 irreversible elementary reactions that occur during combustion. These radical reactions can be divided into four categories: (i) initiation reactions, which mark the beginning of the process by breaking stable molecules into radicals; (ii) propagation reactions, during which the radical concentration is constant; (iii) chain branching reactions, through which the quantity of radicals doubles and ignition occurs; and (iv) termination reactions, which allow for the recombination of radicals into stable compounds. The *z24_nox20* mechanism is optimal for estimating NO_x emissions precisely because it contains the representative reactions of the main NO_x formation processes, detailed in the following section. The operation of the Cantera software and the characteristics of the kinetic mechanism are recalled and discussed later where necessary.

2.4.2 Hydrogen-Air combustion emissions

As mentioned earlier, the combustion of hydrogen with air is inherently less impactful compared to the combustion of traditional fossil fuels in combination with air. The use of hydrogen fuel allows for the elimination of carbon emissions, particularly CO_2 and CO, producing only H_2O and NO_x as exhaust compounds. In particular, the main NO_x compound produced during combustion is NO, while other nitrogen oxides such as NO_2 are produced in less significant quantities and mainly participate in the formation processes of NO. A summary regarding H_2O and NO_x emissions is reported below, specifying in particular the mechanisms of formation of the latter emissions.

H2O – Water Vapour emissions

The radiative forcing due to aviation water vapor emissions has long been assumed to be negligible, and their climate impact has only recently been studied in detail. Today, the climate impact of aviation indicates a very large uncertainty regarding the contribution of radiative forcing from these emissions. Indeed, both horizontal and vertical resolutions must be taken into consideration when calculating stratosphere to troposphere exchange, which increases complexity when evaluating the climate impact of water vapor emissions. Only emissions of water vapor occurring in the stratosphere significantly perturb the environmental humidity and hence have a radiative effect due to the low humidity present in the upper layers of the atmosphere and their persistence. Water vapor acts as a catalyst in the destruction of ozone through multiple mechanisms. The ozone loss through water vapor emissions is greater than that caused by NO_x emissions for altitudes higher than about 40 km [22]. The impact of these emissions is expected to double in the future due to the transition to hydrogen-fuelled supersonic aircraft for civil aviation, mostly operating in the stratosphere. For this reason, the detailed study of these emissions and their impact will be of fundamental importance in the coming years.

NOx – Nitrogen Oxides emissions

The majority of all NO_x produced during air-hydrogen combustion consists of nitric oxide (NO), while other compounds such as NO_2 are produced in much smaller proportions [7]. These compounds of oxides of nitrogen (NO_x) form during combustion from the nitrogen (N_2) present in atmospheric air, which dissociates due to the high flame temperatures reached in the combustion chamber, initiating a chain reaction leading to the formation of various intermediate substances. These pollutants do not directly contribute to warming the Earth's surface but generate a radiative effect by interacting with other atmospheric elements. The effect of such interaction processes is highly sensitive to the spatiotemporal resolution of NO_x emissions. Regarding emissions in the troposphere, NO_x has two main effects characterized by different timescales. Emissions of NO_x in the troposphere initially lead to a short-term local increase in ozone production (O_3) over weeks to months. Additionally, in the presence of high levels of NO_x and O_3, there is an increase in hydroxyl radical (OH) production, which, in turn, leads to the long-term global destruction of ambient methane (CH_4) over decades. The short-term increase in O_3 causes a significant positive effect of radiative warming, while the long-term CH_4 depletion causes a smaller, absolute negative effect of radiative forcing. Despite the long-term negative cooling effects, the short-term warming from O_3 dominates, leading to a net positive warming effect overall. Regarding the impact of NO_x emissions beyond the troposphere, it is particularly difficult to evaluate due to the complexity and high spatiotemporal sensitivity of the catalytic cycles of ozone chemistry. As reported in [6], [7] and [8], this effect can contribute positively and negatively to radiative forcing, depending on the ambient conditions at the emission point. In general, in the stratosphere, the role of NO_2 in the catalytic cycles of ozone chemistry becomes particularly relevant [7]. Since the determining factor in the formation processes of NO_x within

the engine is the flame temperature reached in the combustion chamber, a higher production of these emissions is expected for high-speed hydrogen-powered aircraft compared to traditional subsonic aircraft, due to the higher temperatures associated with the former. For the purposes of this thesis, it is important to examine the different mechanisms responsible for the formation of NO_x during air-hydrogen combustion. In particular, only the mechanisms of NO formation integrated within the kinetic scheme *z24_nox20*, which is chosen to be used for modelling the air-hydrogen combustion in the SABRE case study for this work, are reported and discussed below.

- **The Zeldovich mechanism (Thermal NO)**

  Thermal NO, also known as Zeldovich NO, originates from the following reactions:

  $$N2 + O \rightarrow N + NO$$

  $$N + O2 \rightarrow NO + O$$

  $$N + OH \rightarrow H + NO$$

  These reactions, particularly the first one, become significant only at high temperatures, around 1800-2000K, hence the term "thermal" attributed to the NO produced by this mechanism. In particular, the first reaction is the rate-limiting step of the thermal NO formation. The activation energy required to break the covalent bond of the N_2 molecule is very high. Consequently, considering the antagonistic contribution of temperature and activation energy in defining the rate constant of the reaction and thus the speed at which the reaction occurs, only at very high temperatures is it possible for the reaction to take place in acceptable times to appreciate the result. When the temperature is low, the reaction occurs extremely slowly, as does the formation of subsequent thermal NO_x, and therefore their production within the engine. Based on these considerations, it is possible to conclude that a reduction of thermal NO can be achieved by decreasing N_2, O, or the rate constant of the first reaction [23].

- **The N/O sub-mechanism (NO generated via nitrous oxide)**

  In general, the N/O sub-mechanism involves the participation of four chemical species, namely nitric oxide (NO), nitrogen dioxide (NO_2), nitrous oxide (N_2O), and nitrogen trioxide (NO_3). Specifically, nitrogen monoxide (NO) plays two main roles in this sub-mechanism. It forms via recombination reactions to eliminate free radicals, as it is a more stable species compared to others. Alternatively, it acts as a chain carrier, participating in other reactions of nitrogenous compounds [24]. Within the *z24_nox20* mechanism, reactions associated with NO_3 are not integrated, but only those associated with NO_2 and N_2O are included, as listed below.

  $$NO2 + M \rightarrow NO + O + M$$

  $$H + NO2 \rightarrow NO + OH$$

  $$NO2 + O \rightarrow NO + O2$$

  $$N2O + O \rightarrow 2\ NO$$

  This mechanism has a significant impact under conditions of high pressure and low temperature. Indeed, the reaction involving these three elements is favoured by high-pressure levels, while

lower temperatures are sufficient to break the bonds in N_2O or NO_2, thanks to the limited activation energy of the respective reactions [24].

- **The H/N/O sub-mechanism**

  The H/N/O sub-mechanism essentially involves the participation of five chemical species, namely nitroxyl (HNO), HON, nitrous acid isomers ($HONO/HNO_2$), and nitric acid isomers ($HONO_2$). Within the *z24_nox20* mechanism, only reactions associated with HNO are included, as listed below.

$$H2O2 + N2 \rightarrow NH + NO + OH$$

$$NH + OH \rightarrow H + HNO$$

$$NH + O2 \rightarrow HNO + O$$

$$HNO + OH \rightarrow H2O + NO$$

$$H + HNO \rightarrow H2 + NO$$

  In particular, the compound HNO originates from the intermediate species NH, which is generated during the recombination reaction of H_2O_2 with N_2. It is useful to note that the resulting species HONO from the reaction between NH and OH can exist in two different forms: trans-HONO and cis-HONO. Despite the superior stability of the trans-HONO species, the dominant products are cis-HONO+NO via the last reaction listed, due to the lower energy barrier. It is worth noting that the chemistry of HNO still has large uncertainties. Direct measurements and theoretical calculations for these reactions are still poorly investigated, particularly at high temperatures [24].

Once the processes of NO_x formation considered by the kinetic mechanism *z24_nox20* used for the 0D simulation of hydrogen-air combustion in the SABRE engine have been discussed, it is possible to identify strategies available for their minimization. The most influential parameter in NO_x formation processes is the flame temperature. This temperature is a function of the equivalence ratio, i.e., the ratio of fuel and air in real conditions compared to the stoichiometric value ($\phi = 1$). The maximum production of NO_x occurs at the maximum flame temperature achievable, which is obtained under stoichiometric combustion conditions. For this reason, the first minimization strategy consists of reducing the flame temperature by selecting mixture compositions different from those ensuring stoichiometric combustion. In hydrogen/air combustion, a lean condition is usually preferred as the excess of H_2 can increase the complexity of reaction pathways to be taken into account in the kinetic scheme. Combustion under lean conditions is preferable to rich conditions also due to the smaller amount of fuel required and therefore carried on board. Another strategy to inhibit NO_x formation is to optimize the residence time, i.e., the time that the reacting flow spends inside the thrust chamber. Increasing the residence time of the flow in the combustion chamber at elevated temperatures also increases the production of NO_x. Therefore, this parameter should be optimized, considering the constraint imposed by the ignition delay time. It is necessary to guarantee the complete combustion required for thrust generation without exceeding the time spent by the reacting gas flow in the chamber. Minimization of the residence time can be achieved by optimizing the volume of the combustor based on the considerations made earlier. Another possibility to optimize the residence time lies in modulating the volumetric flow rate entering the chamber. Regarding the scope of this thesis, the objective is not to minimize NO_x emissions. In fact, the volumetric flow rate entering the combustion chamber, equivalence ratio, and flame temperature inside it are constrained by the inputs provided by the manufacturing company and the proposed propulsive-emission modelling. However, considering this analysis of NO_x formation processes within the engine, it is possible to conduct an analysis of the existing

correlations between the chemical-propulsive parameters of the engine and the NO_x produced. This allows the identification of a set of influential parameters with which to modify the original formulations of emission estimation methods present in the literature to adapt them to the high-speed and hydrogen-fuel case study.

Chapter 3 - Case Study

3.1 Skylon SSTO

This chapter briefly presents SKYLON, the case study to which the developed methodology has been applied. SKYLON is an SSTO spaceplane fully reusable, currently under development by the British company Reaction Engines Limited (Reaction) since 2009. This vehicle takes off and lands on a runway like a conventional aircraft, thus belonging to the category of Horizontal Take-Off Landing (HTOL) vehicles. This aspect constitutes a significant advantage in its operational management; for instance, it can be prepared for departure in a hangar near the runway, thereby avoiding the complex and expensive transportation challenges associated with launch facilities. To increase the achievable mass ratio for an SSTO, SKYLON exploits the SABRE engine technology, a combined-cycle LO_X/LH_2 engine able to cover the entire mission of the vehicle by working both in airbreathing mode and rocket mode. The obtained mass ratio is estimated to be approximately 23 per cent more than using a pure rocket system. The engine's airbreathing mode, used by the take-off phase, is switched to pure rocket mode after accelerating the vehicle to Mach 5.14 at 28.5 km altitude, until reaching Low Earth Orbit. Once the climb phase and the subsequent insertion into orbit are completed, the payload is deployed and the orbital operations are accomplished. After that, the vehicle returns to Earth. The re-entry interface is passed at an altitude of 120 km, where the vehicle manoeuvres to control temperatures and thermal loads and to meet the pre-calculated requirements for return to the spaceport. Following a gliding approach similar to the Space Shuttle, it reaches the landing runway.

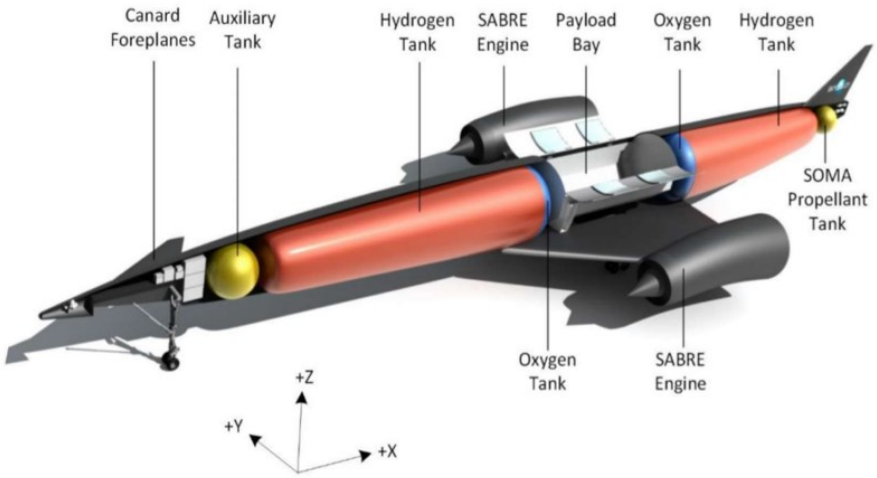

Figure 3.1 - Skylon layout, [25]

As it can be seen in Figure 3.1, the SKYLON configuration has a slender airframe which, in contrast to designs of other SSTO spaceplanes, features a distinct separation between the fuselage and the delta wing (positioned approximately halfway up the fuselage). This characteristic has been demonstrated to be optimal in terms of weight, lift, and volume, but poses challenges in the management of heat flows, as it gives rise to localized high heat fluxes that necessitate an active cooling system. The payload bay of this vehicle is positioned at the wing attachment point, and the payload is loaded from above. The axial symmetric nacelles, on which the SABRE engines are mounted, are positioned on the wingtips. The majority of the fuselage is dedicated to housing the hydrogen cryogenic tanks, with a smaller portion reserved for the liquid oxygen tanks. This allocation is facilitated by the fact that, during the initial phase of ascent, the oxidizer is sourced from the outside air, in addition to the low density of hydrogen that leads to larger fuel tanks. The placement of the tanks is associated with equilibrium problems that impact the vehicle. These challenges were resolved through meticulous aerodynamic design and the implementation of differential burning of the propellant in the two tanks. The SKYLON is equipped with control surfaces for atmospheric flight, including canard foreplanes for pitch control, ailerons for roll control, and an aft fin for yaw control. During the pure rocket phase, control is achieved through differential engine thrust. Additionally, it features a SOMA (SKYLON Orbital Manoeuvring Assembly) module with engines designed for orbital manoeuvres, fed by a specific propellant tank. Regarding the materials, the primary structure consists of a frame composed of titanium struts reinforced with silicon carbide, while the aluminium tanks are suspended using Kevlar ties. The frame is further covered with sheets of reinforced glass ceramic material, serving as both the aeroshell and the primary thermal protection system, supplemented by a multilayer metallic heat shield. The dimensional and mass characteristics of the SKYLON are reported in Table 3.1.

Fuselage Length	83.1 m
Wing Span	26.8 m
Height	13.5 m
Max Payload Mass	15.0 tons
Gross Take-Off Mass	325.0 tons
Dry Mass	53.4 tons

Table 3.1 - Dimensional and mass characteristics of the SKYLON spaceplane [25]

3.2 SABRE engine

The Synergistic Air-Breathing Rocket Engine (SABRE) is the key component of the Skylon, enabling the single-stage-to-orbit vehicle to operate in both air-breathing and rocket modes. This unique engine concept operates like a turbojet, utilizing hydrogen as fuel in combination with air from take-off until the transition point, set at an altitude of 25 km, enabling the engine to reach a Mach number of 5. Once this speed regime is reached, the engine transitions to rocket mode, during which air is replaced by liquid oxygen (LO_X), ensuring a specific energy release during combustion compatible with the levels required for ascent to low

Earth orbit. The transition of the SABRE to rocket mode occurs at an altitude where it is no longer feasible to sustain LH_2-external air combustion due to the rarefied conditions of the atmosphere at that altitude. However, the advantages of this innovative engine design are significant, as the air-breathing operating mode allows for a reduction in the amount of propellant needed to be stored inside the Skylon to ensure access to the target orbit, consequently increasing the payload mass that can be transported to its destination. The architecture of the SABRE is well summarized by Figure 3.2 provided by V. Fernandez Villacé [26].

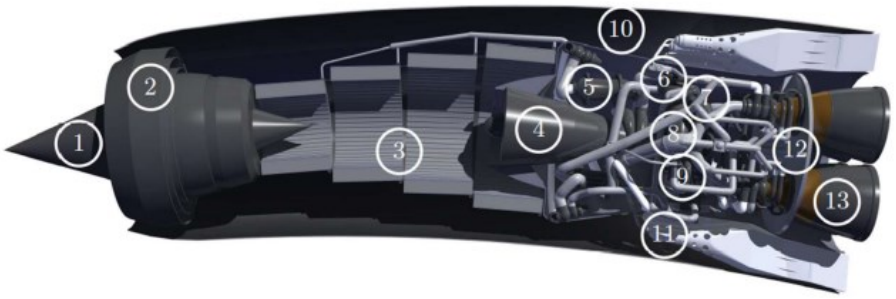

Figure 3.2 - SABRE section: 1) movable spike 2) intake 3) precooler 4) air compressor 5) pre-burner and reheater (HX3) 6) helium circulator 7) H2 pump 8) He turbine and regenerator (HX4) 9) LOx pump 10) spill duct 11) ramjet burners 12) heat shield 13) thrust chamber, [26]

Regarding its air-breathing operating mode, the SABRE falls into the category of deeply precooled combined cycle engines, where the primary air cycle is coupled with a secondary regenerative cycle using helium for thermal management of the engine. This solution allows for the regeneration of a portion of the heat extracted from the hot incoming airflow into the engine, extending its operation in air-breathing mode up to a Mach regime exceeding 5 without performance degradation, particularly in specific impulse. Additionally, the SABRE involves a two-stage combustion process occurring in two different combustion chambers: the PreBurner (PB) and the main Combustion Chamber (CC), enabling the regeneration of a portion of the heat produced during the initial combustion segment, again utilizing the helium cycle. The regenerated heat through the helium cycle is utilized to heat the cold flow of hydrogen stored at a temperature close to 0K to maintain its liquid state during storage, as well as to power the compressor involved in the primary air cycle. As reported in V. F. Villàcé, the incoming air captured by the intake is deeply cooled by a flow of cold helium inside the PreCooler (PC), then passes through the high-pressure ratio Air Compressor (AC), downstream of which the flow is split with a variable splitting ratio depending on the flight Mach number and redirected to the two combustion chambers. The two-stage combustion takes place first in the PB, where a portion of the air is burned under fuel-rich conditions. The exhaust gases from the PB, after exchanging some of their heat in a heat exchanger with helium, rejoin with the second airflow from the splitting at the main CC, where combustion is completed again under fuel-rich conditions. Finally, the combustion products from the main CC expand in the nozzle, generating thrust. Additionally, bypass burners are provided for a portion of the incoming airflow at the intake, optimizing engine performance and efficiency. Regarding the engine operation in rocket mode, the engine cycles are shorter as the air intake is closed, and the two-stage hydrogen-air combustion is replaced by a single stage of hydrogen-oxygen combustion. Oxygen in this configuration contributes to heat regeneration by cooling the nozzle walls, thereby recovering some of the heat produced during the hydrogen combustion. As reported in the Skylon User Manual, this engine can provide a gross thrust of approximately 2 MN per nacelle in both of its operating modes. In the air-breathing phase, it offers a specific impulse ranging from 40,000 to 90,000 Ns/kg. However, in the rocket phase, the specific impulse value is around 4500 Ns/kg. The architecture of the SABRE engine is indeed custom-designed for space access, offering significant advantages. It provides a high thrust-to-weight ratio during air-breathing operation, coupled with moderate specific fuel

consumption, which enables efficient propulsion during the initial phase of flight. Furthermore, as it transitions to rocket mode, it maintains a high specific impulse, ensuring optimal performance during the phase of reaching the target orbit.

3.2.1 SABRE characteristics

The following table and figure summarize the input data regarding the SABRE, which serves as the basis for constructing the propulsion modelling of the engine, as discussed in the subsequent chapters.

	Parameters	Value	References
Preliminary	Free stream Mach number	0 - 5	[26]
	Altitude	0 – 25000 m	[26]
	Air mass flow	77.3 – 92 Kg/s	[26]
	Helium mass flow rate	17 – 22 Kg/s	[26]
Intake	Intake total pressure recovery	0.12 – 0.95	[27]
Precooler	PC pneumatic efficiency	72%	[26]
	PC outlet temperature,	97 K	[26]
Air compressor	AC efficiency	0.8	[28]
	AC pressure ratio	65 - 180	[27]
Liquid Hydrogen Tank	fuel/air equivalence ratio	2.5 - 2.8	[27]
	Tank temperature	18 K	[26]
	Tank pressure	1 bar	[26]
Liquid Hydrogen Pump	Efficiency	0.8	[27]
	LHP compression ratio	257	[26]
Hydrogen Turbine	Efficiency	0.8	[28]
Helium Turbine	Efficiency	0.8	[28]
	Turbine inlet temperature	1000 K	[26]
Helium compressor	Compressor efficiency	0.8	[28]
Node CC-PB	$\dot{m}_{PB}/\dot{m}_{tot}$	0.45 – 0.6	[27]
Preburner	Combustion efficiency	0.9	[28]
	Pneumatic efficiency	0.95	[28]
	Lower calorific value	120.9e6 J/kg	[28]
Combustion Chamber	Combustion efficiency	0.9	[28]
	Pneumatic efficiency	0.95	[28]
	Lower calorific value	120.9e6 J/kg	[28]
Nozzle	Pneumatic efficiency	0.98	[28]
	Efficiency	0.95	[28]
	Area ratio at separation	20-100	[26]

Table 3.2 Main characteristics of SABRE engine

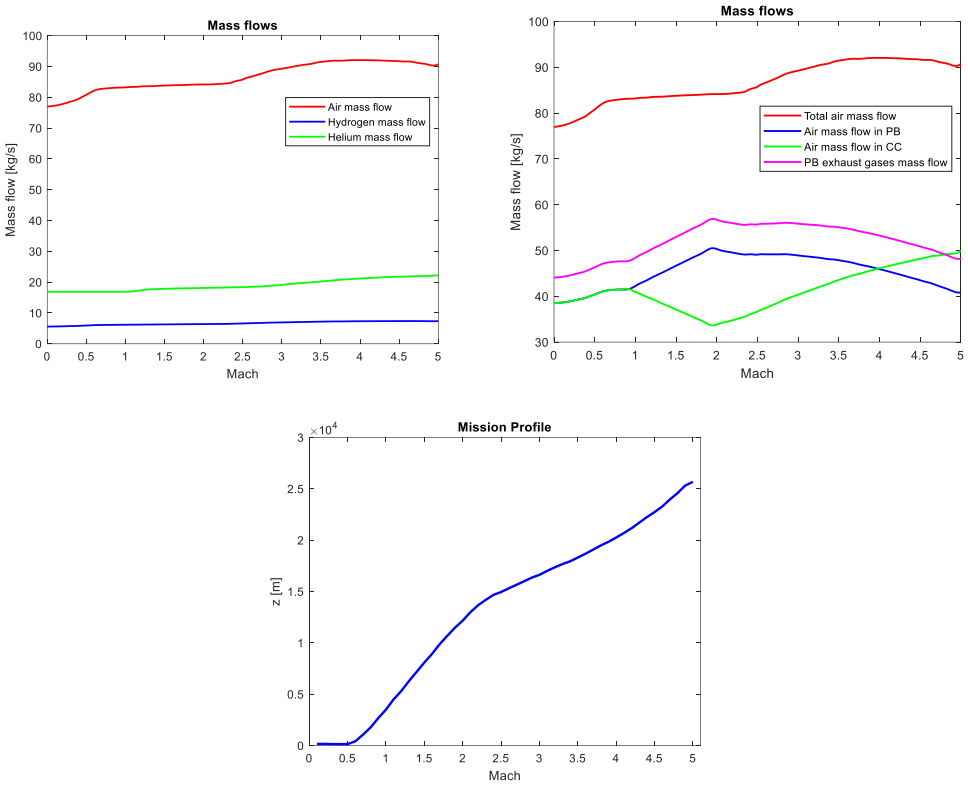

Figure 3.3 - SABRE engine mass flows and Skylon mission profile, as a function of Mach

Chapter 4 - State-of-the-Art in Propulsion and Emission Modelling

The first phase of the research involved a comprehensive review of the state-of-the-art about the following two topics: (1) SABRE propulsion system and combustion modelling and (2) methods and tools for emission indices estimations compatible with the conceptual design stage of the aircraft. In this regard, the Matlab propulsion model developed by Giovanni Grimaldi and described in [27] has been used as a reference in the present work. This chapter provides a brief description of this propulsion model, highlighting the need for improvements to enhance its accuracy. An approach to upgrading the model developed by G. Grimaldi based on the analysis discussed below is proposed in Chapter 5. Regarding the chemical-kinetic modelling of the SABRE combustion process and the subsequent engine emission modelling, reference is made to the recent publication [29]. To generate the only emission database available in the literature for SABRE, the study [29] proposes the use of the Cantera software for modelling chemical-kinetic processes, utilizing the output parameters of the propulsion model [27] as input. Transitioning to the methods for estimating NO_x emissions, the research focused on a range of methodologies specifically studied for subsonic aircraft configurations powered by traditional fuels. This choice is driven by the lack of specific emission estimation methodologies for high-speed flight conditions, such as those relevant to the SABRE case study, which is also powered by an unconventional fuel (H_2). This thesis aims to bridge this gap by proposing new formulations of classical methods for predicting emission indices for pollutants and greenhouse gases, optimized for the SABRE case study within the context of its NO_x emissions. Despite the specificity of the newly derived formulations, the methodology described in Chapter 5 for upgrading and adapting traditional estimation methods may potentially apply to the entire category of high-speed aircraft engines powered by non-traditional eco-fuels. In the latter part of this chapter, the two methods used as input for generating the new formulations, namely the BFFM2 and P3T3 methods, are described. Besides presenting different application procedures, these two methods differ primarily in the specificity of the data required for their use. The BFFM2 method, in fact, only requires knowledge of the fuel flow trend during the mission and the mission profile itself to derive variations in environmental conditions. The P3T3 method, on the other hand, requires knowledge of the pressure and temperature trends at the inlet of the combustion chamber, which is usually proprietary engine data and thus more difficult to obtain or estimate accurately. The distinctions between these two methods lead to differing levels of accuracy in the emission estimates they produce. The P3T3 method demonstrates greater precision compared to the BFFM2 method, both in its original formulation and in the updated formulations, as outlined in the results and conclusions chapter.

4.1 Propulsion modelling of the SABRE

The model introduced above was developed by G. Grimaldi [27] and it is representative of the operation of the SABRE during the air-breathing phase of its mission profile, which extends from sea level to an altitude of 25 km, reaching a flight Mach number of 5 as indicated by Reaction Engines Limited (REL). This model is assumed to represent the state-of-the-art in propulsion modelling of the SABRE in conceptual design. The engine comprises four thrust chambers, two preburner-reheater units, two hydrogen turbo-pumps, two regenerators, and two helium circulators, each driven by a hydrogen turbine. This configuration allows the propulsion modelling to be scaled down by a quarter, considering only a single unit of each component in the Matlab model, making it representative of 1/4 of the actual engine. The fundamental assumptions underlying this modelling are two: the fraction of incoming air destined for the ramjet burners is assumed to be identically zero throughout the mission profile, and the intake is assumed to perform with nominal pressure recovery while matching the mass flow demanded by the air compressor.

Figure 4.1 illustrates the model developed by G. Grimaldi. This model comprises three distinct thermodynamic cycles: the complete air cycle, the hydrogen cycle, and the regenerative helium cycle. Grimaldi's modelling primarily focuses on the complete air cycle, representing the thermodynamic cycle of the air flow entering the engine through the intake. After passing through the intake, the airflow is cooled by a cold helium stream within the precooler (PC), then compressed in the air compressor (AC), and subsequently split into two different streams at the PB-CC node regulating the air flow directed to the two combustion stages of the engine. One part of the airflow undergoes rich fuel combustion with hydrogen in the PB, with the exhaust gases exchanging heat again with the helium before rejoining the remaining part of the airflow before the main combustion chamber (CC), where combustion with the hydrogen surviving the PB is completed. The total exhaust gas flow from the main CC is finally expanded in a nozzle.

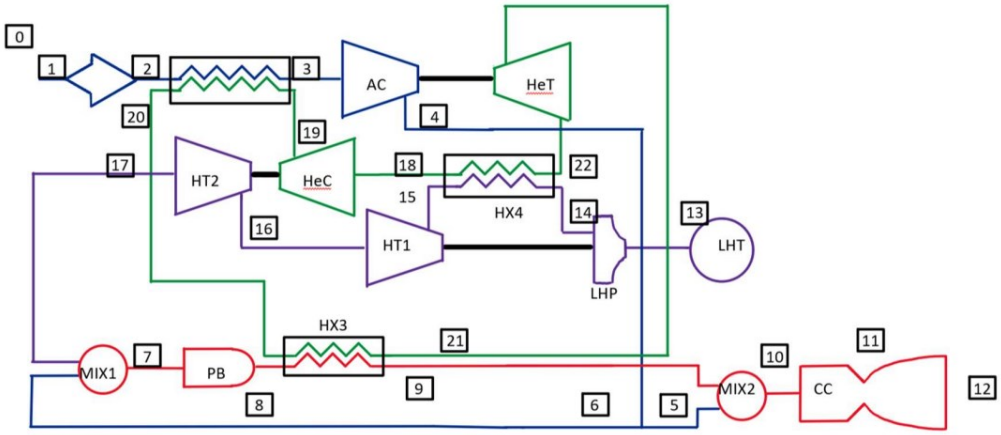

Figure 4.1 - Cycle scheme of the complete model [27]

The SABRE is a particularly complex engine, with a large number of components resulting in a dense and intricate network of thermal and power balances. In order to make the discussion clear, a brief description of G. Grimaldi's propulsion model is reported below, organized according to the numbering shown in Figure 4.1. This description provides an overview of the thermodynamic evolution of the three gas streams involved in the engine operation.

- 0: Ambient conditions at flight altitude. Air properties are assessed using an atmospheric model from literature [28].
- 1 – 2: Air passes through the intake and its velocity is decreased through an adiabatic process until it reaches subsonic values compatible with the compressor demand.
- 2 – 3: Air passes through the PreCooler (PC) where it is cooled down to the inlet temperature of the air compressor. The heat exchanges are modelled as isobaric processes.
- 3 – 4: Air is compressed through an adiabatic process in a single spool Air Compressor (AC).
- 4 – 5/6: At the PB-CC node, air is split into two mass flows that go into the first mixer or the second mixer, respectively coupled to the preburner and the main combustion chamber.
- 6 – 7: In the first Mixer (MIX1), the air is mixed with all the hydrogen that feeds the engine, creating a rich mixture.
- 7 – 8: The hydrogen-rich mixture from MIX1 undergoes combustion in the first stage of the combustion process in the PreBurner (PB). The temperature rises, and the outlet gases primarily consist of nitrogen, water vapor, and unburned hydrogen due to insufficient oxidant. This process is modelled as isobaric.
- 8 – 9: PB exhaust gases go through Heat Exchanger 3 (HX3) where they are cooled down by the helium stream on the other side. The heat exchanges are modelled as isobaric processes.
- 9 – 10: In the second Mixer (MIX2), the PB combustion gases, still rich in hydrogen, are mixed with the remaining portion of the air mass flow from the PB-CC node. Once again, the mixture is hydrogen-rich, however, in this case, it includes a fraction of water vapor in addition to the predominant molecular nitrogen.
- 10 – 11: The hydrogen-rich mixture from MIX2 undergoes combustion in the second stage of the combustion process in the main Combustion Chamber (CC). Unlike the PB, the temperature and pressure values in the main CC are high enough to result in a non-negligible mass fraction of NO in the exhaust gases. This process is modelled as isochoric.
- 11 – 12: The combustion products of the main combustion chamber are expanded through a nozzle.
- 13 – 14: Hydrogen undergoes a transition from the conditions at the Liquid Hydrogen Tank (LHT) to the outlet conditions of the Liquid Hydrogen TurboPump (LHTP). The pump compression ratio is considered constant.
- 14 – 15: Hydrogen flow goes through Heat Exchanger 4 (HX4) where it is heated by the helium stream on the other side. The heat exchanges are modelled as isobaric processes. The thermodynamic properties of hydrogen (density, specific heats, and adiabatic expansion coefficient) are considered constant and fixed at their mean value throughout the cycle.
- 15 – 16: Hydrogen flows through the first Hydrogen Turbine (HT1) where it cools down and decreases in pressure. HT1 is mechanically linked to the Liquid Hydrogen TurboPump (LHTP). The same considerations apply to HX4 regarding thermodynamic properties.
- 16 – 17: Hydrogen flows through the second Hydrogen Turbine (HT2) where it cools down and decreases in pressure. HT2 is mechanically linked to the helium compressor (HeC). The same considerations apply to HX4 regarding thermodynamic properties.
- 18 – 19: Helium is compressed in the Helium Compressor (HeC) thanks to the power extracted by the hydrogen turbine HT2. The thermodynamic properties of helium (density, specific heats, and adiabatic expansion coefficient) are assumed to be constant and fixed at their mean value throughout the cycle.
- 19 – 20: The cold helium flows through the precooler where it cools down the air coming from the intake. The same considerations apply to HeC regarding thermodynamic properties. The heat exchanges are modelled as isobaric processes.
- 20 – 21: The cold helium flows through the HX3 where it is heated up by the combustion products of the PB. The same considerations apply to HeC regarding thermodynamic properties. The heat exchanges are modelled as isobaric processes.

- 21 – 22: The hot helium stream flows through the helium turbine (HeT) where its temperature and pressure decrease, while the extracted energy is used to power the air compressor (AC). The same considerations apply to HeC regarding thermodynamic properties.
- 22-18: The still warm helium flow from the HeT turbine heats the cold hydrogen flow exiting the turbopump within the heat exchanger HX4. The heat exchanges are modelled as isobaric processes.

The Matlab propulsion model developed by G. Grimaldi effectively implements and describes the main engine cycle, namely the air cycle. However, this model does not incorporate the study and implementation of the auxiliary thermodynamic cycle involving helium. The helium flow rate is assumed to be constant and fixed at 22 kg/s, with no consideration given to the evolution of its pressure within the cycle. Furthermore, the thermodynamic characteristics of helium (specific heat and adiabatic exchange coefficient) are treated as constant and fixed at their mean values throughout the cycle. The regenerative cycle of helium, which forms the basis for the thermal balance between the involved gas flows in the engine, is of particular importance for a deeply precooled combined cycle like the SABRE. Therefore, integrating this regenerative cycle into the main model represents a key aspect of the propulsion model update. Similar to the simplified modelling of the helium cycle, the thermodynamic evolution of the hydrogen flow within the engine is also simplified in Grimaldi's propulsion model. Specifically, constant thermodynamic characteristics are assumed for hydrogen, fixed at their mean values throughout the cycle. Additionally, Grimaldi introduces the assumption of a constant compression ratio of the hydrogen turbopump throughout the mission. This assumption, particularly influential regarding the pressure of the hydrogen flow and consequently the pressure at the two combustion chambers, directly impacts the NO_x emissions produced by the SABRE, which are deeply dependent on chamber pressure. Updates to the propulsion model are required in this regard as well. Finally, concerning the two processes of mixing and combustion within the SABRE, Grimaldi proposes a classical modelling approach based on enthalpy balances under isobaric and isochoric conditions. Despite the acceptable accuracy of the results obtained through this enthalpy-based modelling of the processes, suitable for the conceptual design phase of the aircraft, significant improvement is possible by integrating specialized software into the propulsion modelling to address thermodynamic balance and equilibrium issues. Also, concerning the evaluation of gas thermodynamic characteristics, greater accuracy can be achieved using dedicated software compared to the Matlab tool employed by Grimaldi. Once these potential areas for improvement were identified to enhance the sophistication of the SABRE propulsion modelling, the actual update of the SABRE propulsion model can be conducted according to the approach outlined in Chapter 5.

4.2 Emission modelling of the SABRE

Regarding the emission modelling of the engine, the study reported in [29] has been used as a reference. A strategy is proposed for updating the original formulation of a method for estimating NO_x emissions, namely the P3T3 method, and its application to the SABRE case study during its air-breathing phase is implemented. The proposed approach for formulating the engine emission database involves utilizing the propulsion model [27] to derive the thermodynamic parameters of the engine necessary for simulating the mixing and combustion processes using dedicated software. Specifically, Cantera, an open-source software for 0D/1D mathematical-chemical modelling, is employed through the Python interface. Cantera conducts 0D time-dependent simulations of homogeneous, isochoric, and adiabatic batch reactors with premixed gaseous reacting hydrogen/oxygen mixtures. For this purpose, the kinetic mechanism i.e., the *z24_nox20* developed by the Swedish Defence Research Agency FOI modelling group was effectively utilized [30]. The modelling of the preburner combustion was conducted under isobaric conditions, while the 0D

simulations for the combustion chamber were executed assuming isochoric conditions. Additionally, the composition of the exhaust gases leaving the preburner was used as input for the combustion chamber after being mixed with the additional air stream from the intake. The input data required by the software are the pressure values characterizing the inlet of the two combustion stages and the temperatures of the flows at the inlet of the two mixers. The outputs are instead the temperature values of the flows exiting the mixers and the temperature and mass fractions of the species present in the chamber at the final instant of combustion. Once the composition of the gas entering and exiting the main combustion chamber is known, the NO_x Emission Indices can be calculated. Specifically, this index is evaluated for each Mach condition studied based on the mass fraction of H_2 injected into the combustion chamber, i.e., at the initial instant of the simulation, and the mass fractions of NO and H_2 out of combustion, i.e., at the final instant of the simulation. The relationship that allows evaluating the EINO in [g_{NO}/kg_{H2}] is as follows:

$$EINO = \frac{Y_{NO}}{Y_{H2inj} - Y_{H2out}} \tag{4.1}$$

Following this approach for 18 different Mach conditions ranging from 0 to 5, a chemical kinetic Emission Inventory was compiled. The trend of the EINO as a function of the calculated Mach, as computed in [29], is presented in Figure 4.2. Please note that for SABRE, and more generally for hydrogen-air combustion, only the mass fraction of NO produced during combustion is useful for estimating the Emission Indices of the engine, as it is several orders of magnitude higher than the other NO_x compounds.

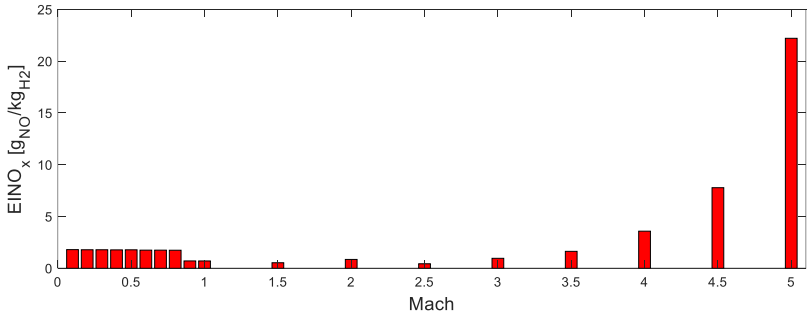

Figure 4.2 - EINO from Cantera 0D kinetic-chemical simulations [29]

4.3 NO_x Emission Index Estimation Methodologies

In literature, numerous methodologies for estimating emissions of pollutants and greenhouse gases from the aviation sector are available, classified based on the required input data and consequently, the resulting accuracy. In particular, the present work is specialized in the estimation of NO_x emissions, thus, the discussion of methods presented below also focuses on these emissions. According to [31], methods for estimating NO_x emission indices can be categorized into five groups: (i) correlation-based models, (ii) P3T3 methods, (iii) Fuel-Flow methods, (iv) simplified physics-based models, and (v) high-fidelity simulations. The last two types of methods are discarded as they are not compatible with the purposes of this discussion. Simplified physics-based models are not widely used in general due to the inability to implement adequate kinetic analysis for NO_x production during combustion. Regarding high-fidelity methods, despite representing the most accurate emissive modelling approach among all those mentioned earlier, they also require the highest level of detail concerning the engine operation and its geometry, which is incompatible

with the limited data available in conceptual design. The correlation-based, P3T3, and FF methods, on the other hand, are of interest for the present study and exhibit similar characteristics, as emerges from the following sections respectively dedicated to the three types of methods. The main differences among these methods lie in the required input data and the extent of their applicability. In particular, correlation-based methods assess the $EINO_x$ of the engine using empirical or semi-empirical relationships built from the analysis of correlations between NO_x emissions and primary or secondary propulsion-emission variables. These methods not only require a large number of variables to be correlated with NO_x production to obtain acceptable but still uncertain results but are also specifically tailored to the engine under analysis and thus not applicable to all engines or categories of engines. Regarding the P3T3 method and FF method, they represent a specialization of Correlation-Based models characterized by a much broader range of applicability. They require a limited number of input data and calculate the $EINO_x$ at Flight Level (FL) based on the $EINO_x$ measured at Sea Level (SL), which must be corrected to the conditions at altitude by utilizing both altitude and ground level combustor operating conditions. The P3T3 method necessitates temperature and pressure profiles at the inlet of the combustion chamber, while FFM requires profiles of ambient conditions and fuel flow. Furthermore, these methods feature unified coefficient formulations intended to apply to every type of subsonic aircraft engine powered by traditional fuels. In particular, it should be emphasized that the FFM methods are derived from the P3T3, addressing the need to formulate a method applicable even in case of lack of proprietary data concerning the engine. There are two different methods based on Fuel Flow: the Boeing Fuel Flow Method 2 developed by Boeing (BFFM2) and the DLR fuel flow method developed by The German Aerospace Centre. These two formulations differ only in the introduced exponential correction factors, and therefore, it is decided to refer only to the BFFM2 below, as it is more commonly used in literature. Although the P3T3 method and BFFM2 have been selected for this thesis work as the methods to update to make them applicable for the high-speed and hydrogen combustion case study, an insert of this subsection is also dedicated to correlation-based methods. This is because the update of the P3T3 and BFFM2 methods is conducted with an approach that can be defined as correlation-based. In fact, the adaptation strategy of the two methods to the case study, as outlined in Chapter 5, is based on updating the mathematical formulations of the P3T3 and BFFM2 by introducing one or more parameters influencing NO_x formation, identified through an analysis of physicochemical correlations during engine operation.

4.3.1 Correlation-based Models

The Correlation-Based models rely on thermodynamic and emissive data derived from engine tests under ground-level conditions. These data are integrated within mathematical formulations to determine $EINO_x$ based on combinations resulting from the analysis of correlations between them and the formation of NO_x inside the engine. These methods are divided into two categories, empirical and semi-empirical, depending on the type of variables included in the final mathematical formulations. Specifically, the variables that characterize an empirical correlation-based method are primary engine parameters, such as inlet temperatures and pressures to the combustion chamber, end-of-combustion temperature, Fuel-to-Air Ratio (FAR), or Water-to-Fuel Ratio (WFR). Semi-empirical methods, on the other hand, require a detailed knowledge of the combustion chamber configuration as they involve the use of specific combustor variables, such as primary zone temperature, flame temperature, combustor volume, and residence time in the chamber. Correlation-based methods can also be classified based on how the variables are incorporated into the mathematical formulations to derive $EINO_x$: direct methods involve the direct use of these variables, while ratio methods employ them in the form of dimensionless ratios between flight-level and sea-level conditions. These methods offer the advantage of a wide range of variables to investigate when generating mathematical formulations for estimating $EINO_x$, with some of these variables being easily estimable or readily available. Consequently, they are recognized as one of the most easily applicable types

of methods in conceptual design. On the downside, achieving an acceptable accuracy in estimations with these methods necessitates using a considerable number of variables. However, considering that each variable is subject to detection or estimation errors, this results in an accumulation of errors, which becomes more significant with an increasing number of variables considered. Furthermore, these methods are highly specialized for the specific engine and combustor under study, and thus cannot provide generalized formulations for different aircraft. At most, they can be adapted to suit specific cases.

4.3.2 The P3T3 method

The P3T3 method is the most used approach for estimating NO_x emission indices. This method directly stems from Correlation-Based Models, focusing on a limited range of parameters of interest, which include the inlet temperature and pressure to the combustor (P_3, T_3), and the Fuel-to-Air Ratio. These variables are included in the compact mathematical formulation provided below.

$$EINO_{X\,FL} = EINO_{X\,SL}\left(\frac{p_{3FL}}{p_{3sL}}\right)^{n}\left(\frac{FAR_{FL}}{FAR_{sL}}\right)^{m}\exp\,(H) \tag{4.2}$$

$$H = 19 * (h_{SL} - h_{FL}) \tag{4.3}$$

where H is the humidity factor introduced to account for the influence of humidity on NO_x formation in the combustion chamber: as this factor increases, the combustion temperature decreases, leading to a reduction in NO_x production. The H factor can be calculated based on the relative increase in specific humidity h $[kg_{H2O}/kg_{DryAir}]$ due to altitude gain. Although the inlet temperature to the combustor, T_3, is not explicitly included in the mathematical formulation, it implicitly influences the application of the method and represents the determining parameter. This is highlighted by the application procedure of the method reported in [31] and outlined below:

1. As a first step, it is necessary to have access to certain proprietary engine data provided directly by its manufacturer rather than estimated through propulsion modelling, corresponding to the four throttle conditions prescribed in the ICAO databank for the Landing Take-Off cycle (LTO). These data include pressure and temperature at the combustor inlet ($p_{3SL,}$ T_3) and FAR_{SL}, all evaluated under Sea Level conditions. Alongside these propulsion data, it is necessary to have access to $EINO_{xSL}$ emissions data, also obtainable from the ICAO Databank rather than estimated using dedicated software. The parameters p_{3SL}, FAR_{SL}, and $EINO_{xSL}$ must then be plotted as functions of T_3 and appropriately interpolated to obtain a good fit.
2. Once the fits in Sea Level conditions are generated, the next step is to derive the values of the same parameters under Flight Level conditions, namely p_{3FL}, T_{3FL}, and FAR_{FL}. Again, this information should be obtained directly from the engine manufacturer rather than through propulsion modelling.
3. Starting from the values of T_{3FL} obtained in step 2, it is possible to deduce the parameters $EINO_{xSL}$, p_{3SL}, and FAR_{SL} using the fits obtained in step 1. Once these parameters are known, as the P3T3 method operates as a ratio-method, ratios between FL and SL conditions need to be constructed, as they are included in the mathematical formulation of the method.
4. Finally, the mathematical formulation of the method mentioned earlier can be applied to evaluate the $EINO_{xFL}$ starting from the appropriately corrected $EINO_{xSL}$, taking into account the evolution ratio of p_3, FAR, and the humidity factor. The generalized formulation that provides the best results

across a broader range of engines involves exponential coefficients *m* and *n*, with *n=0.4* and *m=0*. However, this methodology allows for the possibility of using optimized coefficients for the specific case study to obtain more accurate results.

4.3.3 The BFFM2

As previously mentioned, the BFFM2 is the most commonly used Fuel Flow method in the literature, derived from the P3T3 method to create an NO_x estimation method capable of predicting these emissions solely based on non-proprietary parameters. In this case as well, the $EINO_{xFL}$ is derived from a correction of the $EINO_{xSL}$. However, for the BFFM2 method, this correction is performed based on the profiles of environmental conditions, the fuel flow profile W_f and the Humidity Factor H. Compared to the P3T3 method, the BFFM2 involves an additional intermediate fitting step concerning the fuel flow parameter. To derive this parameter under SL conditions from that under FL conditions, a mathematical formulation is provided which includes the Mach number. The fuel flow parameter is not directly included in the final mathematical formulation of the method used for evaluating $EINO_{xFL}$. However, it is the parameter based on which $EINO_{xSL}$ are plotted and interpolated, which are then used for environmental correction leading to $EINO_{xFL}$. The following steps described in [32] must be implemented for the application of the classic formulation of the BFFM2 method:

1. As a first step, it is necessary to derive the fuel flow values at sea level corresponding to the four throttle settings prescribed by the ICAO Databank for the Landing Take-off (LTO) cycle by applying the following correction to the fuel flow values in FL conditions obtained from the ICAO Databank or estimated from propulsion engine modelling.

$$w_{fSL} = w_{fFL} \frac{\theta_{amb}^{a}}{\delta_{amb}^{b}} \exp\left(c * M^2\right) \tag{4.4}$$

$$\theta_{amb} = T_{amb}[K]/288.15 \tag{4.5}$$

$$\delta_{amb} = p_{amb}[Pa]/101325 \tag{4.6}$$

   It is possible to use exponential coefficients specifically tailored for the engine under study, although the original formulation of the method prescribes the following values: *a=3.8, b=1, c=0.2*.

2. The $EINO_{xSL}$ values from the ICAO Databank or estimated using appropriate modelling software are then curve-fitted as a function of the corrected fuel flow in SL conditions obtained in the previous step, W_{fSL}. The original formulation of the BFFM2 method prescribes as a formality the plotting of these parameters on a log-log scale.

3. Given the value of W_{fFL}, it is possible to derive W_{fSL} using the correction mentioned in point 1. From there, $EINO_{xSL}$ can be obtained using interpolation from point 2. Finally, once $EINO_{xSL}$ is determined, it is possible to estimate $EINO_{xFL}$ using the following formulation:

$$EINO_{X\,FL} = EINO_{X\,SL} \left(\frac{\delta_{amb}^{d}}{\theta_{amb}^{e}}\right)^{f} \exp\left(H\right) \tag{4.7}$$

In this case as well, it is possible to use exponential coefficients specifically tailored for the engine under study, although the original formulation of the method prescribes the following values: *d=1.02, e=3.3, f=0.5*. H is the humidity factor introduced previously for the P3T3 method. It's worth noting that, despite the BFFM2 appearing at first glance as a direct method, it is actually a ratio method because the parameters delta δ and theta θ represent the ratios between environmental conditions at varying altitudes and those under SL conditions.

4.3.4 Simplified Physics-based Models

Simplified physics-based models are developed to outline the combustion process from a physical perspective. These models involve dividing the combustion chamber into distinct regions, each governed by various specific assumptions and characteristic species concentrations. The combustor is then modelled as a network of multiple ideal reactors, each appropriately simplified based on the governing assumptions of the respective region. This approach makes the simulation computationally less expensive compared to studying the combustor as a whole. Lately, physics-based reduced-order models have been predominantly used, especially for combustor conceptual design. These models employ a control volume approach, dividing the burner into finite volumes where similar flow phenomena occur. Within each volume, governing physical and chemical equations are iteratively solved, resulting in consistent outcomes with less reliance on combustor configuration compared to correlation-based models. Despite their higher demand for computational resources, they offer lower computational costs than CFD-based methods. Among these models, the Chemical Reactor Network (CRN) approach is prominent. In this approach, each control volume is represented by one or more chemical reactors, such as plug flow, perfectly stirred, and partially stirred reactors, which simulate the combustion process for a predetermined fuel-to-air ratio. While CRN models demonstrate lower accuracy compared to CFD-based methods, they strike a balance between computational efficiency and predictive capability [33]. Nevertheless, these models fall short of capturing the intricate kinetic pathways of pollutant formation, restricting their suitability for hydrogen-powered aeronautical applications.

4.3.5 High-fidelity Simulations

High-fidelity simulations represent the most accurate but computationally expensive approach for estimating emissions, requiring a detailed understanding of combustor geometry and NO_x formation kinetics. When referring to high-fidelity simulations, the use of Computational Fluid Dynamics (CFD) tools is envisaged for in-depth simulation of the combustion process. Among the most common high-fidelity simulation methodologies are Reynolds-Averaged Navier-Stokes (RANS) solutions, applicable only when combustor boundary conditions are known, Direct Numerical Simulations (DNS), known for their simulation efficiency yet computationally demanding for non-ideal configurations, and Large-Eddy Simulations (LES), which integrate small-scale turbulence modelling into combustion. While these techniques offer high accuracy, their computational costs make them impractical for emissions estimation during conceptual design. Given the high level of detail required in engine knowledge and the substantial computational cost, these techniques remain unsuitable for preliminary design stages. Therefore, 1D, 2D, or 3D CFD analyses are primarily employed for later design stages, typically occurring after the conceptual stage.

Chapter 5 - Updating Methods for NO_x Emissions Estimation

5.1 Methodology

In a landscape transitioning towards greener practices in the aerospace sector, with a growing focus on the climate impact of space access activities, the ability to estimate non-CO_2 emissions during the conceptual design phase of an aircraft is becoming increasingly important. Thus, this capability lays the groundwork for developing new strategies to reduce these emissions and mitigate their impact from the early stages of the project. In this thesis, a methodology is proposed to update the classical formulations of existing methods for estimating pollutants and greenhouse gas emissions for subsonic aircraft powered by traditional fuels. The aim is to develop new formulations applicable to aircraft powered by more sustainable fuels and operating at higher Mach numbers, which are compatible with space access missions. The methodology illustrated by the block diagram in Figure 5.1 aims to be general to enhance its applicability across a wide spectrum of flight regimes, mission profiles, and fuel types. This methodology is then specialized for estimating NO_x emissions from the SABRE hydrogen-powered case study in the second part of this section. The methodology involves an initial phase of designing or updating the propulsion modelling of the engine under study to generate a comprehensive and reliable propulsion database. The generation of this database serves as the foundation for the adaptation and improvement of emission estimation methods for the case study. These methods include the BFFM2 and P3T3 methods introduced in earlier chapters. Firstly, the propulsion modelling involves gathering data on the engine and the mission under study. Based on this data, a Matlab model of the thermodynamic evolution of the involved flows in thrust generation is constructed or updated. Finally, a validation of the performance analysis results is conducted. The propulsion modelling phase is particularly crucial as it provides inputs for the second modelling step outlined in the methodology, which is the emission modelling. In the second block of the workflow depicted in Figure 5.1, the methodology involves the kinetic chemical simulation of the mixing and combustion processes within the engine using the Cantera software. This software, whose capabilities are further explored in subsequent chapters, takes input from the engine propulsion database and outputs thermodynamic characteristics and mass fractions of species present in the combustion products. Starting from these mass fractions, it is possible to calculate the Emission Index, which forms the emissions database used as a reference for updating the selected estimation methods. Additionally, the use of Cantera for simulating mixing and combustion processes can be integrated into the Matlab-based propulsion modelling of the engine. This integration enhances the reliability of the results and strengthens cohesion in the approach adopted for formulating the two databases. Once the databases have been constructed to serve as a resource for applying the BFFM2 and P3T3 methods in their original and updated formulations, a series of parameters are selected. These parameters result from a correlation-based research investigating the correlations between chemical-propulsive variables and the formation of NO_x in the combustor. The selected parameters are considered particularly influential in shaping the emissions profile of the engine under study. The

parameters selected for updating the original formulations of the methods may vary depending on the fuel used by the engine, its operation, and potentially the mission phase under consideration. During the final phase of the workflow, these parameters are utilized to update the original formulations of the methods and adapt them to the case study. Finally, a comparison of the results of the new formulations of the emission estimation methods is conducted with those calculated using the chemical kinetic simulations of Cantera. The described methodology simplifies when an official database concerning the engine, particularly regarding its emissions, is already available. However, integrating Cantera appropriately into the Matlab-based propulsion modelling of the engine for simulating thermodynamic mixing and combustion processes enhances the reliability of the propulsive database. This integration also represents an initial step towards investigating the possibility of simultaneously formulating both propulsion and emission databases using a unified model of the engine in conceptual design. This possibility is not yet entirely feasible because the Matlab interface of Cantera only allows for the implementation of thermodynamic equilibrium simulations to be smoothly integrated into propulsion modelling. While the results from these simulations are useful for propulsion modelling purposes, they are not as reliable as those obtained from Cantera's kinetic chemical simulations, which are currently only implemented through the Cantera Python interface. Additionally, the Matlab interface of Cantera does not yet implement some useful functionalities for mixing modelling, which can only be implemented through the Cantera Python interface. Therefore, at the current state of the art, the two blocks concerning propulsion and emission modelling of the engine are connected but still separate in Figure 5.1.

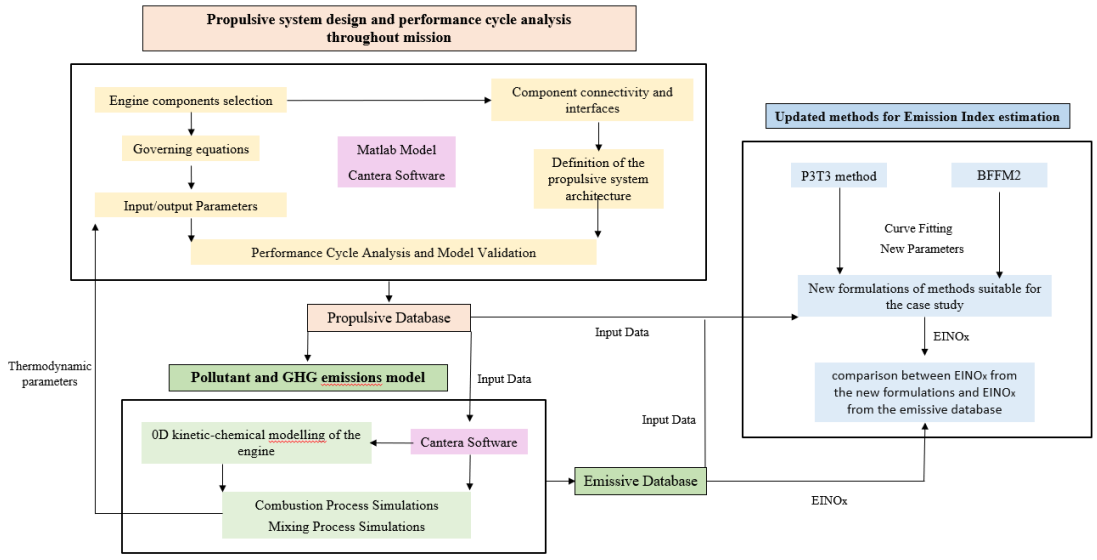

Figure 5.1 - Workflow for Updating Emission Estimation Methods in Conceptual Design

Regarding the application of the described methodology to the SABRE case study for estimating its NO_x emissions, it's useful to make some preliminary observations. For this purpose, the block diagram of the general methodology is specialized for the SABRE case study in Figure 5.2 concerning propulsion and emission modelling, and in Figure 5.3 regarding the actual method updates. Starting from the propulsion modelling, an existing Matlab-based propulsion model from the literature [27], developed by G. Grimaldi, is utilized as a reference to be updated. To this model, three main modifications are made to increase its accuracy: (i) the introduction of the regenerative thermodynamic cycle of helium, (ii) the simulation of thermodynamic equilibrium in the two combustion chambers using Cantera in Matlab, and (iii) the integration of results from the mixing processes modelling using Cantera in Python. Based on this updated

modelling, the propulsive database is constructed containing temperature and pressure data of the flows involved in combustion within the engine. These temperatures and pressures are then utilized for the kinetic chemical modelling of mixing and combustion processes of the SABRE using Cantera in Python, thus constructing the emissive database. Specifically, this database contains the mass fractions of chemical species in the inlet and outlet flows of the two combustion stages of the SABRE, along with the resulting NO_x Emission Indices, which are then used as references in the final phase of the work.

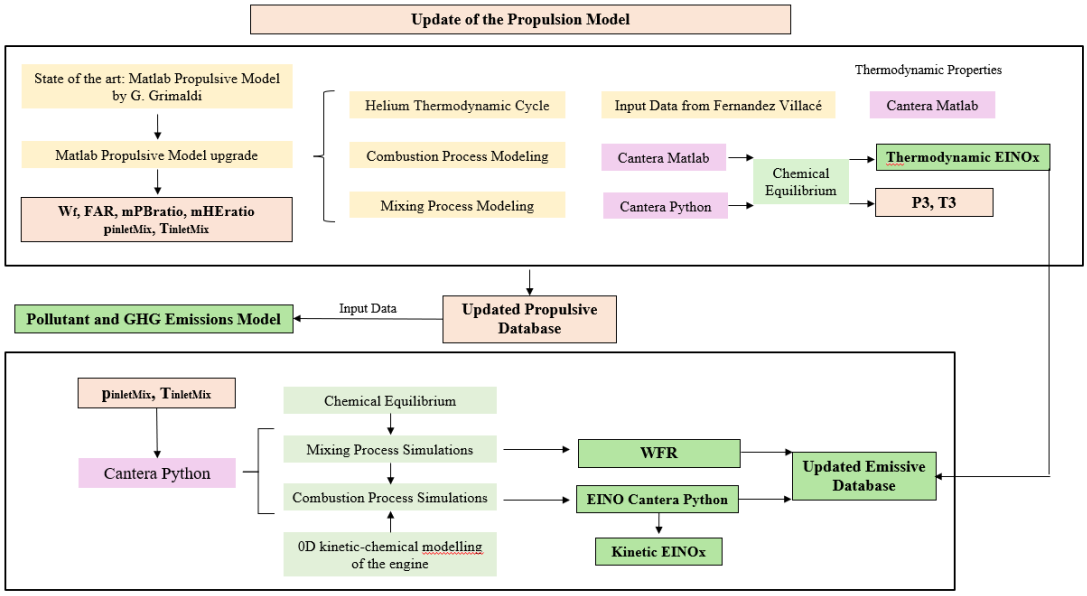

Figure 5.2 - Workflow for updating the propulsive and emissive databases

Once the two databases are updated, the next step involves selecting parameters to integrate into the classical formulations of the BFFM2 and P3T3 methods for their update and adaptation to the case study. During this phase, particular importance must be given to the unique propulsion configuration of the SABRE, along with the study of factors that chemically and thermally influence NO_x formation. In addition to introducing parameters intuitively associated with NO_x production by the engine, such as the Mach number or the fuel-to-air ratio (FAR), parameters specifically studied for the SABRE are introduced. Due to the two-stage combustion configuration, the parameter PBratio is introduced, defined as the ratio between the air flows sent to the PreBurner (PB) and to the main Combustion Chamber (CC) after the split downstream of the air compressor. Moving on to consider the hydrogen-air combustion proposed for the SABRE, the Water-to-Fuel Ratio (WFR) is selected as a parameter, representing the ratio between the flows of H_2O and H_2 entering the main CC, to account for the significant fraction of water resulting from combustion in the PB and the effect of its presence in the main CC on NO_x formation. Finally, since the SABRE is classified as a deeply precooled combined cycle engine, the HEratio parameter is introduced, defined as the ratio between the flows of helium and total air managed by the engine, to include the relevance of the helium cycle in the engine thermal management into the formulations. All these new parameters are variables along the mission profile of the SABRE and are integrated into the new formulations of the BFFM2 and P3T3 methods as ratios between the conditions at Flight Level (FL) and the conditions at Sea Level (SL), evaluated using Matlab fitting functionalities based on available data at sea level conditions, ensuring continuity with the approach proposed by the original formulations of the methods. The physical and chemical role of these new parameters in the NO_x formation process is explained in their respective dedicated sections, highlighting the reasons for their integration into the new

formulations. These ratios are integrated into the new formulations of the NO_x emissions estimation methods in various combinations and with different exponent coefficients. These coefficients are optimized for each formulation using the *lsqcurvefit* function in Matlab, with reference to the $EINO_x$ from the emissive database.

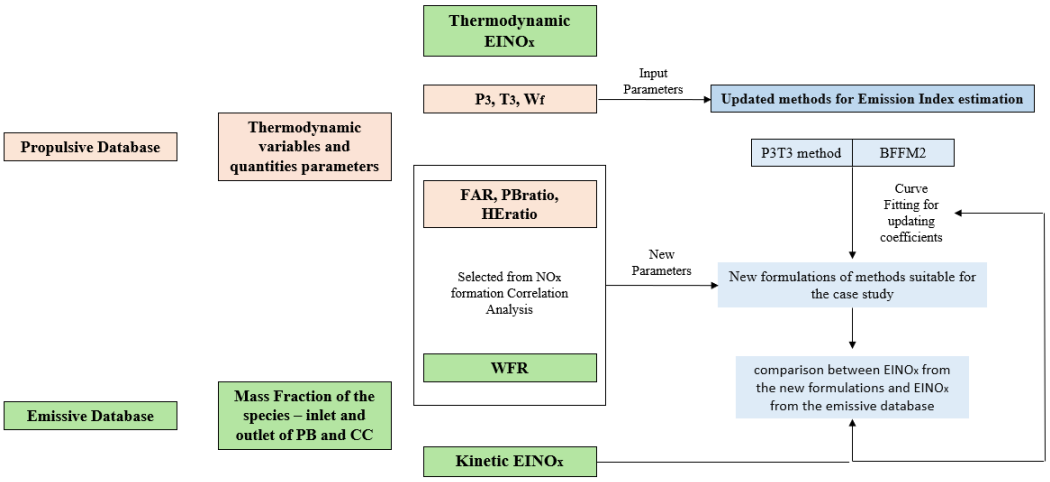

Figure 5.3 - Workflow for updating the P3T3 and FF original methods

The subsequent sections describe the workflow undertaken, detailing the propulsion model update process, the generation of the updated emissive database, and the analysis of correlations leading to the selection of parameters to be integrated as ratios in the new formulations. Finally, in Chapter 6, the new mathematical formulations of the methods are presented, incorporating the new parameters and numerically optimized coefficients calculated using Matlab fitting tools. The results of the newly formulated P3T3 and BFFM2 methods, adapted for estimating NO_x emissions in the context of SABRE H_2-Air combustion, are reported and discussed in Chapter 7. These results are compared with the $EINO_x$ derived from Cantera kinetic chemical simulations retrieved from the emissive database. Starting from the proposed comparison, absolute and relative errors of the results of the new formulations derived with reference to the $EINO_x$ of the emissive database are evaluated to assess their estimation accuracy. However, validation of the results is currently not possible due to the lack of an officially certified emissive database for the engine, which is still under study and therefore not yet tested. The application of the methodology to both the P3T3 method and the FF method is useful to verify its applicability regardless of the method chosen for adaptation.

5.2 Propulsive Database

The development of a comprehensive Propulsive Database, accurately representing the real-world functioning and performance of the studied engine, is crucial for achieving the most accurate estimation possible of its emissions during the conceptual design phase. The data from the Propulsive Database are used as inputs for the kinetic-chemical modelling of the engine, and consequently for the development of the Emissive Database. Concerning the SABRE, which features a two-stage combustion process, it is necessary to evaluate, through thermodynamic and propulsion modelling of the engine, the temperature and

pressure values of the flows entering the Mixers preceding the PreBurner and the main Combustion Chamber. These temperature and pressure data are used to evaluate the mass fractions of species present in the exhaust gases of the two combustion stages of the SABRE using dedicated software. In this work, the Cantera software is utilized due to its high reliability in solving problems involving chemical kinetics, thermodynamics, and transport processes. This open-source suite of tools is particularly well-suited for evaluating the thermodynamic properties of gases, as well as the mass fractions of combustion products. The mass fractions of gases exiting the PreBurner (PB) and the main Combustion Chamber (CC) of the SABRE, evaluated using Cantera, are then utilized to calculate the NO_x Emission Indices. These indices form the comprehensive Emissive Database of the engine, elaborated in Chapter 5.3 and subsequently discussed in detail in Chapter 7. The evaluated Emission Indices are used as a reference to update the emission estimation methods and to compare their results in order to probe the accuracy of their estimation. Regarding these new formulations, the role of propulsion modelling is twofold. Indeed, the data comprising the Propulsive Database not only serve as the basis for evaluating the Emission Indices used as references in the new formulations but also appear directly within them as dimensionless ratios. The data contained in the Propulsive Database are particularly relevant for the accuracy of this work. Therefore, the aim of this phase of work is to modify, update, and enhance the reliability of the results of the SABRE propulsion model available to the author. This conceptual design model was previously developed by G. Grimaldi and implemented in Matlab [27]. The new version of the model leaves unchanged much of the engine complete air cycle modelling developed by G. Grimaldi but introduces significant innovations regarding the modelling of the helium (He) auxiliary cycle, combustion processes modelling and mixing processes modelling. Additionally, the accuracy of evaluating thermodynamic quantities has been improved. At this stage of conceptual design, given the limited availability of proprietary data, a reverse engineering approach is employed to derive the trends as a function of Mach number of those thermodynamic and propulsive parameters concerning the helium and hydrogen flows that were considered constant in the original version of the model. For this purpose, the numerical results from the high-level modelling of the SABRE conducted by V. Fernández Villacé using the simulation framework EcosimPro [26] are utilized. To further increase the accuracy of the results, the Matlab interface of Cantera is employed to evaluate the intermediate thermodynamic properties of gases within each component, both for helium and hydrogen. Given the opportunity to leverage some functionalities of the Cantera software through its Matlab interface, the combustion processes in the PreBurner (PB) and the main Combustion Chamber (CC) are modelled using Cantera and directly integrated into the Matlab propulsion model, replacing the simplified combustion models previously proposed. Despite the cohesive structure of the final code, the Matlab interface of Cantera is not yet developed to the extent that it allows seamless integration of its functionalities into the Matlab propulsion model. In particular, the Matlab interface of Cantera currently does not allow simulation of mixing processes, which are therefore implemented using the Python interface of Cantera. The results of these Mixer modelling for the SABRE, in terms of mass fractions of species in the flows entering the PB and the CC, are subsequently integrated into the main Matlab model. Additionally, regarding combustion processes, simulations conducted by Cantera via Matlab are thermodynamic in nature, rather than chemical kinetic. Therefore, these simulations are not reliable for evaluating mass fractions of species in the combustion exhaust gases but remain reliable for estimating pressures and temperatures at the end of the process. In this case as well, the Python interface of Cantera is utilized for more reliable kinetic-chemical combustion simulations that yield the mass fractions upon which the Emissive Database of the SABRE is built. Indeed, the current Matlab model does not facilitate the simultaneous formulation of the Emissive and Propulsive Databases. Nonetheless, it serves as an illustration of the mutual influence of one of the databases on the process that led to deriving the data of the other, and vice versa.

5.2.1 Advancements in SABRE Propulsive Modelling

As anticipated in the previous sections, an updated version of an existing Matlab propulsion model is used for formulating the SABRE Propulsive Database. Various modifications are made to the reference model to increase its reliability in replicating the actual engine operation in the conceptual design phase. The update of the propulsive model involves some minor modifications, such as the introduction of the ISA standard for air properties and some improvements regarding the modelling of the thermodynamic evolution of the H_2 fuel. However, the areas that require more focus for intervention are threefold: (i) modelling of the regenerative cycle of helium, (ii) refinement of the modelling of combustion processes, and (iii) refinement of the modelling of mixing processes. Regarding the modelling of the helium cycle, it is made possible by using the Matlab interface of the Cantera software, which allows for the evaluation of the specific heats and adiabatic expansion coefficients of the gas for each intermediate temperature and pressure condition within each component. This differs from what was done in the previous model version, where these values were considered constant and fixed at their mean value within the cycles. Data regarding the helium flow rate and its inlet pressure profile to the HeT turbine are obtained from [26]. These parameters are fundamental inputs for the cycle modelling. Furthermore, the Cantera software is utilized in the context of propulsion modelling for simulating the mixing processes and the two combustion stages of the SABRE. Additionally, the capabilities of Cantera are leveraged for the thermodynamic modelling of hydrogen, similar to what is done for helium. Moreover, concerning the hydrogen flow, starting from the power outputs from the SABRE modelling by V. Fernández Villacé, the compression ratio of the hydrogen turbopump LHTP is recalculated. This parameter, which was also considered constant in the previous version of the model, is now being reevaluated. The combination of all these modifications results in relative errors in the assessment of SABRE performance compared to those provided by Reaction Engine Limited which are absolute values below 20%. Despite this result not deviating much from the ones of the previous version of the propulsion model, the results in terms of pressures and temperatures are much more compatible with those reported in the study by V. Fernández Villacé. In this study [26], the SABRE was modelled using the EcosimPro simulation framework. It is reasonable to consider the results of this high-level study more reliable than those of the original Matlab model, and thus it can be concluded that the temperature and pressure outputs of the updated Matlab model are also more realistic. The following sections provide a description of the three main updates made in the new version of the model, also mentioning the modifications made in the modelling of hydrogen within the section dedicated to the modelling of the helium cycle, due to the significant similarities that exist. The modelling of most of the components involved in the complete air cycle remains unchanged from G. Grimaldi's model and is therefore not further elaborated here, but the reader is referred to reference [27]. The fundamental assumptions underlying this modelling are two, and they are the same as those of the previous version: the fraction of incoming air destined for the ramjet burners is assumed to be identically zero throughout the mission profile, and the intake is assumed to perform with nominal pressure recovery while matching the mass flow demanded by the air compressor.

5.2.2 Helium Thermodynamic Cycles and Hydrogen Thermodynamic Evolution

The helium cycle is a closed auxiliary cycle that allows for the regeneration of part of the energy contained in the incoming air flow at the intake through the precooler and part of the energy produced during combustion in the preburner via the heat exchanger HX3. This energy is regenerated by heating the cold hydrogen stream at the heat exchanger HX4 and by powering the air compressor. This cycle plays a fundamental role in managing the thermal and power flows of the SABRE. The hydrogen cycle is closely

connected to that of helium, as the hydrogen turbine HT2 is mechanically linked to the helium compressor HeC. Additionally, the temperature of the hydrogen entering the preburner (PB) is determined by the hydrogen-helium heat exchanger HX4. Given the limited availability of proprietary data related to the helium and hydrogen cycles, the present work relies on existing literature to obtain the necessary input data. Similarly to how it was done for the propulsion model [27], the data from the high-level simulation of the SABRE conducted by V. Fernández Villacé using EcosimPro are also employed for modelling the helium and hydrogen cycles. EcosimPro is a top-tier simulation tool for modelling continuous-discrete systems, so it is believed that this modelling is of excellent quality and is therefore a good representation of the engine's real operation.

Regarding the helium cycle, its variable flow profile and the inlet pressure profile to the HeT turbine, shown in Figure 5.4, are derived from [26] and used as inputs for the cycle modelling. The inlet temperature to the HeT turbine is considered constant and set at 1000K. The temperature of the helium exiting from heat exchanger HX4 is considered constant throughout the air-breathing phase of the engine and is fixed at 50 K, in line with [26].

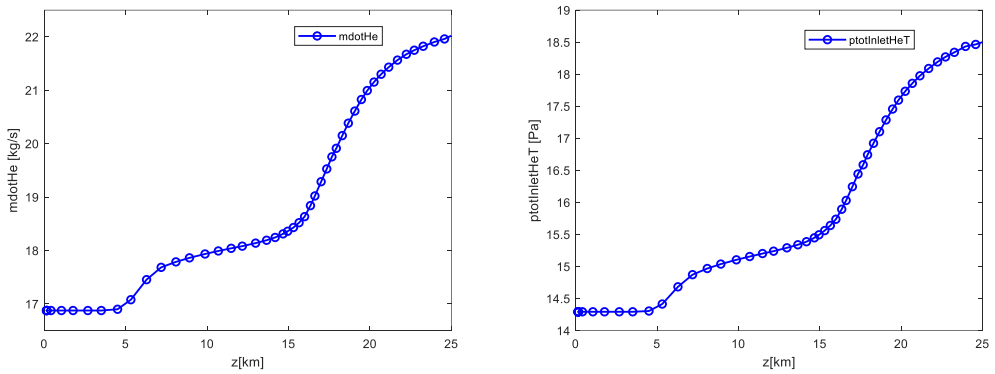

Figure 5.4 - Helium mass flow and HeT inlet pressure over altitude [26]

Additionally, the output of the modelling [26], in terms of power of the hydrogen turbopump LHTP, is used to recalculate the compression ratio of the turbopump as a function of flight Mach. Figures 5.5 illustrate the power of the hydrogen turbopump LHTP reported in [26] and the trend of compression ratio recalculated using the same balance equation that is subsequently reused multiple times for modelling the two cycles.

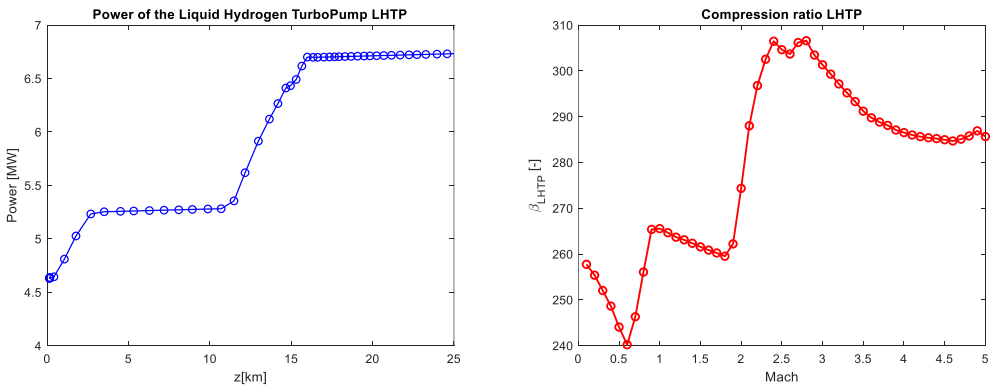

Figure 5.5 - Power of the Liquid Hydrogen TurboPump LHTP [26] and recalculated LHTP compression ratio

Using these new input data, it is possible to model the cycles of helium and hydrogen with the relationships and balance equations provided below, integrating these two cycles into the original model [27]. The relationships used are the same as those employed by G. Grimaldi in his preliminary modelling of the two cycles. However, besides eliminating the assumptions of constant helium flow rate and compression ratio of LHTP, the updated model examines the evolution of helium and hydrogen flows within each component and recalculates the outlet parameters based on average thermodynamic characteristics (i.e., average specific heats and average adiabatic expansion coefficients). The chemical models *Kéromnès* and *z24_nox20* are utilized through the Cantera Matlab interface to assess the thermodynamic properties of helium and hydrogen at each intermediate pressure and temperature condition within the components involved in their respective cycles.

Resuming the numbering of the stations as indicated in Figure 4.1:

Helium Turbine 21-22

The inlet temperature of the helium turbine is considered constant for each Mach and altitude condition, set equal to its design value of 1000K. The following equations can be used to model the helium turbine, considering an efficiency η_{HeT} of 0.8 as done by Moino [28]. The outlet temperature, the turbine pressure ratio, and consequently the outlet pressure are calculated based on the power extracted from the turbine, equal to the power required by the air compressor calculated as in [27].

$$W_{HeT} = -W_{AC} \tag{5.1}$$

$$T°_{22} = T°_{21} + \frac{W_{HeT}}{c_{pHeTmean} * \dot{m}_{He}} \tag{5.2}$$

$$\beta_{Het} = \left(\frac{1}{\eta_{HeT}}\left(\frac{T°_{22}}{T°_{21}} - 1\right) + 1\right)^{\frac{-\gamma_{HeTmean}}{\gamma_{HeTmean}-1}} \tag{5.3}$$

$$p°_{22} = \frac{p°_{21}}{\beta_{Het}} \tag{5.4}$$

Heat exchanger HX4 22-18

In this heat exchanger, the hot helium flow from the turbine heats the cold hydrogen flow from the turbo pump. The engine heat exchangers can be considered isobaric components, so the pressure of the helium flow is assumed constant in each of them. The temperature of the helium exiting from heat exchanger HX4 is considered constant throughout the air-breathing phase of the engine and is fixed at 50 K, in line with [27]. This temperature is used as an input for the complete propulsion model of the engine to recalculate the heat exchanged at the HX4 under the average conditions of the helium flow between inlet and outlet to the exchanger according to the following balance equation.

$$\dot{Q}_{HX4} = c_{pHeHX4mean} * \dot{m}_{He} * (T°_{18} - T°_{22}) \tag{5.5}$$

$$p°_{18} = p°_{22} \tag{5.6}$$

Helium Compressor HeC 18-19

Considering the pressure of the helium flow constant through each heat exchanger within the cycle, the compression ratio of the helium compressor is set equal to that of the only other component of the cycle that modifies the gas pressure, namely the helium turbine HeT. This ensures the consistency of pressures within the cycle. Consequently, the outlet pressure and temperature from the helium compressor are derived using the following relationships, considering an efficiency η_{HeC} of 0.8 as done by Moino [28]:

$$\beta_{HeC} = \beta_{HeT} \tag{5.7}$$

$$T°_{19} = \left(1 + \frac{1}{\eta_{HeC}}\left(\beta_{HeC}^{\frac{\gamma_{HeCmean}-1}{\gamma_{HeCmean}}} - 1\right)\right) \tag{5.8}$$

$$p°_{19} = p°_{18} * \beta_{HeC} \tag{5.9}$$

Precooler 19-20

Upon reaching the precooler, the cold helium flow is heated by the hot air flow exiting the intake. The heat exchanged at the precooler is calculated by G. Grimaldi assuming a constant temperature of the air exiting the precooler, set at 97K. The pressure is assumed to be constant inside the precooler, as well as in the other heat exchangers.

$$T°_{20} = T°_{19} + \frac{\dot{Q}_{PC}}{c_{pHePCmean} * \dot{m}_{He}} \tag{5.10}$$

$$p°_{18} = p°_{22} \tag{5.11}$$

Heat Exchanger HX3 20-21

Through this heat exchanger, which marks the closure of the cycle, the helium regenerates a portion of the heat produced in the preburner during the first stage of the SABRE combustion. Similarly to the other exchangers, to model HX3 the thermal balance equation can be used, and the condition of constant pressure was imposed. Recalling that the inlet temperature to the HeT turbine is constant and set at 1000K for every flight condition, it is possible to calculate the heat exchanged at the heat exchanger.

$$\dot{Q}_{HX3} = c_{pHeHX4mean} * \dot{m}_{He} * (T°_{21} - T°_{20}) \tag{5.12}$$

$$p^{\circ}_{21} = p^{\circ}_{22} \tag{5.13}$$

For the evaluation of the thermodynamic properties of helium under its intermediate conditions within each component, the *Keromnes* chemical model is utilized. This model, named after its creator, provided the necessary information when appropriately called within the code using the Matlab interface of the Cantera software. The Matlab code for evaluating the specific heats and the adiabatic expansion coefficient of helium as functions of its temperature and pressure using the Cantera Software is reported below.

```
helium= Solution('keromnes.yaml');
set(helium,'T',Ttot(i),'P',ptot(i),'Y','He:1');
cp_he(i)=cp_mass(helium);
cv_he(i)=cv_mass(helium);
gamma_he(i)=cp_he(i)/cv_he(i);
```

Figure 5.6 - Utilization of the Keromnes chemical model via the Cantera Matlab interface for evaluating the properties of helium

Regarding the modelling of the evolution of the hydrogen flow inside the engine, the equations used are the same as those presented for helium components modelling and therefore are not repeated here. Similarly to helium, for hydrogen, the Matlab interface of the Cantera software is used for evaluating the thermodynamic properties under intermediate conditions within each component. The chemical model utilized is the *z24_nox20*, which is the same chemical model used for generating the emission database and specialized for evaluating the NO_x produced from the combustion between air and hydrogen. An example of using this chemical model to evaluate the thermodynamic characteristics of hydrogen via Cantera through Matlab is shown in the following figure.

```
gasH2= Solution('z24_nox.yaml');
set(gasH2,'T',Ttot(i),'P',ptot(i),'Y','H2:1');
cp_H2(i)=cp_mass(gasH2);
cv_H2(i)=cp_mass(gasH2);
gamma_H2(i)=cp_H2(i)/cv_H2(i);
```

Figure 5.7 - Utilization of the z24_nox20 chemical model via the Cantera Matlab interface for evaluating the properties of hydrogen

5.2.3 Combustion Process Simulation using Cantera Software

The second area addressed in the upgrade of the propulsion modelling of the SABRE engine directly pertained to the combustion process. The initial model involved a combustion modelling based on simple equilibrium and balance equations in the combustion chamber under stoichiometric, isobaric or isochoric conditions, respectively for the preburner (PB) and the main combustion chamber (CC). This type of modelling has been replaced by a simulation of the combustion process until reaching chemical equilibrium conditions using the dedicated software Cantera. Cantera is an open-source suite specifically used for 0D/1D kinetic-chemical modelling. The capabilities of this software are further explored in the chapter

dedicated to the formulation of the emissive database. The Python interface of Cantera allows launching time-dependent simulations through which it's possible to study the kinetic-chemical evolution of gases in the combustion chamber, modelled as a batch reactor under isochoric conditions in the case of the main combustion chamber. For propulsion modelling purposes, the Cantera software is directly integrated into the engine model using its Matlab interface, which has limited functionality compared to the Python interface but is still functional for the purposes of this work. Within the Matlab model, Cantera is specifically utilized for assessing the chemical equilibrium conditions during combustion, employing the "*equilibrate*" command. Input data include the pressure and temperature of the inflow into the chamber, along with its composition expressed in terms of mass fraction of species present in the mixture. The Cantera Matlab interface allows for retrieving flow characteristics upon reaching chemical equilibrium. Among these outputs are equilibrium pressure and flame temperature, specific heats, mass fractions of species in the exhaust gases, their average molecular weight, and density. The following Matlab code implements the resolution of chemical equilibrium within the main combustion chamber.

```
MAINCCinletgas=Solution('z24_nox.yaml');
 set(MAINCCinletgas,'T',Ttot_inlet(1),'P',ptot_inlet(1),'Y', ['H2:0.0542792512856512'
                                                             'O2:0.1071870708706257'
                                                             'H2O:0.120731910055463'
                                                             'N2:0.7178017668148612'
                                                             'NO:0.0000000009733969']);

 equilibrate(MAINCCinletgas,'UV');
 Ttot_outlet(1) = temperature(MAINCCinletgas);
 ptot_outlet(1) = pressure(MAINCCinletgas);
 cp_gas_outlet(1)=cp_mass(MAINCCinletgas);
 cv_gas_outlet(1)=cv_mass(MAINCCinletgas);
 gamma_gas_outlet(1)=cp_gas_11/cv_gas_11;
 MM_outlet(1)=meanMolecularWeight(MAINCCinletgas);
 rho_outlet(1)=density(MAINCCinletgas);
YH2_outletMAINCC(1)=massFraction(MAINCCinletgas,'H2');
YH2O_outletMAINCC(1)=massFraction(MAINCCinletgas, 'H2O');
YN2_outletMAINCC(1)=massFraction(MAINCCinletgas,'N2');
YNO_outletMAINCC(1)=massFraction(MAINCCinletgas,'NO');
```

Figure 5.8 - Chemical equilibrium in the main CC via the Cantera Matlab Interface

The "*equilibrate*" command requires specifying the combustion conditions for which the chemical equilibrium is being calculated. For the main combustion chamber, a process with constant internal energy (U) and specific volume (V) is considered, thus 'UV' is chosen to represent an isochoric process. Meanwhile, for the preburner, a process with constant enthalpy (H) and pressure (P) is considered, hence 'HP' is used to represent an isobaric process. The "*equilibrate*" command calls the Cantera chemical equilibrium solver for single-phase solutions, known as "*ChemEquil*", as the first attempt to calculate chemical equilibrium. This solver utilizes an element potential method, which is one of a class of equivalent nonstoichiometric methods. This method introduces the fundamental concept of element potential, which is the chemical potential of the elemental species per atom. This parameter is defined such that one element potential exists for each independent atom in the system. The method of element potentials relates the mole fractions of each chemical species to quantities called element potentials, and it utilizes a damped Newton method to solve a number of nonlinear algebraic equations equal to the number of element potentials present in the mixture [34]. The equations that the method solves are derived from the classical equations for minimizing Gibbs free energy but are specialized for element potentials. The advantage of nonstoichiometric methods is to solve a significantly smaller number of nonlinear algebraic equations compared to stoichiometric methods. In the case of stoichiometric methods, such as Gibbs minimization, this number is equal to the number of species present in the mixture to be chemically equilibrated. The

specialized boundary conditions for the chemical equilibrium using the chemical potential method can be summarized in the following form:

$$\mu_k = \sum_m \lambda_m * a_{km} \qquad (5.14)$$

where μ_k is the chemical potential of species k, a_{km} is the number of atoms of element m in species k, and λ_m is the chemical potential of the elemental species per atom. When the condition of chemical equilibrium is reached, the chemical potential of each species is thus the linear sum of contributions from all its atoms. The non-stoichiometric methods like the element potential method assert that every intermediate state is a valid chemical equilibrium state but does not necessarily satisfy the element constraints. These methods are faster when they converge, however, they are not as robust as stoichiometric ones. For this reason, in case of instability and consequent non-convergence of the element potential method, Cantera automatically provides the option to replace the non-stoichiometric solver "*ChemEquil*" with the stoichiometric solver "*VCS*," designed to set a mixture containing one or more phases to a state of chemical equilibrium. The Villars-Cruise-Smith (VCS) algorithm, developed by Smith and Missen and detailed in "Chemical Reaction Equilibrium Analysis: Theory and Algorithms" is utilized. Since this method is stoichiometric, each intermediate state evaluated satisfies the element constraints but may not be a state of chemical equilibrium. The VCS algorithm has a higher computational cost compared to the element potentials but offers greater reliability [35].

The approach proposed here, which involves modelling combustion processes by calculating chemical equilibrium in the combustion chamber, results in mass fractions that differ significantly from those obtained from 0-D time-dependent kinetic chemical simulations conducted in the context of the emissive database formulation. Since the kinetic-chemical simulations carried out via Cantera Python are more reliable than the calculation of chemical equilibrium alone via Cantera Matlab, the mass fractions evaluated using the procedure described in this section are considered invalid. However, for propulsion purposes, the modelling described is considered acceptable and more accurate than the one presented previously in [27]. In the case of combustion in the preburner, no correction is provided for the chemical equilibrium temperature calculated by the Cantera solver at chemical equilibrium. This is because this stage of combustion has not yet been studied from a chemical kinetics standpoint, and thus, there is no more realistic comparison target data available. In the case of the main combustion chamber, however, it is necessary to consider that the temperature derived at the chemical equilibrium condition will be overestimated compared to the actual temperature of the exhaust gases from the combustor. This overestimation arises from the difference between the time required to reach chemical equilibrium and the actual residence time of the gases in the chamber. This overestimation of the gas temperature at the combustor outlet results in an unacceptable overestimation of the engine performance. Therefore, it is necessary to correct this temperature using a correction factor. This correction factor is closely related to the difference between the timescale of chemical equilibrium and the timescale of the effective time that gases spend in the chamber. Both the timing of chemical equilibrium, being an ideal condition, and the residence time in the chamber, not having the volume of the chamber available, are indefinite. Assuming that the residence time in the chamber is greater than the ignition delay time but not excessively large to avoid excessive emissions, it is possible to estimate this corrective factor from the time histories generated by the 0D kinetic-chemical simulations of the Cantera software. The corrective parameter is set equal to the ratio between the estimated residence time in the chamber, assumed to be twice the ignition delay time, and the delay time for reaching chemical equilibrium in the chamber, assumed to be the instant when the temperature profile reaches a plateau in the chamber. This results in a correction factor to be applied to the combustor exit temperature, in terms of a time scale ratio averaged over Mach number variations, equal to 0.71.

5.2.4 Mixing Process Simulation using Cantera Software

The third and final intervention made to the reference model involved updating the modelling of the mixing processes preceding the preburner and the main combustion chamber. The formulation of the SABRE emission database, as illustrated in Chapter 5.3, also includes modelling the mixing processes alongside the kinetic-chemical simulation of combustion processes. Considering the Cantera software capabilities in calculating the mixed states properties, it is decided to integrate the results of this mixing modelling into the original Matlab propulsion model [27] to enhance its accuracy. Therefore, the mixing modelling through Cantera is explained in this section and is not repeated later in the emission modelling chapter. Firstly, it's essential to highlight the difference between what's described for the combustion processes modelling in Chapter 5.2.3 and the chosen modelling approach for the mixers. Cantera allows evaluating chemical equilibrium in the combustion chamber using its Matlab interface but doesn't enable modelling mixing processes through the same interface. Therefore, to address mixing, it is necessary to utilize the Cantera Python interface and then integrate the outcomes of this modelling into the Matlab model. Instead of using the command "*equilibrate*" to calculate the chemical equilibrium of the mixture in the mixers, as used for assessing the chemical equilibrium in the combustion chamber, the modelling of the mixing processes involves the use of another Cantera command that is currently not implemented in its Matlab interface. This command, the "*quantity*" command, allows assigning a parameter to the two streams entering the mixer that identifies their quantity, particularly the molar flow rate. Quantifying the streams that are mixed in the mixer is crucial for evaluating the properties of the mixed state. In contrast, it is not necessary to quantify the single flow of mixed gases that undergo combustion to evaluate the chemical equilibrium of the combustion mixture. The input parameters for the scripts shown in Figure 5.9, which evaluate the mixed state, are almost the same as those used for evaluating the chemical equilibrium in the combustion chamber. Among these parameters are the values of temperature, pressure, and composition in terms of mass fractions of the two incoming streams, to which the two molar flow rates are added in this case. The molar flow rate [mol/s] is easily calculated from the mass flow rate of the considered stream by dividing it by its average molecular weight.

```
gas = ct.Solution('z24_nox.yaml')
Air = ct.Quantity(gas)
T_air=542.614
p_air=12349914.98
Air.TPY = T_air, p_air, 'O2:0.23 N2:0.77'
Air.moles = 1339.38718

PBexhaust = ct.Quantity(gas)
T_PBexhaust=1187.139670
p_PBexhaust=11733289.7
PBexhaust.TPY = 1187.139670, 11733289.7, 'H2:0.101652328465957 H20:0.226102598812458 N2:0.672244463414168'
PBexhaust.moles = 3849.21868

M = A + F
print(M.TPY)
```

Figure 5.9 - Chemical equilibrium of the mixed state via the Cantera Python Interface

Due to the relatively low temperature of the two streams arriving at the mixers, no combustion reactions occur at these components. The Cantera software utilizes the molar flow rates provided as input for the two streams in the mass balance used to evaluate the mass fractions of the mixed state. Cantera allows retrieving as output all the thermodynamic parameters of the mixed state under chemical equilibrium conditions. In

particular, for the continuation of the propulsion modelling, parameters such as the temperature and pressure of the gases exiting the mixers, their specific heats and adiabatic exchange coefficient, the average molar mass, density, and mass fractions of the mixed species are stored and subsequently integrated into the Matlab propulsion model.

5.2.5 Propulsive Performances of the updated Propulsive Model

After implementing the described updates to the reference propulsion model [27], it is possible to evaluate the engine performance in terms of gross thrust, uninstalled thrust, specific thrust, and specific impulse. These four parameters resulting from the performance analysis are plotted below and compared with the values for the SABRE published by the manufacturer REL. The relative errors of these four parameters evaluated with respect to the official SABRE data are also reported.

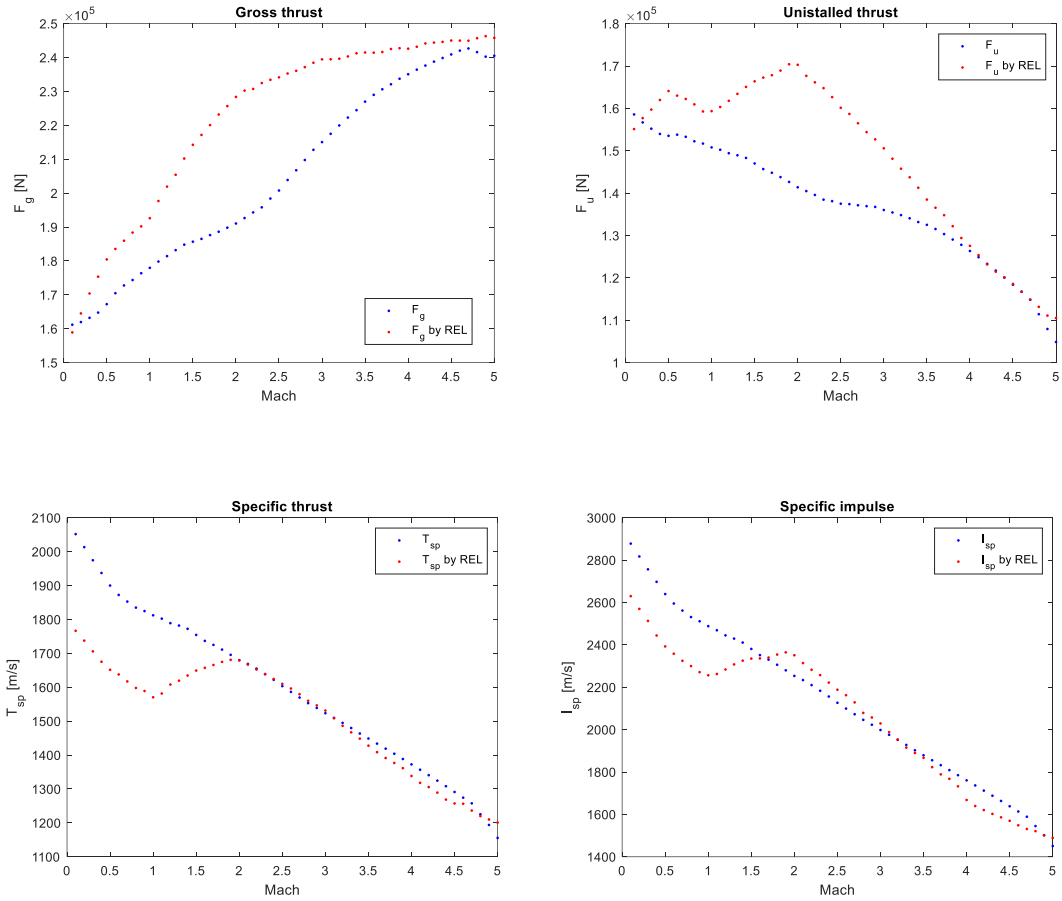

Figure 5.10 - Propulsive Performances of the updated Propulsive Model

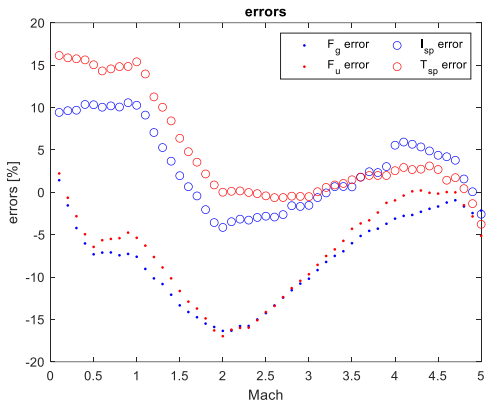

Figure 5.11 Performances relative errors of the updated Propulsive Model

As can be seen from the trends above, the relative errors resulting from the performance analysis generally remain below 20%. This result is considered acceptable in a conceptual design phase. Specifically, the maximum error for gross thrust and net thrust is around 16% negative. Additionally, the maximum error for specific impulse and thrust also lies around 16% positive. However, errors around 15% for all four parameters are observed within a restricted Mach range compared to the entire speed regime analysed. Specifically, for gross and uninstalled thrusts, errors are below 10% outside the Mach 1.5-3 range, where the largest deviation from the REL trends occurs. On the other hand, for specific thrust and specific impulse, errors are below 5% if the first phase of the mission from zero to Mach 1 is exclude. The main advantage of this model is its capacity to provide insight into the helium and hydrogen cycles, thus allowing for a more comprehensive understanding of the engine operation. Furthermore, modelling the mixing and combustion processes using dedicated software, i.e., Cantera, enhances the sophistication of the propulsion model overall. Finally, the definitive version of the current propulsion model, integrating the Cantera kinetic-chemical modelling software internally, stands as a model that aims to operate a combined formulation of both propulsion and emission databases within the proposed methodology. Unfortunately, due to the limited functionality of the Cantera Matlab interface, this combined formulation is not yet possible. Indeed, the NO_x mass fractions resulting via Cantera Matlab chemical equilibrium are not reliable compared to those derived from more plausible 0D time-dependent kinetic-chemical simulations implemented via Cantera Python in the context of the emission modelling discussed in Chapter 5.3. Upon completing the validation of the performance analysis results of the current propulsion model, all necessary parameters for formulating the emission database and updating NO_x emission estimation methods have been gathered. These parameters will be invoked as needed subsequently and are thus not detailed in this chapter.

In order to quantitatively demonstrate the effect of the modifications made, in Figure 5.12 are reported the recalculated trends of temperatures and pressures at the inlet to the two combustion stages of the SABRE, compared with the trends resulting from the original modelling [27].

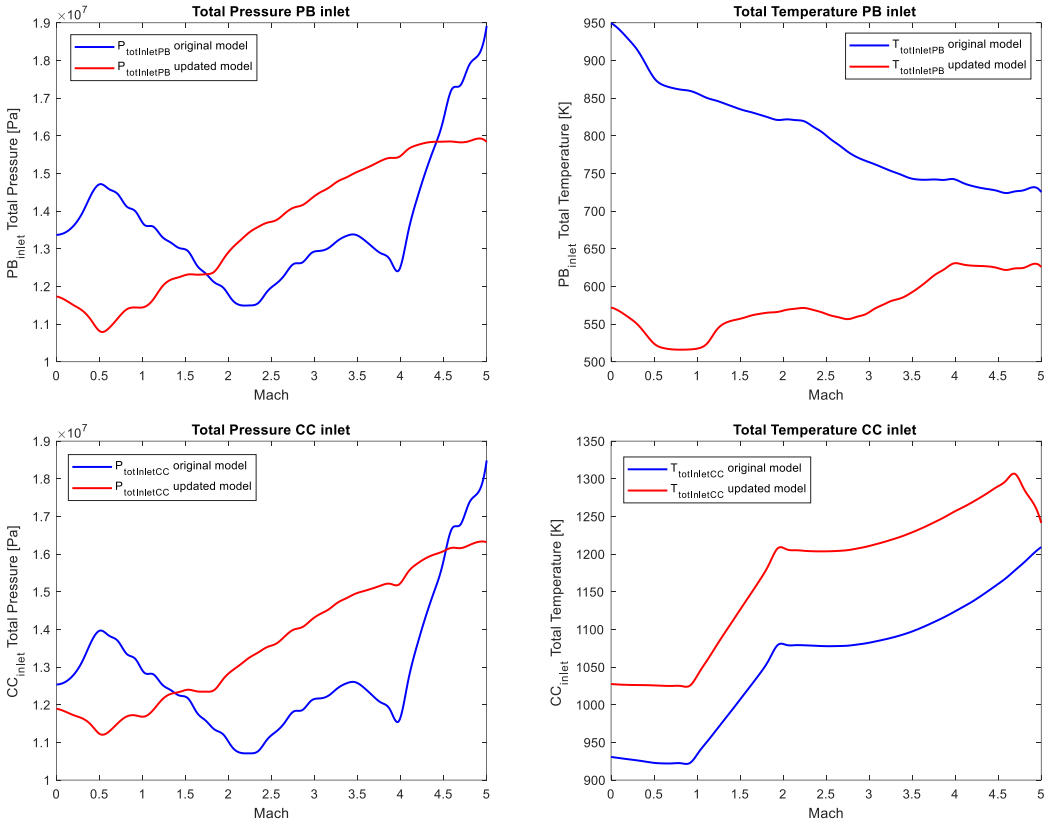

Figure 5.12 - Pressure and Temperature at the inlet of the PB and the CC, comparison between original and updated model

5.3 Emissive Database

The emissive database is expanded by considering 50 equispaced Mach conditions between 0.1 and 5 and updated with the recalculated pressure and temperature inputs resulting from the new propulsion modelling. Indeed, the chemical-emissive modelling of the engine is conducted simultaneously with the propulsion modelling. The mixing processes are modelled via Cantera under the Python interface, and the pressures and temperatures of the mixed states entering the two combustion stages are integrated into the propulsion model. The modelling of the mixing processes is based on quantitative inputs, such as molar fractions, as well as thermodynamic variables, such as pressures and temperatures. This type of modelling is only possible through the Python interface of Cantera, as it requires associating quantitative properties with mixing flows. For the study of mixing and combustion processes, the kinetic mechanism i.e., the *z24_nox20* developed by the Swedish Defence Research Agency FOI modelling group is utilized, as done in [29]. This mechanism is specialized for evaluating NO_x emissions resulting from hydrogen-air combustion. As for the kinetic-chemical modelling of combustion processes, it remains unchanged from what was reported in [29]. In particular, combustion in the preburner is associated with reaching chemical equilibrium under isobaric conditions, and therefore, its results can be derived from modelling through Cantera under the Matlab interface described in the previous section. Regarding the main combustion chamber (CC), both the chemical equilibrium of the mixed gases and their time-dependent kinetic-chemical evolution within ideal constant volume reactors are simulated. The result of the kinetic modelling of the main CC is a time history that captures the chemical and thermodynamic evolution of the mixture during combustion. Starting from

the temporal evolution profiles of mass fractions of species present in the combustion chamber resulting from kinetic simulations, kinetic EINO can be evaluated. The kinetic EINO are evaluated at the end time of the simulation, set at 2 seconds. It is believed that kinetic EINO represents the real evolution of gases within the combustor, unlike those evaluated under the ideal condition of chemical equilibrium. For this reason, these kinetic EINO are considered more reliable than thermodynamic EINO, which are determined under conditions of chemical-thermodynamic equilibrium. Both sets of EINO are reported in Chapter 7, along with a discussion regarding their reliability, similarities, and differences. Ultimately, kinetic EINO are assumed as reference EINO for updating the fuel flow method for NO_x estimation. Please note that for SABRE, and more generally for hydrogen-air combustion, only the mass fraction of NO produced during combustion is useful for estimating the engine $EINO_x$, as it is several orders of magnitude higher than the other NO_x compounds.

A comparison between EINO from the original [29] and the updated emissive database is shown in Figure 5.13. For a numerical comparison between the two sets of EINO, please refer to Chapter 7.1.

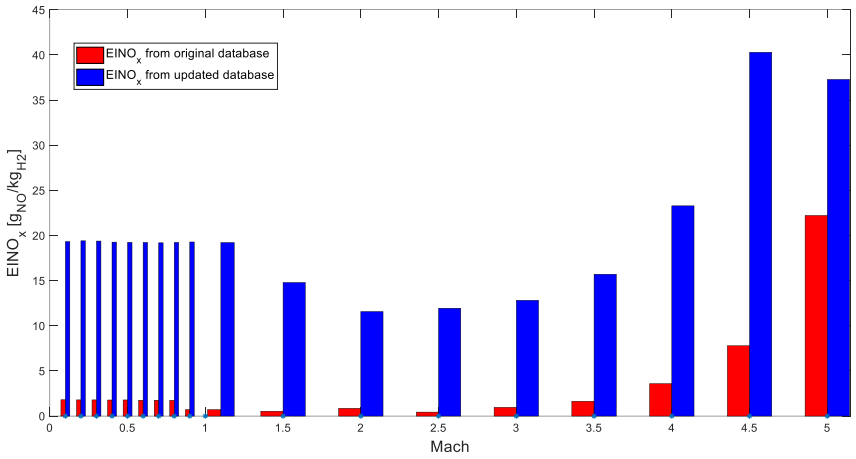

Figure 5.13 - Comparison between EINO from the original [29] and updated emissive databases

5.4 Chemical-Physical Discussion and Correlation Analysis of EINO Trends

In the absence of a certified standard reference for the $EINO_x$ produced by the SABRE engine, to update the emissive database with recalculated EINO, it is necessary to ensure that the trend evaluated as a function of Mach is supported by chemical-physical justification. This involves an analysis of the correlations between the recalculated EINO trend and the chemical-propulsive parameters of the engine that generates it. The correlation analysis phase is important not only to certify the physical-chemical coherence of the results obtained from emissive modelling but also to identify tailored parameters specific to the SABRE engine for updating the original formulations of NO_x emissions estimation methods. Firstly, it is necessary to verify that the trend evaluated for EINO as a function of Mach corresponds to that of the temperature reached during combustion evaluated as a function of Mach. It is well known that the temperature and pressure conditions reached in the combustion chamber are key factors in the formation processes of NO_x. The conditions reached during combustion are influenced by the initial pressure and temperature of the

mixture, along with the chemical composition of the mixture entering the chamber. Since combustion in the main chamber occurs under isochoric conditions, the pressure remains constant between the inlet and outlet of the chamber. Therefore, initially, it is possible to study the effect of inlet conditions on NO_x formation in terms of their impact on the temperature reached in the chamber. For the purpose of comparing the two trends, Figure 5.14 and Figure 5.15 respectively depict the trend of the recalculated emissive EINO database and the temperature reached during combustion, both as a function of flight Mach.

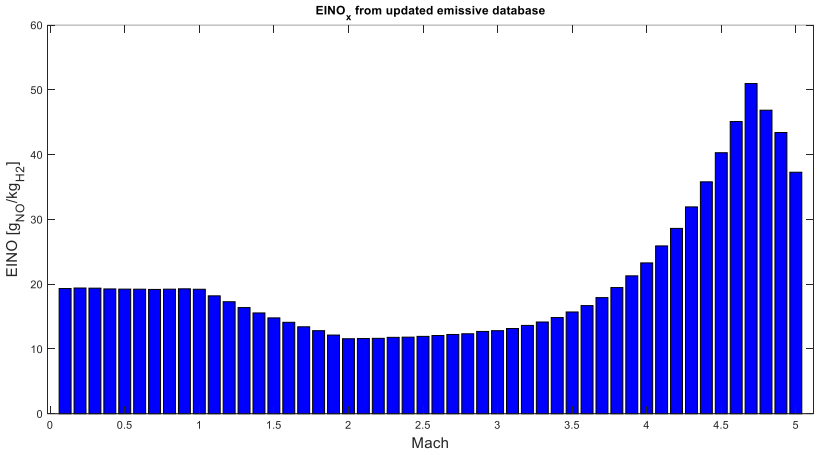

Figure 5.14 - EINO from the updated emissive databases

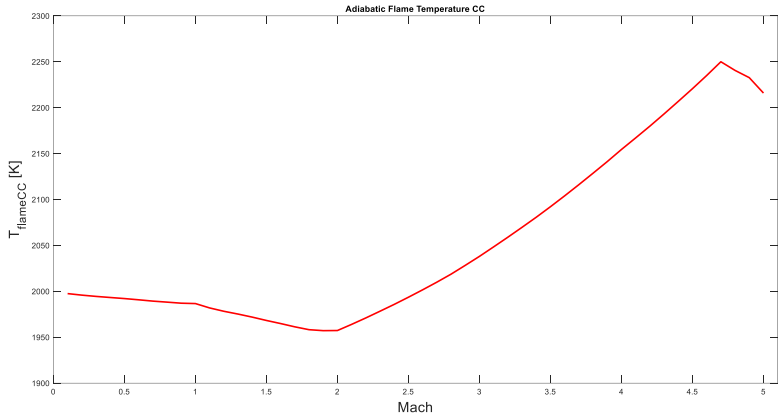

Figure 5.15 – Temperature reached during combustion

The trend of EINO closely mirrors the trend of the temperature, as expected. The comparison between these trends validates the behaviour of the calculated EINO from a standpoint of physical consistency. However, a more thorough analysis of the correlations between the Flame Temperature (FT) and the inlet conditions to the chamber is necessary to provide a comprehensive understanding of the complex network of dependencies characterizing this engine. In this regard, the combination of parameters that justifies the FT trend includes the inlet pressure and temperature conditions and the mass fractions of H_2, O_2 and H_2O of the incoming mixed flow. In particular, with an increase in temperature and pressure at the combustor inlet, one would expect an increase in the temperature reached in the chamber and thus in the NO_x produced during combustion. Considering the fuel-rich conditions of combustion, i.e., equivalence ratios greater than 1, an increase in the ratio between mass fraction of H_2 and mass fraction of O_2 at the chamber inlet would

be expected to result in a reduction in the temperature achieved. Finally, considering the presence of a substantial mass fraction of H_2O in the incoming flow to the main combustion chamber (CC) due to combustion in the preburner (PB), an increase in this mass fraction would be expected to lead to a decrease in the temperature reached in the chamber. Water vapor has three effects on the NO_x formation process. As reported in [36], water vapor dilution of the combustion mixture reduces NO_x emission in premixed flames by (i) lowering flame temperature, (ii) oxygen deficiency, and (iii) chemical action. In this regard, study [36] compares the effects on NO_x formation of substituting a fraction of nitrogen with a fictional fraction of water during combustion, analysing various conditions. In particular, the aim is to evaluate the relative importance of the three chemical and physical effects of water on NO_x formation and flame temperature. First, the effect of a fraction of H_2O associated with the real chemical-physical characteristics of water was studied, resulting in a decrease in NO_x produced due to the combined effects of the three. Subsequently, the effect of a fictional fraction of water with the physical properties of H_2O (thermochemistry and transport) but that does not react in the chemical scheme was studied. This demonstrated the predominance of the thermal and kinetic effects over the chemical one. In other words, the effect of the decrease in flame temperature (i) and that of the third body coefficients of H_2O in radical reactions (iii) are more important than the effect of the deficiency of oxygen-containing species (ii). Finally, to separately study the thermal and kinetic effects, the third body coefficients of the fictional fraction of H_2O were replaced with those of nitrogen. What is observed is a predominance of the thermal effect among the three, attributable to the decrease in flame temperature, confirming that, due to the high temperatures, the primary mechanism for NO_x formation in the combustion chamber is the Zeldovich mechanism (thermal NO_x). Furthermore, regarding the chemical effect of the deficiency of oxygen-containing radical species, in the case of fuel-rich combustion like that of the SABRE, this effect is reversed, favouring the formation of NO_x. However, at the high temperatures characteristic of the SABRE, the chemical and kinetic effects can be considered negligible compared to the thermal effect. In general, therefore, the presence of H_2O at the inlet to the main CC has an inhibitory effect on NO_x formation.

After clarifying the impact of the inlet conditions of the combustion chamber on the flame temperature, it is possible to analyse their combined effect as Mach varies. In this regard, Figure 5.16 depicts the trends of pressure, temperature, ratio between mass fraction of H_2 and mass fraction of O_2, and mass fraction of H_2O at the inlet of the main CC as a function of Mach.

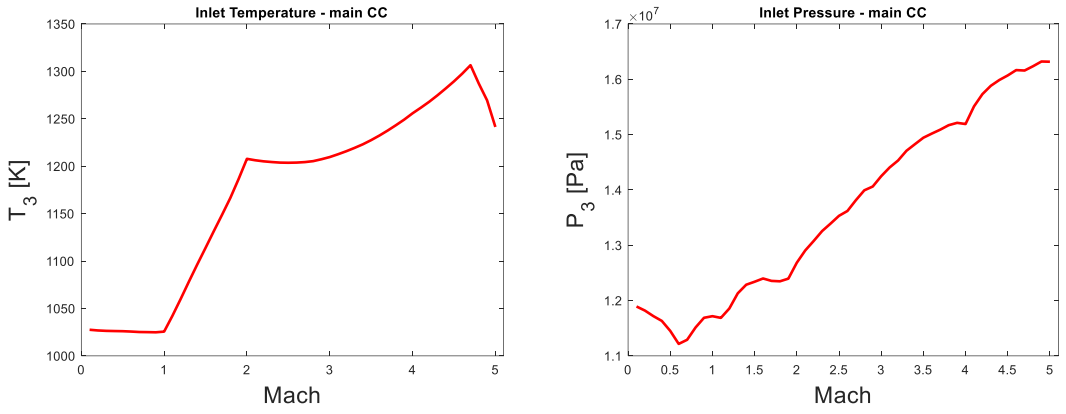

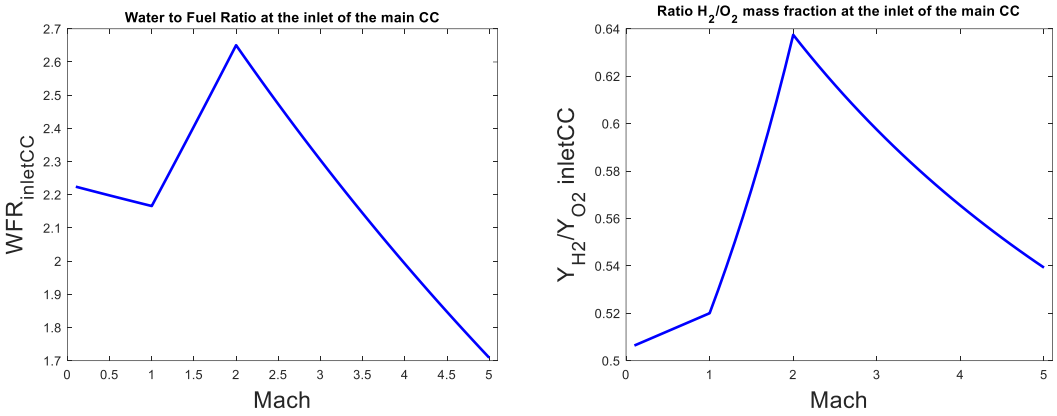

Figure 5.16 – a) Pressure, b) temperature, c) mass fraction of H2 and d) mass fraction of H2O at the inlet of the main CC

From the comparison between the trends reported in Figure 5.15 and the trend of the temperature reached in the chamber, the following observations can be made:

- For Mach values between 0 and 1, the combined effect of the decrease in T_3, the decrease in p_3, and the increase in the mass fraction of incoming H_2 relative to that of O_2 outweighs the effect of the slight decrease in the WFR, resulting in a slight decrease in the flame temperature.
- For Mach values between 1 and 2, the combined effect of the increase in WFR and the significant increase in the ratio between the mass fractions of H_2 and O_2 predominates over the increase in T_3 and p_3, resulting in a decrease in the flame temperature.
- For Mach values between 2 and 4.7, there is an increase in T_3 and p_3 and a decrease in WFR and the ratio between the mass fractions of H_2 and O_2. All four parameters are therefore characterized by trends that favor an increase in the flame temperature, which indeed reaches its maximum value.
- Finally, for Mach values between 4.8 and 5, there is a decrease in T_3 that outweighs all other effects, resulting in a decrease in the flame temperature compared to its maximum value.

Through this brief analysis of the correlations between the chemical-propulsive parameters of the engine and the mechanisms of NO_x formation, it is possible to attribute a solid chemical-physical foundation to the trend of the flame temperature and consequently to that of the $EINO_x$. Some of the parameters mentioned, such as p_3 and T_3, appear directly in the original formulation of the P3T3 method for estimating NO_x emissions. As for the WFR, it is instead selected as one of the parameters to be used in updating the original formulations of the P3T3 and BFFM2 methods to adapt them to the case study. Although estimating the WFR requires a thorough knowledge of the engine for the conceptual design phase, it is decided to integrate this parameter into the new formulations due to its widely studied importance [36], [37] as a thermo-regulator in the combustion chamber. With the exception of the WFR, the approach chosen for selecting the parameters to update the original formulations of the NO_x estimation methods involves the fundamental requirement of being able to easily access these parameters, consistent with the conceptual design phase for which the proposed methodology is tailored. To meet this requirement, it is decided to integrate into the new formulations of the estimation methods not the ratio between the mass fractions of H_2 and O_2 at the inlet of the main CC, but rather the two propulsive parameters from which this trend arises: the FAR and the PBratio. These two parameters together quantitatively describe the management of gas flows involved in combustion. In particular, the FAR is uniformly increasing with Mach, while the airflow directed to the PB remains constant up to Mach 1, increases between Mach 1 and 2, and decreases from Mach 2 to Mach 5. Starting from the uniform trend of the FAR and the segmented trend of the PBratio, considering that the fraction of air not sent to the PB is used to dilute the exhaust gases of the PB before concluding combustion in the main CC, it is possible to reconstruct the trend of the ratio between the mass fractions of H_2 and O_2

at the inlet of the main CC through the principle of superposition of effects. Figure 5.17 represents the trends of PBratio and FAR, and it also allows to notice the close correlation between PBratio and WFR, whose trends are approximately identical.

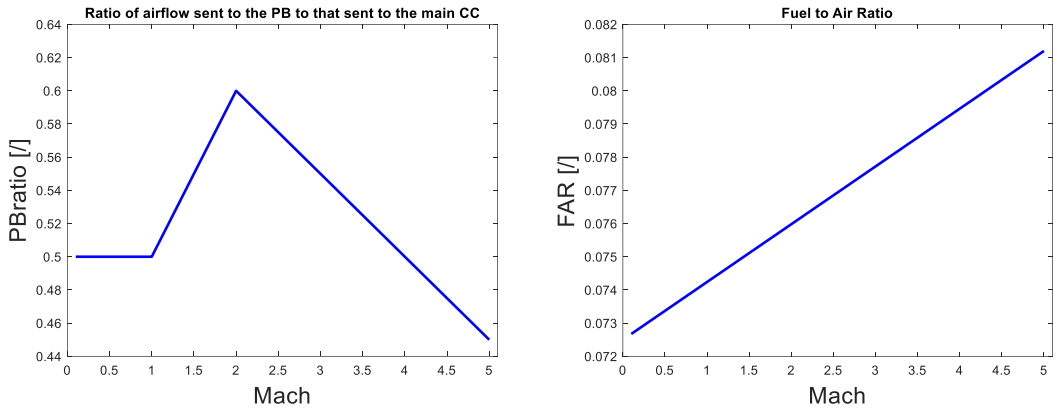

Figure 5.17 – a) PBratio and b) FAR as a function of Mach

Finally, considering the thermal management of the engine by the closed and regenerative cycle of helium, it is decided to introduce the parameter HEratio into the new formulations as well. HEratio is defined as the ratio between the mass flow of helium at the turbine inlet and the total air mass flow at the air compressor inlet powered by the helium turbine. This parameter, of fundamental importance for the deeply precooled combined cycle configuration of the SABRE, is represented in Figure 5.18.

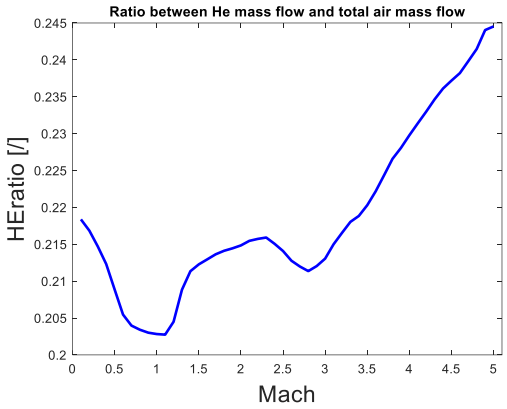

Figure 5.18 – Heratio as a function of Mach

Although this trend may not appear to be directly connected with the trends presented earlier for the other selected influential parameters, it remains of particular importance for characterizing the SABRE and is therefore still selected for adapting the original formulations of the NO_x estimation methods for the case study. Additionally, the regenerative cycle of helium plays a fundamental role in defining the temperature at the inlet of the combustion chamber, as it contributes to the thermal regulation of the PB exhaust gases before the mixing stage preceding the main CC. For this reason, it would be more consistent to construct the HEratio as the ratio of thermal flows exchanged in the heat exchanger. However, for the sake of data

availability for the new emission estimation techniques, it is chosen to stick to the data available to the reader, thus constructing this ratio based on the mass flows.

Chapter 6 - Updated Methods for Estimating NO_x Emission Index

The final part of the methodology involves modifying the classical formulations of the P3T3 and the Fuel-Flow methods to tailor their applicability to the characteristics of the case study. Specifically, the new formulations of these methods are suited for estimating NO_x emissions from high-speed engines using non-conventional fuels. As previously mentioned, this adaptation and enhancement process from the original P3T3 and BFFM2 is carried out through two modifications: the inclusion of new parameters in the form of ratios between FL and SL conditions, coupled with the curve fitting of the resulting mathematical formulations based on the $EINO_x$ from emissive database. The parameters selected for integration into the new formulations in Chapter 5.3 are Mach, FAR, WFR, PBratio, and HERatio. These parameters, expressed as ratios FL/SL, feature in the new mathematical relationships that calculate the $EINO_{xFL}$ as a correction of the $EINO_{xSL}$. Each proposed new formulation entails a different combination of these parameters. Different combinations of parameters yield different curve fitting optimization coefficients and consequently result in varying errors for the modified formulations. As the number of introduced parameters increases, the accuracy of estimation progressively improves.

6.1 Input Data from Propulsive and Emissive Databases

Both the P3T3 and the Fuel Flow method are classified as ratio methods. This implies that every parameter appearing in both the original and updated formulations is expressed in terms of the ratio between Flight Level and Sea Level conditions. To generate and analyse the Sea Level conditions, the propulsive model and the emissive database must be utilized. The following tables numerically present the results of the propulsive and emissive modelling, from which to derive the ratios. Specifically, Table 6.1 pertains to Sea Level conditions, encompassing Mach conditions from 0.1 to 0.4, indicating that the SABRE operates at a considerably low altitude, thus referred to as Sea Level. On the other hand, Table 6.2 corresponds to Flight Level conditions.

Mach	T_3	p_3	FAR	PBratio	WFR	HEratio	H	EINO
[/]	[K]	[Pa]	[/]	[/]	[/]	[/]	[/]	[g_{NO}/kg_{H2}]
0,1	1027,53	1,19E+07	7,27E-02	0,500	2,224	0,218	-0,023	19,32

0,2	1026,79	1,18E+07	7,28E-02	0,500	2,218	0,217	-0,023	19,41
0,3	1026,37	1,17E+07	7,30E-02	0,500	2,211	0,215	-0,024	19,38
0,4	1026,17	1,16E+07	7,32E-02	0,500	2,204	0,212	-0,024	19,27

Table 6.1 - SL conditions for the SABRE

Mach	**T_3**	**p_3**	**FAR**	**PBratio**	**WFR**	**HEratio**	**H**	**EINO**
[/]	[K]	[Pa]	[/]	[/]	[/]	[/]	[/]	[g_{NO}/kg_{H2}]
0,5	1026,01	1,15E+07	7,34E-02	0,500	2,198	0,209	-0,024	19,24
0,6	1025,64	1,12E+07	7,35E-02	0,500	2,192	0,205	-0,013	19,23
0,7	1025,15	1,13E+07	7,37E-02	0,500	2,185	0,204	0,012	19,19
0,8	1025,03	1,15E+07	7,39E-02	0,500	2,179	0,203	0,035	19,23
0,9	1024,86	1,17E+07	7,41E-02	0,500	2,172	0,203	0,058	19,28
1	1025,58	1,17E+07	7,42E-02	0,500	2,166	0,203	0,074	19,22
1,1	1042,20	1,17E+07	7,44E-02	0,510	2,214	0,203	0,089	18,20
1,2	1060,02	1,19E+07	7,46E-02	0,520	2,261	0,204	0,098	17,29
1,3	1078,41	1,21E+07	7,48E-02	0,530	2,309	0,209	0,106	16,38
1,4	1096,37	1,23E+07	7,49E-02	0,540	2,358	0,211	0,111	15,56
1,5	1113,83	1,23E+07	7,51E-02	0,550	2,406	0,212	0,114	14,79
1,6	1131,49	1,24E+07	7,53E-02	0,560	2,454	0,213	0,117	14,12
1,7	1148,84	1,24E+07	7,55E-02	0,570	2,503	0,214	0,118	13,42
1,8	1166,59	1,23E+07	7,56E-02	0,580	2,552	0,214	0,119	12,82
1,9	1186,58	1,24E+07	7,58E-02	0,590	2,601	0,214	0,119	12,15
2	1207,78	1,27E+07	7,60E-02	0,600	2,651	0,215	0,119	11,57
2,1	1206,27	1,29E+07	7,62E-02	0,595	2,614	0,215	0,119	11,60
2,2	1205,13	1,31E+07	7,63E-02	0,590	2,578	0,216	0,119	11,64
2,3	1204,39	1,33E+07	7,65E-02	0,585	2,543	0,216	0,119	11,79
2,4	1203,79	1,34E+07	7,67E-02	0,580	2,508	0,215	0,119	11,82
2,5	1203,64	1,35E+07	7,69E-02	0,575	2,473	0,214	0,119	11,94
2,6	1203,82	1,36E+07	7,70E-02	0,570	2,438	0,213	0,119	12,07
2,7	1204,33	1,38E+07	7,72E-02	0,565	2,404	0,212	0,118	12,24
2,8	1205,33	1,40E+07	7,74E-02	0,560	2,371	0,211	0,118	12,34
2,9	1207,34	1,41E+07	7,75E-02	0,555	2,337	0,212	0,118	12,70
3	1209,63	1,42E+07	7,77E-02	0,550	2,304	0,213	0,118	12,82
3,1	1212,60	1,44E+07	7,79E-02	0,545	2,272	0,215	0,118	13,15
3,2	1215,79	1,45E+07	7,81E-02	0,540	2,239	0,217	0,118	13,64
3,3	1219,32	1,47E+07	7,82E-02	0,535	2,207	0,218	0,118	14,16
3,4	1223,10	1,48E+07	7,84E-02	0,530	2,176	0,219	0,118	14,84
3,5	1227,50	1,49E+07	7,86E-02	0,525	2,144	0,220	0,118	15,71
3,6	1232,34	1,50E+07	7,88E-02	0,520	2,113	0,222	0,118	16,69

3,7	1237,61	1,51E+07	7,89E-02	0,515	2,082	0,224	0,118	17,92
3,8	1243,28	1,52E+07	7,91E-02	0,510	2,052	0,227	0,118	19,47
3,9	1249,19	1,52E+07	7,93E-02	0,505	2,022	0,228	0,118	21,28
4	1255,77	1,52E+07	7,95E-02	0,500	1,992	0,230	0,117	23,28
4,1	1261,68	1,55E+07	7,96E-02	0,495	1,962	0,231	0,117	25,90
4,2	1267,87	1,57E+07	7,98E-02	0,490	1,933	0,233	0,116	28,61
4,3	1274,69	1,59E+07	8,00E-02	0,485	1,904	0,235	0,116	31,93
4,4	1281,94	1,60E+07	8,02E-02	0,480	1,875	0,236	0,115	35,80
4,5	1289,47	1,61E+07	8,03E-02	0,475	1,847	0,237	0,115	40,29
4,6	1297,60	1,62E+07	8,05E-02	0,470	1,819	0,238	0,114	45,10
4,7	1306,52	1,62E+07	8,07E-02	0,465	1,791	0,240	0,113	50,97
4,8	1287,11	1,62E+07	8,09E-02	0,460	1,763	0,241	0,112	46,86
4,9	1269,45	1,63E+07	8,10E-02	0,455	1,736	0,244	0,110	43,41
5	1241,40	1,63E+07	8,12E-02	0,450	1,709	0,245	0,109	37,28

Table 6.2 - FL conditions for the SABRE

6.2 New Formulations of the P3T3 Method

After updating the two databases and collecting the necessary input data for the application of the method in its original and updated versions, it is possible to resume the steps for applying the original P3T3 method outlined in Chapter 4.4.2, adapting them to the derivation of the new formulations. The propulsion and emissive models of the engine are designed to study the behaviour of thermodynamic and chemical variables, and consequently, the resulting $EINO_x$, as functions of Mach number. Therefore, it was decided to maintain this parameter as the independent variable for studying the variables involved in the application of the updated formulations of the P3T3 method. All the ratios featured in the new formulations of the methods are studied as functions of Mach number since the reference variables, including T_3, are expressed as functions of Mach. The Mach number is selected as the x-axis variable due to its ability to capture point variations along the mission profile. Indeed, a change in the mission phase entails a variation in altitude, which consequently affects air pressure, temperature, and Mach number. Therefore, plotting the input variables at flight level against Mach enables the generalization of the new formulations of the P3T3 method, thanks to its characteristic of not only tracking flight speed but also flight level variation.

As the initial step, it is necessary to construct fits based on the known data under Sea Level conditions collected in Table 6.1, in order to study their trend with varying flight conditions. The parameters p_{3SL}, FAR_{SL}, $PBratio_{SL}$, WFR_{SL}, $HEratio_{SL}$, and $EINO_{SL}$ obtained from the updated propulsive and emissive databases must be interpolated as functions of T_3. For the SABRE engine, reference Sea Level conditions as a function of the main combustor inlet temperature can be mathematically expressed with the following equations:

$$p_{3SL} = 1.809 * 10^5 * T_3 - 1.74 * 10^8 \quad (6.1)$$

$$FAR_{SL} = 12.09 * \exp(-0.004977 * T_3) \quad (6,2)$$

$$PBratio_{SL} = 10^{-17} * T_3 + 0.5 \tag{6.3}$$

$$WFR_{SL} = 0.01365 * T_3 - 11.8 \tag{6.4}$$

$$HEratio_{SL} = 8.155 * 10^{-10} * \exp(0.01889 * T_3) \tag{6.5}$$

$$EINO_{SL} = 0.01584 * T_3 + 3.082 \tag{6.6}$$

The most commonly used interpolation method is linear polynomial interpolation; however, in the case of FAR and HEratio, it is preferable to use exponential interpolation to avoid encountering erroneously negative values of these parameters as T_3 increases. The trends of these fits are graphed in Figure 6.1, compared to the values under Sea Level conditions reported in Table 6.1.

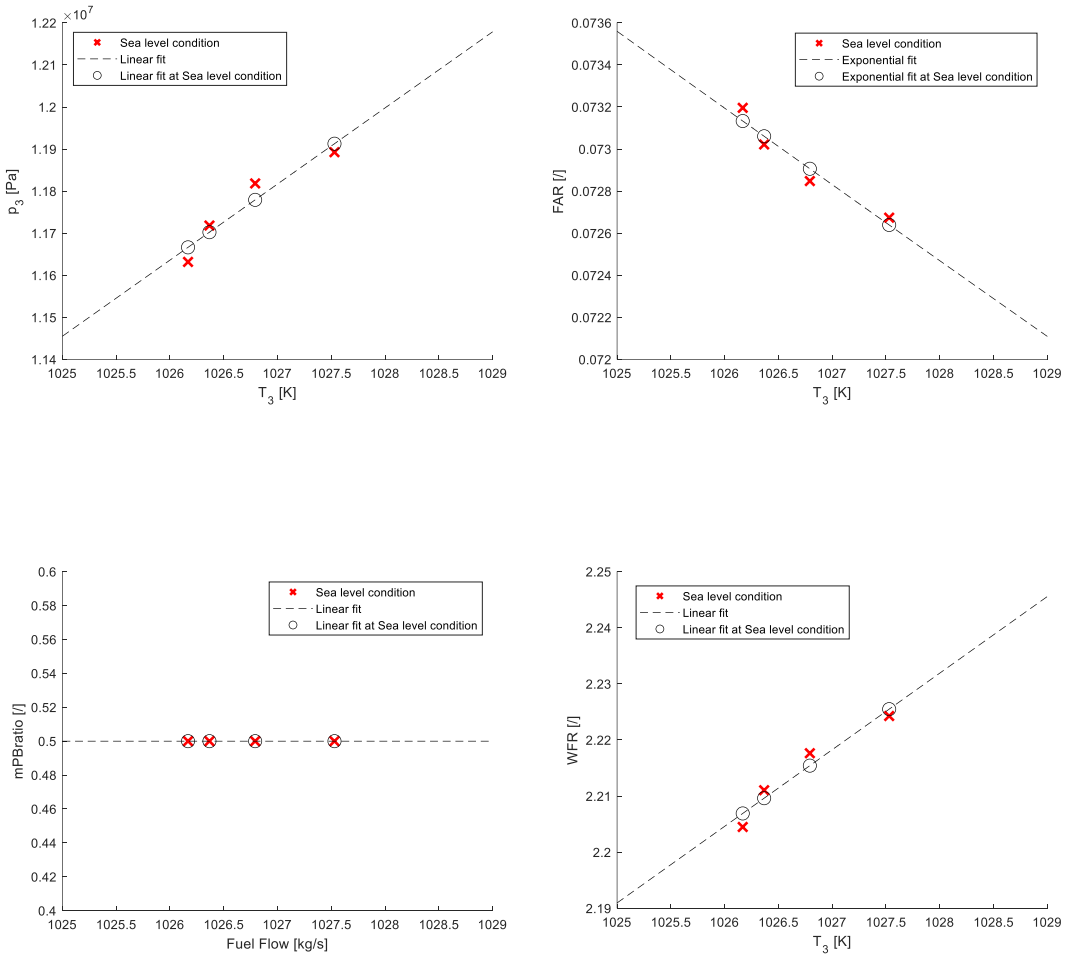

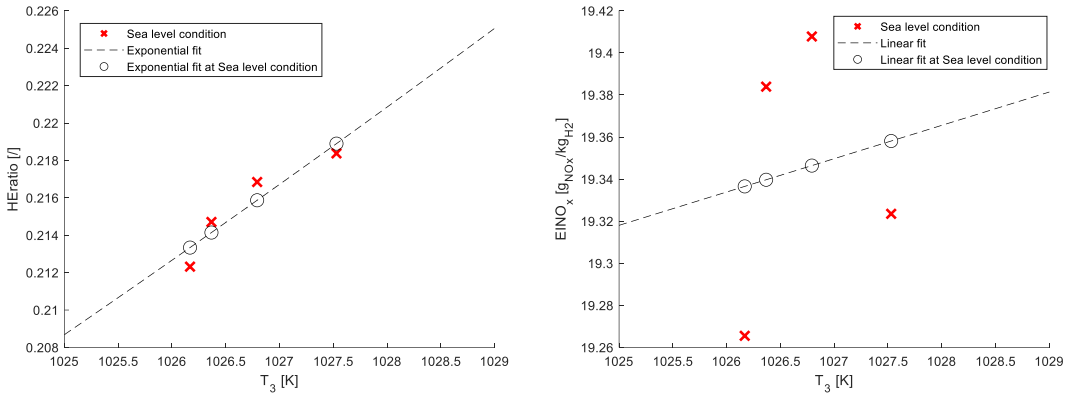

Figure 6.1 - Sea level conditions as a function of the combustion inlet temperature, in terms of a) pressure at the inlet of the combustion chamber, b) Fuel to Air Ratio, c) air mass flow rate PB ratio, d) Water to Fuel Ratio at the inlet of the combustion chamber, e) He-air mass flow rate HE ratio, f) NO Emission Index

Table 6.3 and Table 6.4 respectively report the absolute and relative errors of the interpolation of Sea Level parameter values.

Mach	**p_3**	**FAR**	**PBratio**	**WFR**	**HEratio**	**EINO**
[/]	[Pa]	[/]	[/]	[/]	[/]	[g_{NO}/kg_{H2}]
0,1	2,02E+04	-3,46E-05	-5,55E-17	1,22E-03	5,22E-04	3,46E-02
0,2	-3,90E+04	5,85E-05	-5,55E-17	-2,21E-03	-9,77E-04	-6,14E-02
0,3	-1,58E+04	3,88E-05	-5,55E-17	-1,42E-03	-5,65E-04	-4,42E-02
0,4	3,46E+04	-6,27E-05	-5,55E-17	2,41E-03	1,02E-03	7,10E-02

Table 6.3 - Interpolation absolute errors at SL conditions

Mach	**p_3**	**FAR**	**PBratio**	**WFR**	**HEratio**	**EINO**
[/]	[Pa]	[/]	[/]	[/]	[/]	[/]
0,1	1,70E-03	-4,77E-04	-1,11E-16	5,50E-04	2,39E-03	1,79E-03
0,2	-3,30E-03	8,03E-04	-1,11E-16	-9,98E-04	-4,51E-03	-3,16E-03
0,3	-1,35E-03	5,32E-04	-1,11E-16	-6,43E-04	-2,63E-03	-2,28E-03
0,4	2,98E-03	-8,57E-04	-1,11E-16	1,09E-03	4,80E-03	3,69E-03

Table 6.4 - Interpolation relative errors at SL conditions

Once the fits for Sea Level conditions are obtained, the subsequent step involves deriving the values of the same parameters under Flight Level conditions, namely p_{3FL}, FAR_{FL}, $Pbratio_{FL}$, WFR_{FL} and $Heratio_{FL}$ through propulsion modelling. These values are contained in Table 6.2 as a function of Mach.

Based on the values of T_{3FL} for a given Mach condition, it becomes possible to derive the values of p_{3SL}, FAR_{SL}, $Pbratio_{SL}$, WFR_{SL}, $Heratio_{SL}$ and $EINO_{SL}$ using the fits obtained previously. Once these parameters are determined, as the P3T3 method operates as a ratio method, ratios between Flight Level and Sea Level conditions need to be constructed, as they are incorporated into the mathematical formulation of the method.

Finally, the new mathematical formulation of the method can be applied to evaluate the $EINO_{FL}$ starting from the appropriately corrected $EINO_{SL}$, considering the evolution of the ratio of p_3, FAR, humidity factor, and one or more of the newly introduced parameters. Regarding the new mathematical formulations, described in the following subsections, the approach used involves first optimizing the exponent coefficients of the original formulation. Subsequently, the factor $k * M^c$ is added to account for the effect of high speed on NO_x formation. From this point onwards, initially, only one ratio between FL and SL conditions of the parameters PBratio, WFR, and HEratio is added, re-optimizing the exponents. Subsequently, new formulations are proposed in which two ratios between FL and SL conditions of the parameters PBratio, WFR, and HEratio are included. Finally, a complete formulation is proposed that encompasses all the ratios, with their respective exponents optimized. All the optimization procedures described above are performed using the built-in function *lsqcurvefit* in Matlab, taking the EINO from the emissive database as reference. Alongside the new mathematical formulations, the trends of the ratios contained therein as functions of Mach are presented below. Additionally, a brief discussion regarding the mathematical contribution of the parameters contained in the formulations in relation to their physical-chemical contribution in the NO_x formation process is provided. Based on this discussion, considerations are made on the exponent coefficients introduced for the parameters and their role in ensuring physical-chemical justification for the mathematical contribution of the parameters in the formulations. The optimized coefficients and the results of the new formulations are reported and further discussed in Chapter 7. Please note that, since the mass fractions of nitrogen oxides other than NO have been considered negligible during the emissive modelling phase in the evaluation of engine emission indices, the following discussion is specialized for estimating the EINO. Considering that most of NO_x produced consists of NO, it is possible, as a first approximation, to consider the overall $EINO_x$ coinciding with the EINO.

6.2.1 Variation N.1 – EINO as a function of p_3 and FAR

The first modification made to the original P3T3 method, as documented in Chapter 4.3.2, focused on optimizing the exponent coefficients *a* and *b* associated with pressure and FAR ratios. The mathematical formulation is reported below, along with the graphs of the parameters appearing therein as functions of Mach. Additionally, a brief discussion regarding the exponents in relation to the physical-chemical justification of their values is provided. These values are updated using the built-in function *lsqcurvefit* in Matlab, taking the EINO from emissive database as reference.

$$EINO_{FL} = EINO_{SL}\left(\frac{p_{3FL}}{p_{3SL}}\right)^{a}\left(\frac{FAR_{FL}}{FAR_{SL}}\right)^{b} e^{H} \tag{6.7}$$

$$EINO_{SL} = EINO_{xSL}(T_3) \tag{6.8}$$

$$p_{3SL} = p_{3SL}(T_3) \tag{6.9}$$

$$FAR_{SL} = FAR_{SL}(T_3) \tag{6.10}$$

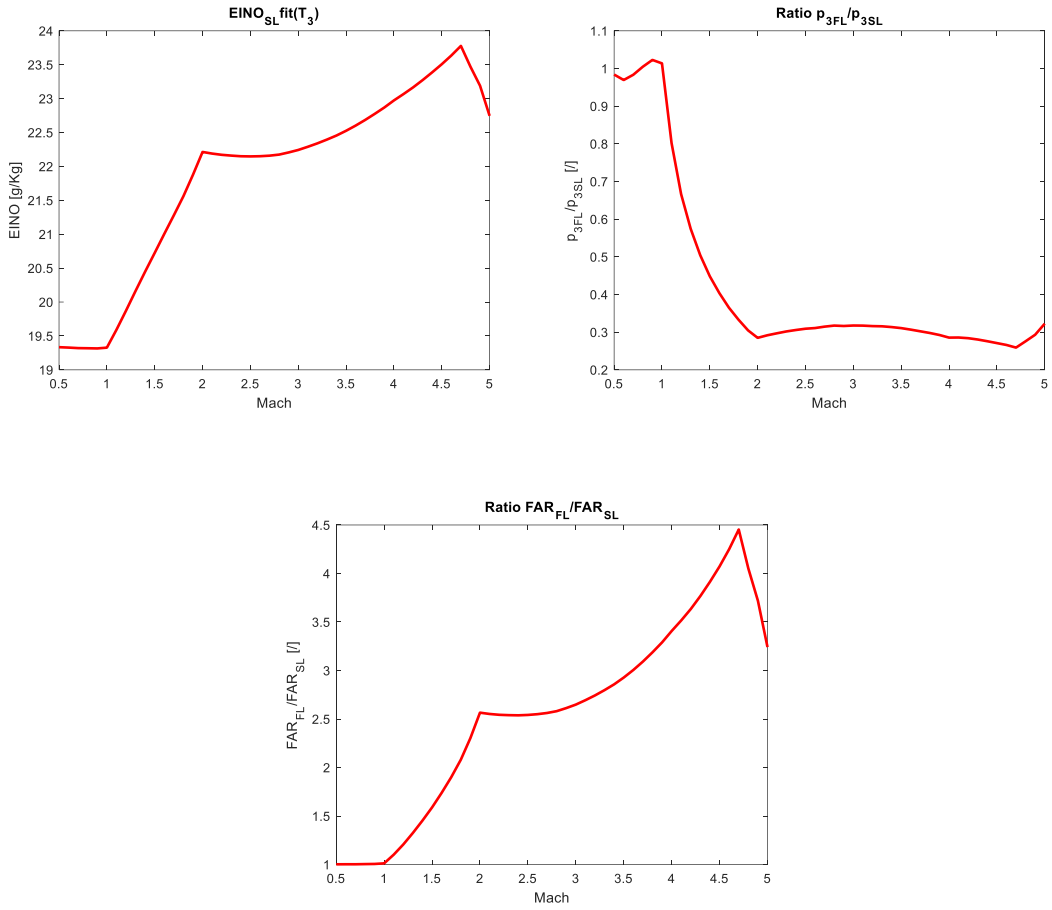

Figure 6.2 – As a function of Mach: a) $EINO_{SL}(T3)$, b) Ratio between Flight Level (FL) and Sea Level (SL) conditions of p_3, c) Ratio between Flight Level (FL) and Sea Level (SL) conditions of FAR

The T_3 generally increases as a function of Mach, except for Mach conditions close to 5, as depicted in Figure 5.16 (*a*). This can be observed from the trend of $EINO_{SL}$ as a function of Mach. In fact, the $EINO_{SL}(T_3)$ fit linearly increases with T_3, and consequently, when expressed as a function of Mach, it perfectly follows the profile of T_3 as a function of Mach. The increasing trend of T_3 with Mach also results in the linear fit of $p_{3SL}(T_3)$ increasing with Mach. Specifically, it increases more rapidly compared to p_{3FL} as a function of Mach. Consequently, the pressure ratio decreases as Mach increases. In particular, it is evident that the trend of the p_3 ratio between FL and SL conditions as Mach increases is approximately inversely proportional to that of T_3 as Mach increases depicted in Figure 5.16. Since p_{3FL} increases with Mach, and an increase in p_{3FL} corresponds to an increase in flame temperature and thus in NO_x production, the contribution of p_3 ratio in the new formulation for EINO must increase with Mach to have physical justification. Since the pressure ratio is less than 1 and decreases as a function of Mach, it is expected that the exponent coefficient *a* has a negative value. A negative coefficient *a* indeed ensures physical justification for the contribution of p_3 ratio as Mach increases. Regarding the ratio between FL and SL conditions of FAR, FAR_{FL} increases with Mach, while the $FAR_{SL}(T_3)$ fit decreases with increasing T_3. Since T_3 increases with Mach, $FAR_{SL}(T_3)$ decreases, and therefore the FAR ratio increases. To have physical justification, the contribution of the FAR ratio to the increase in Mach must be negative in the mathematical

formulation of EINO. Indeed, as Mach increases, FAR increases, leading to a decrease in flame temperature since combustion occurs under fuel-rich conditions, beyond the stoichiometric FAR conditions. A decrease in flame temperature results in a reduction in NO_x production, and thus in the corresponding EINO. The coefficient *b* of the FAR ratio, which has a value greater than 1 and increases with Mach, must therefore be negative to have physical justification. Please note that a positive contribution refers not to a specific value of the ratio raised to its respective optimized coefficient greater than 1, but rather to the increase of this value as Mach increases, which positively contributes to the increase of EINO with Mach.

6.2.2 Variation N.2 - EINO as a function of p_3, FAR and Mach

The second variation involves introducing the factor $k * M^c$ and optimizing all coefficients. The resulting mathematical formulation is as follows.

$$EINO_{FL} = k * EINO_{SL} \left(\frac{p_{3FL}}{p_{3SL}}\right)^a \left(\frac{FAR_{FL}}{FAR_{SL}}\right)^b M^c \, e^H \tag{6.11}$$

Regarding Mach, since it is between 0 and 5, the corresponding coefficient *c* must be positive to have physical justification. With an increase in Mach, one would expect an increase in NO_x formation during combustion due to the higher temperatures and pressures in the combustion chamber required to achieve higher speeds. Therefore, the contribution of $k * M^c$ must increase as Mach increases to be consistent with the physics of the process. Regarding $EINO_{SL}(T_3)$, p_3 ratio, and FAR ratio, the considerations made previously remain valid.

6.2.3 Variation N.3 - EINO as a function of p_3, FAR, Mach and PBratio

The third modification involves introducing, starting from the updated formulation including Mach, the ratio between $PBratio_{FL}$ and the linear fit $PBratio_{SL}(T_3)$. In particular, the $PBratio_{SL}(T_3)$ fit remains constant and equal to 0.5, given the constancy of PBratio as T_3 increases up to Mach 1 condition. The trend of this ratio between FL and SL conditions thus perfectly reflects that of the original parameter PBratio as a function of Mach. This becomes evident when comparing the trend of the ratio between FL and SL conditions, as shown in Figure 6.3, with the trend of the original parameter PBratio, as depicted in Figure 5.17 (*a*).

$$EINO_{FL} = k * EINO_{SL} \left(\frac{p_{3FL}}{p_{3SL}}\right)^a \left(\frac{FAR_{FL}}{FAR_{SL}}\right)^b \left(\frac{\dot{m}_{PBratioFL}}{\dot{m}_{PBratioSL}}\right)^d M^c \; e^H \tag{6.12}$$

$$\dot{m}_{PBratio} = \frac{\dot{m}_{AirPB}}{\dot{m}_{AirTot}} \tag{6.13}$$

$$\dot{m}_{PBratioSL} = \dot{m}_{PBratioSL}(T_3) \tag{6.14}$$

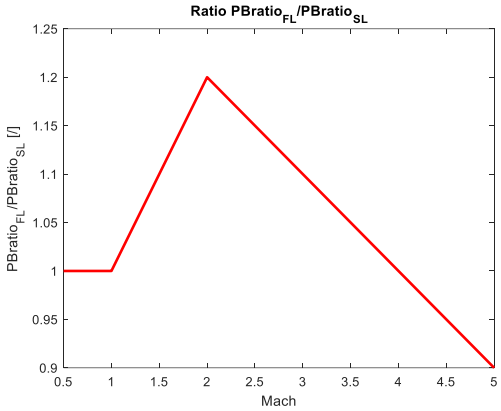

Figure 6.3 - Ratio between Flight Level (FL) and Sea Level (SL) conditions of PBratio as a function of Mach

The trend of this ratio between FL and SL conditions increases up to Mach 2 and then decreases until Mach 5. Furthermore, the value of this ratio oscillates as Mach increases, being greater than 1 until Mach 4 and then less than 1 until Mach 5. With an increase in $PBratio_{FL}$, and therefore the corresponding ratio between FL and SL conditions, a decrease in NO_x production is expected as the combustion segmentation between the two combustion stages increases, leading to a decrease in the temperature reached in the main combustion chamber. Additionally, as PBratio increases, WFR also increases, leading to another reason for the decrease in temperature and hence NO_x. The contribution of the ratio between FL and SL conditions must therefore decrease as Mach increases up to Mach 2 and then increase until Mach 5. For the mathematical contribution of the PBratio ratio to have physical-chemical justification, the coefficient *d* must be negative.

6.2.4 Variation N.4 - EINO as a function of p_3, FAR, Mach and WFR

This new formulation introduces, compared to Variation No. 3, the ratio between FL and SL conditions of the WFR parameter. The trend of WFR as a function of Mach is shown in Figure 5.16 (*c*) and it is appropriately almost identical to that of PBratio shown in Figure 5.17 (*a*). In fact, as the airflow rate into the PB increases, the amount of H_2O produced during this combustion stage increases, consequently increasing the mass fraction of H_2O entering the main CC and thus the WFR. Specifically, WFR_{FL} slightly decreases with increasing Mach up to Mach 1, then increases until Mach 2, and finally decreases until Mach 5. On the other hand, the linear fit $WFR(T_3)$ uniformly increases with increasing T_3, which also increases with Mach. The result of these two trends is the decreasing trend of the WFR ratio between FL and SL conditions as shown in Figure 6.4. The trend of the WFR ratio between FL and SL conditions is therefore almost inversely proportional to that of T_3 as Mach increases, similar to the behaviour observed with the ratio of p_3 between FL and SL conditions. The resulting mathematical formulation is as follows and includes the new exponents that must be subject to optimization.

$$EINO_{FL} = k * EINO_{SL} \left(\frac{p_{3FL}}{p_{3SL}}\right)^a \left(\frac{FAR_{FL}}{FAR_{SL}}\right)^b \left(\frac{WFR_{FL}}{WFR_{SL}}\right)^e M^c \, e^H \qquad (6.15)$$

$$WFR = \frac{\dot{m}_{H20}}{\dot{m}_{fuel}} \qquad (6.16)$$

$$WFR_{SL} = WFR_{SL}(T_3) \tag{6.17}$$

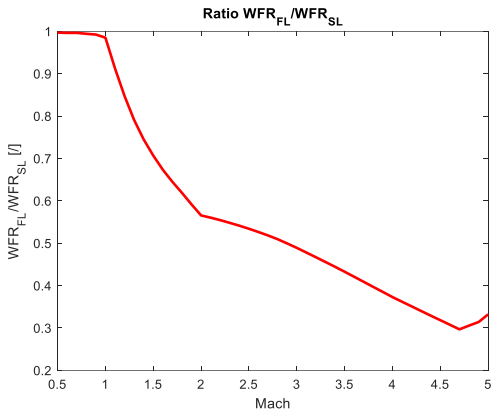

Figure 6.4 - Ratio between Flight Level (FL) and Sea Level (SL) conditions of WFR as a function of Mach

As mentioned earlier, water generated during combustion in the PB intervenes in the main combustion process with three contributions: thermal regulation, oxygen deficiency, and chemical reactions. The thermal contribution predominates over contributions related to the reaction of water in the chamber. Consequently, an increase in WFR generally leads to a decrease in the flame temperature and thus in NO_x production. Considering the trend of WFR as a function of Mach and its effect on NO_x formation, it can be concluded that the mathematical contribution of the WFR ratio between FL and SL conditions in the formulation for EINO should decrease with increasing Mach up to Mach 2 and then increases from Mach 2 to Mach 5. Since this ratio is less than 1 and decreases as Mach increases from Mach 1 to Mach 5, no coefficient can ensure a negative mathematical contribution of the WFR ratio until Mach 2 and then positive from Mach 2 to Mach 5 in the formulation of EINO. Given that the WFR ratio is constant up to Mach 1, decreases from Mach 1 to Mach 4.7, and then increases from Mach 4.7 to Mach 5, a negative exponent *e* is expected. A negative exponent *e* leads to an increasing mathematical contribution from Mach 1 until Mach 4.7 in the EINO formulation. A contribution to the increase in estimated EINO that grows with Mach has physical-chemical justification over a wider Mach range, from 2 to 4.7. Once again, please note that a positive contribution refers not to a specific value of the ratio raised to its respective optimized coefficient greater than 1, but rather to the increase of this value as Mach increases, which positively contributes to the increase of EINO estimated with Mach.

6.2.5 Variation N.5 - EINO as a function of p_3, FAR, Mach and HEratio

This new formulation introduces, compared to Variation No. 3, the ratio between FL and SL conditions of the HEratio parameter. The trend of HEratio as a function of Mach is depicted in Figure 5.18. This parameter oscillates as Mach increases up to Mach 2, then grows uniformly up to Mach 5. On the other hand, the $HEratio_{SL}(T_3)$ fit exponentially increases with increasing T_3, which itself grows with Mach. The result is a decreasing trend of the HEratio ratio between FL and SL conditions as Mach increases up to Mach 2, and approximately constant thereafter, as shown in Figure 6.5. The resulting mathematical formulation is as follows and includes the new exponents that must be subject to optimization.

$$EINO_{FL} = k * EINO_{SL} \left(\frac{p_{3FL}}{p_{3SL}}\right)^{a} \left(\frac{FAR_{FL}}{FAR_{SL}}\right)^{b} \left(\frac{\dot{m}_{HEratioFL}}{\dot{m}_{HEratioSL}}\right)^{f} M^{c}\, e^{H} \tag{6.18}$$

$$\dot{m}_{HEratio} = \frac{\dot{m}_{He}}{\dot{m}_{air\_AC\_inlet}} \tag{6.19}$$

$$HEratio_{SL} = HEratio_{SL}(T_3) \tag{6.20}$$

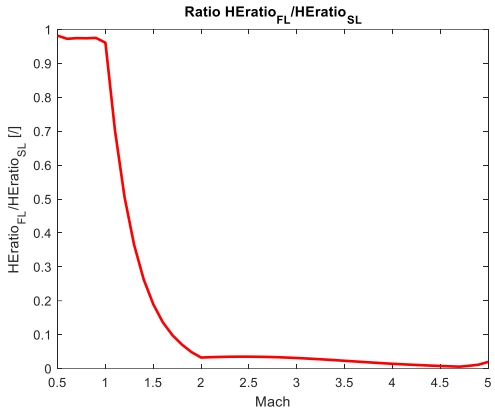

Figure 6.5 - Ratio between Flight Level (FL) and Sea Level (SL) conditions of HEratio as a function of Mach

The HEratio parameter indicates the thermal power developed by the engine and managed by the helium regenerative cycle. An increase in the HEratio corresponds physically to an increase in the flame temperature and thus in NO_x production. Therefore, it is expected a decreasing mathematical contribution of the HEratio ratio between FL and SL conditions as Mach increases up to Mach 2, followed by an increasing contribution up to Mach 5. Since the HEratio ratio between FL and SL conditions has a value less than 1 and follows the trend shown in Figure 6.5, there is no exponent *f* that can ensure a decreasing mathematical contribution as Mach increases up to Mach 2 and then an increasing contribution up to Mach 5. However, a positive coefficient *f* ensures a decreasing contribution as Mach increases up to Mach 2 and a nearly constant contribution between Mach 2 and Mach 5. Therefore, it is expected an optimized positive coefficient *f* to provide physical justification for the trend of the mathematical contribution in the formulation for EINO as Mach increases.

6.2.6 Variation N.6 - EINO as a function of p_3, FAR, Mach, PBratio and WFR

Once the effect of introducing one parameter at a time among the FL/SL ratios of PBratio, WFR, and HEratio has been studied, the analysis proceeds to examine the introduction of a combination of these parameters. The following formulation involves the simultaneous introduction of the FL/SL ratios of PBratio and WFR. As the number of new parameters introduced increases, an improvement in the estimation accuracy of the formulation is expected.

$$EINO_{FL} = k * EINO_{SL} \left(\frac{p_{3FL}}{p_{3SL}}\right)^{a} \left(\frac{FAR_{FL}}{FAR_{SL}}\right)^{b} \left(\frac{\dot{m}_{PBratioFL}}{\dot{m}_{PBratioSL}}\right)^{d} \left(\frac{WFR_{FL}}{WFR_{SL}}\right)^{e} M^{c}\, e^{H} \qquad (6.21)$$

The considerations made earlier regarding the FL/SL ratios, their exponent coefficients, and the resulting assumptions based on the physical-chemical justification of trends remain valid. Therefore, a negative exponent *d* is expected for the FL/SL ratio of PBratio, and a negative exponent *e* for that of WFR. However, it must be considered that the *lsqcurvefit* function in Matlab performs purely mathematical optimization of the exponent coefficients, without taking into account the physical-chemical justifications of the trends. The introduction of an increasing number of parameters in different combinations, characterized by different trends with increasing Mach, may lead to oscillations in the optimized exponents that may not be consistent with the physical-chemical justifications of the trends described earlier. This reasoning applies to all subsequent proposed formulations, and it should be taken into account in the analysis of results in terms of optimized coefficients.

6.2.7 Variation N.7 - EINO as a function of p_3, FAR, Mach, PBratio and HEratio

This formulation proposes the combination of FL/SL ratios of the parameters PBratio and HEratio, according to the following relationship.

$$EINO_{FL} = k * EINO_{SL} \left(\frac{p_{3FL}}{p_{3SL}}\right)^{a} \left(\frac{FAR_{FL}}{FAR_{SL}}\right)^{b} \left(\frac{\dot{m}_{PBratioFL}}{\dot{m}_{PBratioSL}}\right)^{d} \left(\frac{\dot{m}_{HEratioFL}}{\dot{m}_{HEratioSL}}\right)^{f} M^{c}\, e^{H} \qquad (6.22)$$

The considerations made earlier regarding the optimized coefficients *d* and *f* remain valid: a negative exponent *d* is expected for the FL/SL ratio of PBratio, and a positive exponent *f* for that of HEratio. Due to the mathematical optimization performed by Matlab, the values of these coefficients may exhibit oscillations in sign that contradict the provided physical-chemical justifications.

6.2.8 Variation N.8 - EINO as a function of p_3, FAR, Mach, WFR and HEratio

This formulation proposes the combination of FL/SL ratios of the parameters WFR and HEratio, according to the following relationship.

$$EINO_{FL} = k * EINO_{SL} \left(\frac{p_{3FL}}{p_{3SL}}\right)^{a} \left(\frac{FAR_{FL}}{FAR_{SL}}\right)^{b} \left(\frac{WFR_{FL}}{WFR_{SL}}\right)^{e} \left(\frac{\dot{m}_{HEratioFL}}{\dot{m}_{HEratioSL}}\right)^{f} M^{c}\, e^{H} \qquad (6.23)$$

The considerations made earlier regarding the optimized coefficients *e* and *f* remain valid: a negative exponent *e* is expected for the FL/SL ratio of WFR, and a positive exponent *f* for that of HEratio.

6.2.9 Variation N.9 - EINO as a function of p_3, FAR, Mach, WFR, PBratio and HEratio

Finally, the formulation proposing the combination of ratios between FL and SL conditions of all previously introduced parameters is presented. Since this formulation includes the maximum number of parameters, it is expected that the estimation accuracy will be maximized as well.

$$EINO_{FL} = k * EINO_{SL} \left(\frac{p_{3FL}}{p_{3SL}}\right)^a \left(\frac{FAR_{FL}}{FAR_{SL}}\right)^b \left(\frac{\dot{m}_{PBratioFL}}{\dot{m}_{PBratioSL}}\right)^d \left(\frac{WFR_{FL}}{WFR_{SL}}\right)^e \left(\frac{\dot{m}_{HEratioFL}}{\dot{m}_{HEratioSL}}\right)^f M^c \, e^H \qquad (6.24)$$

The considerations made earlier regarding the ratios between FL and SL conditions remain valid. However, the introduction of the maximum number of parameters, while maximizing the expected estimation accuracy, also maximizes the probability of oscillation in the sign of the mathematically optimized exponents.

6.3 New Formulations of the BFFM2 Method

The same procedure proposed for updating the P3T3 method in Chapter 6.2 is now suggested for the Fuel Flow method, particularly for its variant BFFM2. As mentioned earlier, Fuel Flow methods are derived from the P3T3 method and utilize non-proprietary engine data for estimating emissions. These methods are highly useful in cases where specific engine data is difficult to obtain, but they sacrifice estimation accuracy. Therefore, a lower estimation accuracy of NO_x emissions from the SABRE engine compared to that obtained with the new P3T3 formulations is expected, despite undergoing the same process of derivation and introducing the same new parameters. It is possible to summarize the steps for applying the original BFFM2 method outlined in Chapter 4.4.3, adapting them to the derivation of the new formulations. Similarly, the considerations expressed in the previous chapter regarding the choice of Mach number as the independent variable for studying the variables involved in the application of the updated formulations of the FF method remain valid. All the ratios featured in the new formulations of the methods are studied as functions of Mach number since the reference variables, including the fuel flow W_f, are expressed as functions of Mach. The Mach number is selected as the x-axis variable due to its ability to capture punctual variations along the mission profile. Therefore, plotting the input variables at flight level against Mach enables the generalization of the new formulations of the FF method, thanks to its characteristic of not only tracking flight speed but also flight level variation.

As a first step, it is necessary to correct the fuel flow values at FL conditions, obtained from the updated propulsive database as a function of Mach, by applying the following correction to obtain the fuel flow profile at sea level, also as a function of Mach. The mathematical relationships used to perform this

correction are the same as those employed in the original version of the fuel-flow method. The equations are provided below.

$$w_{fSL} = w_{fFL} \frac{\theta_{amb}^{a}}{\delta_{amb}^{b}} \exp\left(c * M^{d}\right) \tag{6.25}$$

$$\theta_{amb} = T_{amb}[K]/288.15 \tag{6.26}$$

$$\delta_{amb} = p_{amb}[Pa]/101325 \tag{6.27}$$

The trend of the fuel flow profile at sea level, evaluated using the exponent coefficients indicated for the classical formulation of the BFFM2, exhibits an exponential increase with rising Mach numbers, as depicted in Figure 6.6 (*a*). Consequently, an initial correction is undertaken by recalculating the exponents of the original mathematical formulation through Matlab's function *lsqcurvefit.* Given the absence of a standardized sea level fuel flow reference, a linear fit is created by interpolating the first 4 fuel flow values corresponding to Mach conditions ranging from 0.1 to 0.4, representing the engine's operation at sea level altitudes. This fit is depicted in Figure 6.6 (*b*) alongside the values of W_{fSL} from the updated propulsive database corresponding to sea level conditions. Evaluating the value of this linear fit for each Mach condition from 0.1 to 5, it is possible to recalculate the exponents *a, b, c* and *d* using curve fitting. The original and updated exponents are listed in Table 6.5. The profile of W_{fSL} as a function of Mach resulting from the application of the W_{fFL} correction with the updated coefficients is presented in Figure 6.6 (*c*).

	a	**b**	**c**	**d**
Original w_{fSL}= f(θ_{amb}, δ_{amb}, M)	3.8	1	0.2	2
Updated w_{fSL}= f(θ_{amb}, δ_{amb}, M)	0.0084	0.0207	0.0089	1.4917

Table 6.5 - Original and updated exponents for fuel flow correction

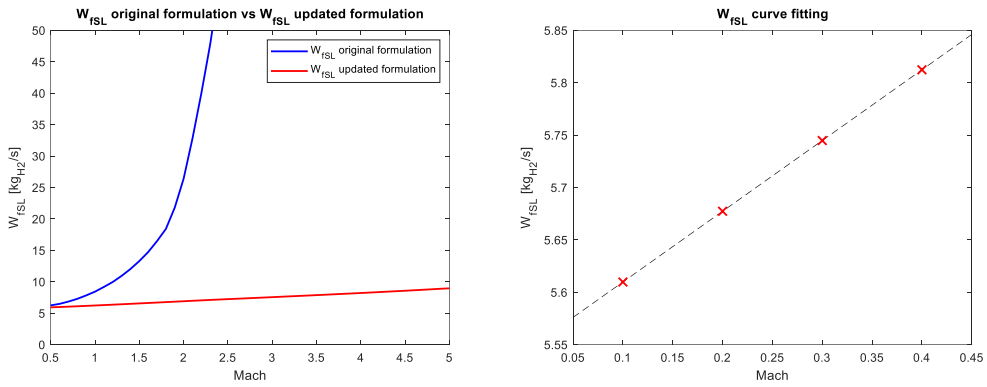

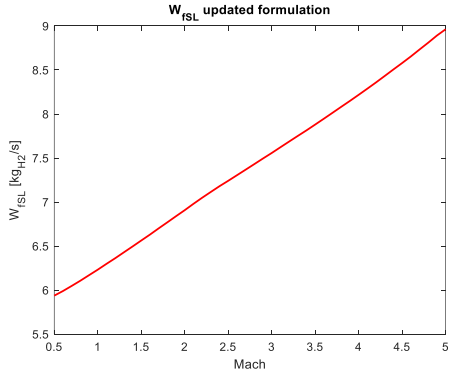

Figure 6.6 – a) W_{fSL} profile from original and updated fuel flow correction as a function of Mach, b) W_{fSL} linear fit as a function of Mach, c) W_{fSL} profile from updated fuel flow correction as a function of Mach

Table 6.6 reports the absolute and relative errors of the interpolation of Sea Level fuel flow values as a function of Mach reported in Figure 6.6 (*b*). Based on the results of this interpolation, the coefficients appearing in the relation for correcting the Fuel Flow at FL to obtain that at SL are updated.

Mach	**W_{fSL} fitting absolute error**	**W_{fSL} fitting relative error**
0,1	3,20E-01	5,71E-02
0,2	3,20E-01	5,64E-02
0,3	3,07E-01	5,35E-02
0,4	2,88E-01	4,96E-02

Table 6.6 - W_{fSL} interpolation absolute and relative errors at SL conditions

Following this correction, $EINO_{SL}$, FAR_{SL}, $PBratio_{SL}$, WFR_{SL}, and $HEratio_{SL}$ obtained from the updated propulsive and emissive databases for the first four Mach conditions, corresponding to sea level conditions due to the contained altitude and reported in Table 6.1, are curve-fitted as a function of the corrected W_{fSL} from the preceding step. For the SABRE engine, reference sea level conditions as a function of the corrected fuel flow at sea level conditions can be mathematically expressed with the following equations:

$$FAR_{SL} = 0.002559 * W_{fSL} + 0.05832 \quad (6.28)$$

$$PBratio_{SL} = 10^{-17} * W_{fSL} + 0.5 \quad (6.29)$$

$$WFR_{SL} = -0.09693 * W_{fSL} + 2.768 \quad (6.30)$$

$$HEratio_{SL} = -0.0301 * W_{fSL} + 0.3875 \quad (6.31)$$

$$EINO_{SL} = 0.4471 * W_{fSL} + 16.83 \quad (6.32)$$

In this case, differently from the update process for the P3T3 method, only linear interpolation is used for the fits in SL conditions of all introduced parameters as functions of the corrected fuel flow. The trends of these fits are graphed in Figure 6.7, alongside the values of the parameters from updated propulsive and emissive databases corresponding to the sea level conditions that generated these fits.

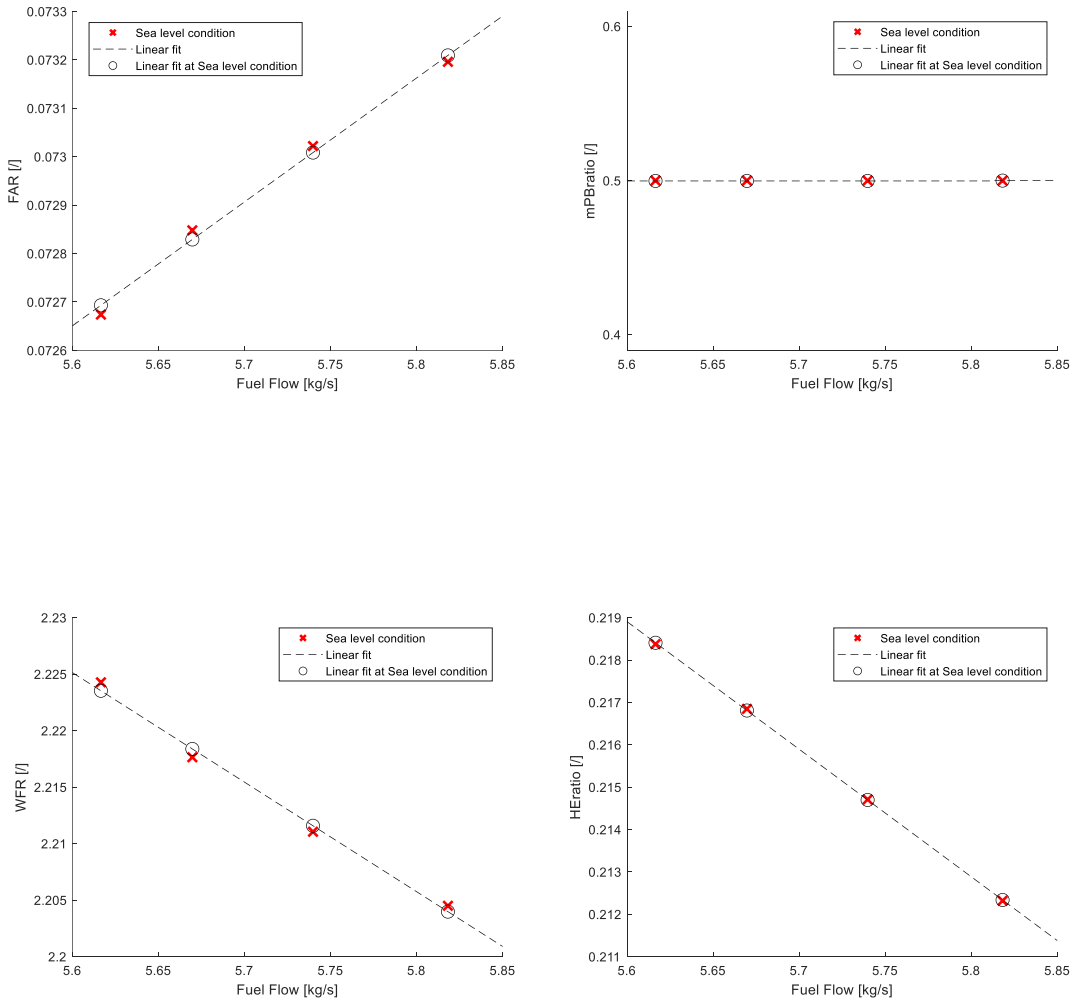

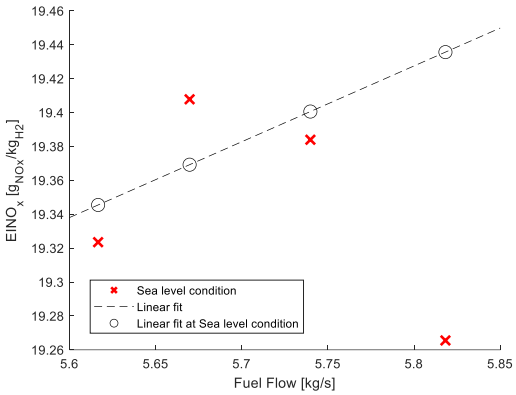

Figure 6.7 - Sea level conditions as a function of the corrected fuel flow, in terms of a) Fuel to Air Ratio, b) air mass flow rate PB ratio, c) Water to Fuel Ratio at the inlet of the combustion chamber, d) Helium-air mass flow rate HEratio, e) NO Emission Index

Table 6.7 and Table 6.8 respectively report the absolute and relative errors of the interpolation of Sea Level parameter values.

Mach	**FAR**	**PBratio**	**WFR**	**HEratio**	**EINO**
[/]	[/]	[/]	[/]	[/]	[g_{NO}/kg_{H2}]
0,1	1,91E-05	-5,55E-17	-7,47E-04	3,26E-05	2,19E-02
0,2	-1,89E-05	-5,55E-17	7,35E-04	-3,83E-05	-3,86E-02
0,3	-1,35E-05	-5,55E-17	5,30E-04	-1,15E-05	1,66E-02
0,4	1,32E-05	0,00E+00	-5,17E-04	1,71E-05	1,70E-01

Table 6.7 - Interpolation absolute errors at SL conditions

Mach	**FAR**	**PBratio**	**WFR**	**HEratio**	**EINO**
[/]	[/]	[/]	[/]	[/]	[/]
0,1	2,64E-04	-1,11E-16	-3,36E-04	1,49E-04	1,14E-03
0,2	-2,59E-04	-1,11E-16	3,31E-04	-1,76E-04	-1,99E-03
0,3	-1,84E-04	-1,11E-16	2,40E-04	-5,35E-05	8,58E-04
0,4	1,80E-04	0,00E+00	-2,35E-04	8,05E-05	8,83E-03

Table 6.8 - Interpolation absolute errors at SL conditions

Once the fits for Sea Level conditions are obtained, the subsequent step involves deriving the values of the same parameters under Flight Level conditions, namely FAR_{FL}, $PBratio_{FL}$, WFR_{FL}, and $HEratio_{FL}$ through propulsion modelling. These values are contained in Table 6.2 as functions of Mach. Based on the values of W_{fSL} for a given Mach condition, it becomes possible to derive the values of FAR_{SL}, $Pbratio_{SL}$, WFR_{SL}, $Heratio_{SL}$, and $EINO_{SL}$ using the fits obtained previously. Once these parameters are determined, as the FF method operates as a ratio method, ratios between Flight Level and Sea Level conditions need to be constructed, as they are incorporated into the mathematical formulation of the method.

Finally, the new mathematical formulation of the method can be applied to evaluate the $EINO_{FL}$ starting from the appropriately corrected $EINO_{SL}$, considering the evolution of the free-stream pressure ratio with respect to the standard SL reference δ, the free-stream temperature ratio with respect to the standard SL reference θ, the humidity factor, and one or more of the newly introduced parameters. Regarding the new mathematical formulations, described in the following subsections, the approach used differs slightly from that adopted for updating the original version of the P3T3. In the case of the FF method, the number of combinations of new parameters introduced is greater than that of the P3T3 update, as the original version of the BFFM2 does not even include FAR. For this reason and considering the lower estimation accuracy of the FF method compared to the P3T3, it is decided to bypass the first step of optimizing the exponent coefficients of the original formulation. In the first proposed updated formulation, the factor $k * M^d$ is directly added to account for the effect of high speed on NO_x formation. The initial optimization of the coefficients is conducted while also considering the factor $k * M^d$. From this point onwards, initially, only one ratio between FL and SL conditions of the parameters FAR, PBratio, WFR, and HEratio is added, re-optimizing the exponents. Subsequently, new formulations are proposed in which two ratios between FL and SL conditions of the parameters FAR, PBratio, WFR, and HEratio are included. Finally, a complete formulation is proposed that encompasses all the ratios between FL and SL conditions, with their respective exponents optimized. All the optimization procedures described above are performed using the built-in function *lsqcurvefit* in Matlab taking the EINO from emissive database as reference. Alongside the new mathematical formulations, the trends of the ratios contained therein as functions of Mach are presented below. Additionally, a brief discussion regarding the mathematical contribution of the parameters contained in the formulations in relation to their physical-chemical contribution in the NO_x formation process is provided. Based on this discussion, considerations are made on the exponent coefficients introduced for the parameters and their role in ensuring physical-chemical justification for the mathematical contribution of the parameters in the formulations. The optimized coefficients and the results of the new formulations are reported and further discussed in Chapter 7. Please note that, since the mass fractions of nitrogen oxides other than NO have been considered negligible during the emissive modelling phase in the evaluation of engine emission indices, the following discussion is specialized for estimating the EINO. Considering that most of NO_x produced consists of NO, it is possible, as a first approximation, to consider the overall $EINO_x$ coinciding with the EINO.

6.3.1 Variation N.1 – EINO as a function of δ_{amb}, θ_{amb} and Mach

The first variation involves introducing the factor $k * M^d$ and optimizing all the exponent coefficients *a, b, c*, and *d* associated with the parameters appearing in the formulation. The mathematical formulation is reported below, along with the graphs of the parameters appearing therein as functions of Mach. Additionally, a brief discussion regarding the exponents in relation to the physical-chemical justification of their values is provided. These values are updated using the built-in function *lsqcurvefit* in Matlab.

$$EINO_{FL} = k * EINO_{SL} \left(\frac{\delta_{amb}^{a}}{\theta_{amb}^{b}}\right)^{c} M^{d}\, e^{H} \qquad (6.33)$$

$$EINO_{SL} = EINO_{SL}(W_{fSL}) \tag{6.34}$$

$$\delta_{amb} = p_{amb}[Pa]/101325 \tag{6.35}$$

$$\theta_{amb} = T_{amb}[K]/288.15 \tag{6.36}$$

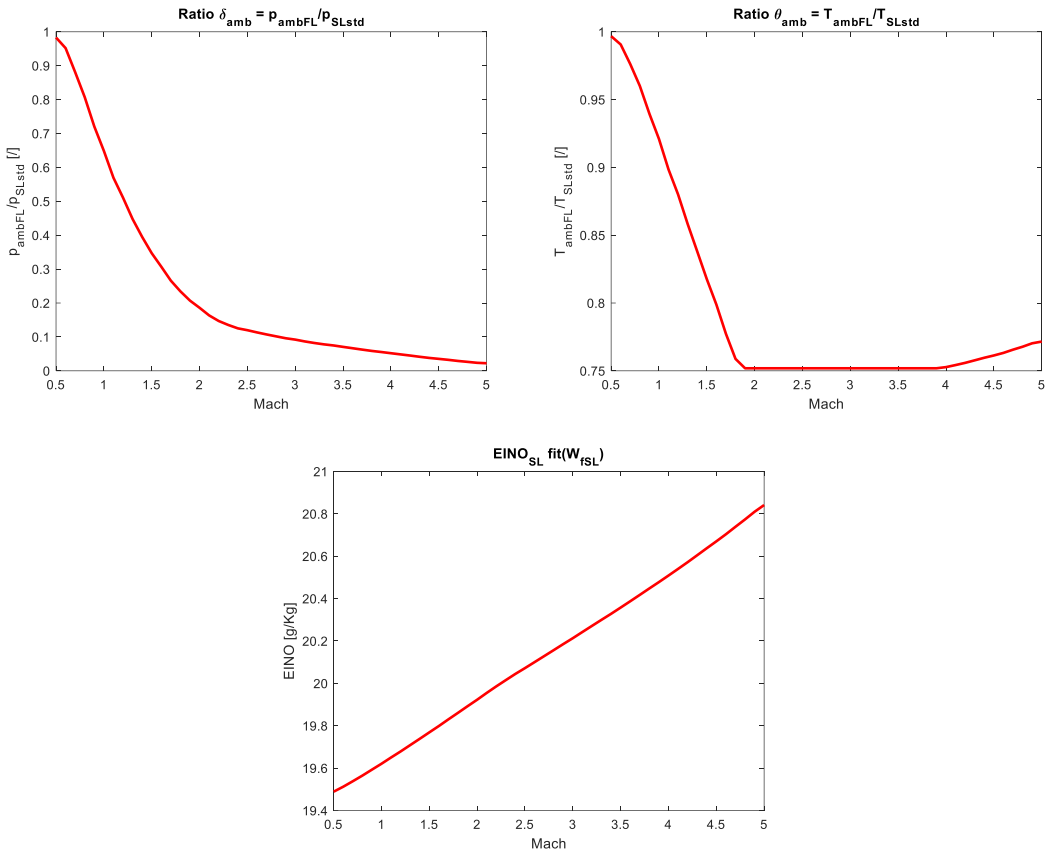

Figure 6.8 – As a function of Mach: a) Ratio between Flight Level (FL) and Standard Sea Level (SL) conditions of ambient pressure (p_{amb}), b) Ratio between Flight Level (FL) and Standard Sea Level (SL) conditions of ambient temperature (T_{amb}), c) $EINO_{SL}(W_{fSL})$

For the ratios between Flight Level (FL) and Standard Sea Level (SL) conditions of pressure and temperature, they are plotted directly as functions of Mach since it is possible to evaluate them given the mission profile as a function of Mach using the Matlab function '*atmosisa*,' which refers to the International Standard Atmosphere model. As altitude increases with Mach, and consequently pressure and temperature tend to decrease, the corresponding ratios between FL and Standard SL conditions also tend to decrease with increasing Mach. As Mach increases, a decrease in atmospheric pressure due to the increase in altitude ideally results in a decrease in the pressure reached in the combustion chamber and thus a decrease in the flame temperature and consequently in the NO_x produced. Therefore, it is expected that as Mach increases, the mathematical contribution of the pressure ratio δ in the formulation for EINO decreases. Since this ratio is less than 1 and exhibits a decreasing trend as a function of Mach, the combined effect of the exponents a and c must be positive to ensure physical justification for the contribution. Similarly, concerning the ambient temperature, as Mach number increases, it tends to decrease, leading ideally to a reduction in the

flame temperature in the combustion chamber and consequently the NO_x produced. Specifically, referring to the trend of the temperature ratio θ reported in Figure 6.8 (*b*), it is expected that as Mach increases from Mach 0.5 to Mach 4, the mathematical contribution of the temperature ratio θ in the formulation for EINO decreases. For Mach between 4 and 5, however, the ambient temperature slightly increases, as does the corresponding ratio, and therefore a slight increase in the mathematical contribution of the ratio in the EINO formulation is expected. Considering the temperature ratio value less than 1, its trend in Figure 6.8 (*b*), and its position as the denominator in the mathematical formulation, it is necessary for the combined effect of exponents *b* and c to be negative to ensure physical justification for this contribution. Regarding the trend as a function of Mach of $EINO_{SL}$ fit evaluated corresponding to the fuel flow at SL obtained previously, it is the result of the combined effect of the increasing trend of the fuel flow as a function of Mach graphed in Figure 6.6 (*c*) and the increasing trend of the $EINO_{SL}$ fit as W_{fSL} increases, graphed in Figure 6.7 (*e*). This trend of $EINO_{SL}$ is corrected through the factors δ, θ, and Mach to obtain the trend of $EINO_{FL}$ through the proposed mathematical formulation.

6.3.2 Variation N.2 – EINO as a function of δ_{amb}, θ_{amb} , Mach and FAR

Starting from this new formulation, a single ratio between FL and SL conditions is added at a time among those of the parameters FAR, PBratio, WFR, and HEratio. In particular, this second variation involves introducing the ratio between FAR_{FL} and the data resulting from the fit $FAR_{SL}(W_{fSL})$. The mathematical formulation is reported below, followed by the representation of the ratio relative to FAR as a function of Mach.

$$EINO_{FL} = k * EINO_{SL} \left(\frac{\delta_{amb}^{a}}{\theta_{amb}^{b}}\right)^{c} \left(\frac{FAR_{FL}}{FAR_{SL}}\right)^{i} M^{d}\, e^{H} \tag{6.37}$$

$$FAR_{SL} = FAR_{SL}(W_{fSL}) \tag{6.38}$$

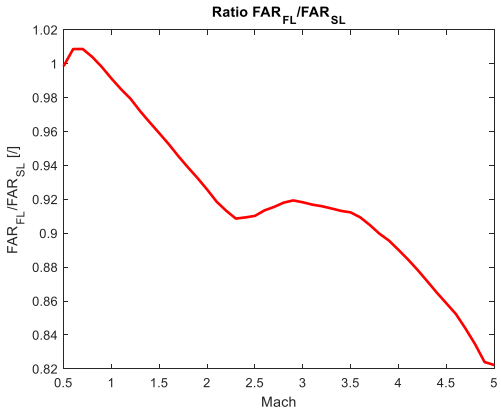

Figure 6.9 - Ratio between Flight Level (FL) and Sea Level (SL) conditions of FAR, as a function of Mach

The variation in the FAR ratio between FL and SL conditions as a function of Mach results from the combined effects of the increasing trend of FAR_{FL} with Mach, as depicted in Figure 5.17 (*b*), and the rising trend of the FAR_{SL} fit with increasing W_{fSL}, shown in Figure 6.7 (*a*). Specifically, the trend of FAR_{FL} is

inverse to that of the corresponding ratio between FL and SL conditions as Mach varies. As Mach increases, FAR_{FL} increases, while the FAR ratio between FL and SL conditions decreases. An increase in FAR_{FL} ideally corresponds to a rise in the fraction of H_2 in the combustion chamber. Due to the fuel-rich conditions during combustion, this increase in the H_2 fraction leads to a decrease in the flame temperature, resulting in reduced NO_x emissions. Consequently, as Mach and FAR increase, a decreasing mathematical contribution is expected in the formulation for $EINO_{FL}$ regarding the FAR ratio between FL and SL conditions. Given the FAR ratio's value being less than unity and its decreasing trend with increasing Mach, ensuring consistency with the physical processes necessitates a positive coefficient *i* for the FAR ratio. The considerations made in the previous section regarding the other parameters featured in the formulation remain applicable to this and subsequent proposed formulations.

6.3.3 Variation N.3 – EINO as a function of δ_{amb}, θ_{amb} , Mach and PBratio

The third modification involves introducing the ratio between $PBratio_{FL}$ and the linear fit $PBratio_{SL}(W_{fSL})$, starting from the updated formulation including Mach. Notably, the $PBratioSL(W_{fSL})$ fit remains constant and equal to 0.5, as observed in Figure 6.7 (*b*), reflecting the constancy of PBratio as W_{fSL} increases up to the Mach 1 condition. Consequently, the trend of this ratio between FL and SL conditions perfectly mirrors that of the original parameter PBratio as a function of Mach. This correlation becomes apparent when comparing the trend of the ratio between FL and SL conditions, as shown in Figure 6.10, with the trend of the original parameter PBratio, as depicted in Figure 5.17 (*a*). The mathematical formulation is reported below, followed by the representation of the ratio relative to PBratio as a function of Mach.

$$EINO_{FL} = k * EINO_{SL} \left(\frac{\delta_{amb}^{a}}{\theta_{amb}^{b}}\right)^{c} \left(\frac{\dot{m}_{PBratioFL}}{\dot{m}_{PBratioSL}}\right)^{i} M^{d}\, e^{H} \tag{6.39}$$

$$\dot{m}_{PBratioSL} = \dot{m}_{PBratioSL}(W_{fSL}) \tag{6.40}$$

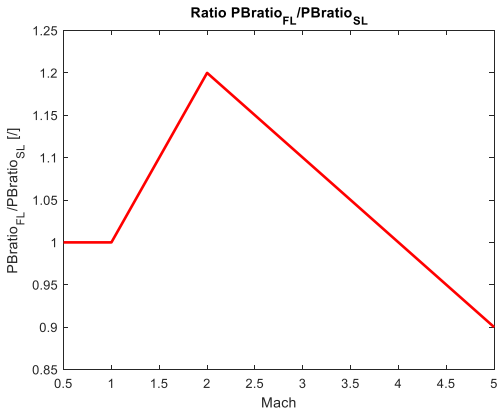

Figure 6.10 - Ratio between Flight Level (FL) and Sea Level (SL) conditions of PBratio, as a function of Mach

The trend of this ratio between FL and SL conditions increases up to Mach 2 and then decreases until Mach 5. Furthermore, the value of this ratio oscillates as Mach increases, being greater than 1 until Mach 4 and then less than 1 until Mach 5. With an increase in $PBratio_{FL}$, and therefore the corresponding ratio between FL and SL conditions, a decrease in NO_x production is expected as the combustion segmentation between the two combustion stages increases, leading to a decrease in the flame temperature reached in the main combustion chamber. Additionally, as PBratio increases, WFR also increases, leading to another reason for the decrease in the flame temperature and hence in NO_x. The contribution of the ratio between FL and SL conditions must therefore decrease as Mach increases up to Mach 2 and then increase until Mach 5. For the mathematical contribution of the PBratio ratio to have physical-chemical justification, the coefficient *i* must be negative.

6.3.4 Variation N.4 – EINO as a function of δ_{amb}, θ_{amb}, Mach and WFR

This new formulation introduces, compared to Variation No. 1, the ratio between FL and SL conditions of the WFR parameter. The trend of WFR as a function of Mach is shown in Figure 5.16 (*c*) and is almost identical to that of PBratio shown in Figure 5.17 (*a*). In fact, as the air flow rate into the PB increases, the amount of H_2O produced during this combustion stage increases, consequently increasing the mass fraction of H_2O entering the main CC and thus the WFR. Specifically, WFR_{FL} slightly decreases with increasing Mach up to Mach 1, then increases until Mach 2, and finally decreases until Mach 5. On the other hand, the linear fit $WFR(W_{fSL})$ uniformly decreases with increasing W_{fSL}, which increases uniformly with Mach. The result of these two trends is the trend of the WFR ratio between FL and SL conditions as shown in Figure 6.11. The trend of the WFR ratio between FL and SL conditions is therefore almost identical to that of WFR_{FL} as Mach increases. The resulting mathematical formulation is as follows and includes the new exponents that must be subject to optimization.

$$EINO_{FL} = k * EINO_{SL} \left(\frac{\delta_{amb}^{a}}{\theta_{amb}^{b}}\right)^{c} \left(\frac{WFR_{FL}}{WFR_{SL}}\right)^{i} M^{d}\, e^{H} \tag{6.41}$$

$$WFR_{SL} = WFR_{SL}(W_{fSL}) \tag{6.42}$$

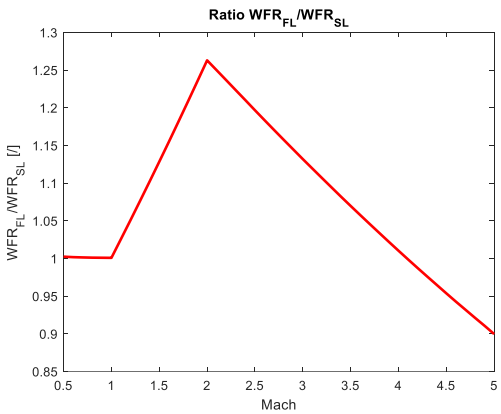

Figure 6.11 - Ratio between Flight Level (FL) and Sea Level (SL) conditions of WFR, as a function of Mach

The water vapor generated during combustion in the PB contributes to the combustion process in the main CC in three ways: thermal regulation, oxygen deficiency, and chemical reactions. The thermal contribution predominates over contributions related to water reaction in the chamber. Consequently, an increase in WFR generally leads to a decrease in flame temperature and thus a decrease in NO_x production. Considering the trend of WFR as a function of Mach and its effect on NO_x formation, it can be concluded that the mathematical contribution of the WFR ratio between FL and SL conditions in the formulation for EINO should decrease with increasing Mach up to Mach 2 and then increase from Mach 2 to Mach 5. The WFR ratio between FL and SL conditions is greater than 1 except for Mach conditions close to 5, and it mirrors the trend of WFR_{FL} as Mach increases. Considering that this ratio follows the trend of WFR_{FL}, a negative exponent *i* is expected to maintain consistency with the physical processes. A negative exponent *i* leads to a decreasing mathematical contribution with increasing Mach from Mach 1 until Mach 2, followed by an increasing contribution from Mach 2 to Mach 5 in the EINO formulation. These contributions to the increase in estimated EINO, as described with increasing Mach, has physical-chemical justification.

6.3.5 Variation N.5 – EINO as a function of δ_{amb}, θ_{amb}, Mach and HEratio

This new formulation introduces the ratio between FL and SL conditions of the HEratio parameter, compared to Variation No. 1. The trend of HEratio as a function of Mach is depicted in Figure 5.18. This parameter oscillates as Mach increases up to Mach 2, then grows uniformly up to Mach 5. Conversely, the $HEratio_{SL}(W_{fSL})$ fit decreases linearly with increasing W_{fSL}, which itself increases with Mach. The result is a uniformly increasing trend of the HEratio ratio between FL and SL conditions as Mach increases from Mach 0.5 to Mach 5, as shown in Figure 6.12. The resulting mathematical formulation includes the new exponents that must be subject to optimization.

$$EINO_{FL} = k * EINO_{SL} \left(\frac{\delta_{amb}^{a}}{\theta_{amb}^{b}}\right)^{c} \left(\frac{\dot{m}_{HEratioFL}}{\dot{m}_{HEratioSL}}\right)^{i} M^{d}\, e^{H} \tag{6.43}$$

$$\dot{m}_{HEratioSL} = \dot{m}_{HEratioSL}(W_{fSL}) \tag{6.44}$$

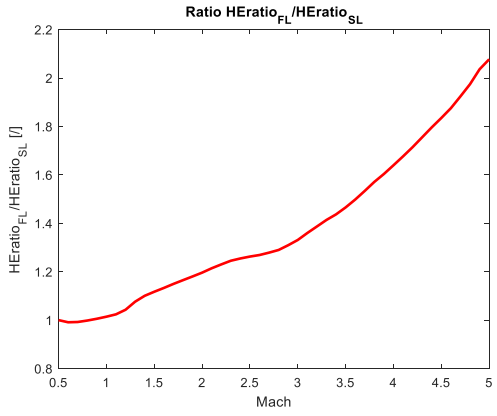

Figure 6.12 - Ratio between Flight Level (FL) and Sea Level (SL) conditions of HEratio, as a function of Mach

The HEratio parameter indicates the thermal power developed by the engine and managed by the helium regenerative cycle. An increase in the HEratio corresponds physically to an increase in the flame temperature and thus in NO_x production. Therefore, it is expected a slightly decreasing mathematical contribution of the HEratio ratio between FL and SL conditions as Mach increases up to Mach 2, followed by a growing contribution. Since the HEratio ratio between FL and SL conditions has a value less than 1 and follows the trend shown in Figure 6.12, a positive coefficient *i* ensures a slightly increasing contribution as Mach increases up to Mach 2 and a growing contribution between Mach 2 and Mach 5. Therefore, an optimized positive coefficient *i* is expected to provide physical justification for the trend of the mathematical contribution in the formulation for EINO as Mach increases.

6.3.6 Variation N.6 - EINO as a function of δ_{amb}, θ_{amb}, Mach, PBratio and FAR

Once the effect of introducing one parameter at a time among the FL/SL ratios of FAR, PBratio, WFR, and HEratio has been studied, the analysis proceeds to examine the introduction of a combination of these parameters. The following formulation involves the simultaneous introduction of the ratios between FL and SL conditions of PBratio and FAR. As the number of new parameters introduced increases, an improvement in the estimation accuracy of the formulation is expected.

$$EINO_{FL} = k * EINO_{SL} \left(\frac{\delta_{amb}^{a}}{\theta_{amb}^{b}}\right)^{c} \left(\frac{\dot{m}_{PBratioFL}}{\dot{m}_{PBratioSL}}\right)^{p} \left(\frac{FAR_{FL}}{FAR_{SL}}\right)^{q} M^{d}\, e^{H} \qquad (6.45)$$

The considerations made earlier regarding the ratios between FL and SL conditions, their exponent coefficients, and the resulting assumptions based on the physical-chemical justification of trends remain valid. Therefore, a negative exponent *p* is expected for the FL/SL ratio of PBratio, and a positive exponent *q* for that of FAR. However, it is essential to consider the purely mathematical nature of the exponent optimization carried out by the Matlab function *lsqcurvefit*. The introduction of an increasing number of parameters in different combinations, characterized by different trends with increasing Mach, may lead to oscillations in the sign of the optimized exponents that may not be consistent with the physical-chemical justifications of the trends described earlier. This reasoning applies to all subsequent proposed formulations, and it should be taken into account in the analysis of results in terms of optimized coefficients.

6.3.7 Variation N.7 - EINO as a function of δ_{amb}, θ_{amb}, Mach, PBratio and WFR

The following formulation involves the simultaneous introduction of the ratios between FL and SL conditions of PBratio and WFR.

$$EINO_{FL} = k * EINO_{SL} \left(\frac{\delta_{amb}^{a}}{\theta_{amb}^{b}}\right)^{c} \left(\frac{\dot{m}_{PBratioFL}}{\dot{m}_{PBratioSL}}\right)^{p} \left(\frac{WFR_{FL}}{WFR_{SL}}\right)^{q} M^{d}\, e^{H} \qquad (6.46)$$

The considerations made earlier regarding the optimized coefficients of the ratios between FL and SL conditions for the parameters PBratio and WFR remain valid. Therefore, a negative exponent *p* is expected for the FL/SL ratio of PBratio, and a negative exponent *q* for that of WFR.

6.3.8 Variation N.8 – EINO as a function of δ_{amb}, θ_{amb}, Mach, PBratio and HEratio

The following formulation involves the simultaneous introduction of the ratios between FL and SL conditions of PBratio and HEratio.

$$EINO_{FL} = k * EINO_{SL} \left(\frac{\delta_{amb}^{a}}{\theta_{amb}^{b}}\right)^{c} \left(\frac{\dot{m}_{PBratioFL}}{\dot{m}_{PBratioSL}}\right)^{p} \left(\frac{\dot{m}_{HEratioFL}}{\dot{m}_{HEratioSL}}\right)^{q} M^{d}\, e^{H} \qquad (6.47)$$

The considerations made earlier regarding the optimized coefficients of the ratios between FL and SL conditions for the parameters PBratio and HEratio remain valid. Therefore, a negative exponent *p* is expected for the FL/SL ratio of PBratio, and a positive exponent *q* for that of HEratio.

6.3.9 Variation N.9 - EINO as a function of δ_{amb}, θ_{amb}, Mach, FAR and HEratio

The following formulation involves the simultaneous introduction of the ratios between FL and SL conditions of FAR and HEratio.

$$EINO_{FL} = k * EINO_{SL} \left(\frac{\delta_{amb}^{a}}{\theta_{amb}^{b}}\right)^{c} \left(\frac{FAR_{FL}}{FAR_{SL}}\right)^{p} \left(\frac{\dot{m}_{HEratioFL}}{\dot{m}_{HEratioSL}}\right)^{q} M^{d}\, e^{H} \qquad (6.48)$$

The considerations made earlier regarding the optimized coefficients of the ratios between FL and SL conditions for the parameters FAR and HEratio remain valid. Therefore, a positive exponent *p* is expected for the FL/SL ratio of FAR, and a positive exponent *q* for that of HEratio.

6.3.10 Variation N.10 - EINO as a function of δ_{amb}, θ_{amb}, Mach, FAR and WFR

The following formulation involves the simultaneous introduction of the ratios between FL and SL conditions of FAR and WFR.

$$EINO_{FL} = k * EINO_{SL} \left(\frac{\delta^a_{amb}}{\theta^b_{amb}}\right)^c \left(\frac{FAR_{FL}}{FAR_{SL}}\right)^p \left(\frac{WFR_{FL}}{WFR_{SL}}\right)^q M^d \, e^H \quad (6.49)$$

The considerations made earlier regarding the optimized coefficients of the ratios between FL and SL conditions for the parameters FAR and WFR remain valid. Therefore, a positive exponent p is expected for the FL/SL ratio of FAR, and a negative exponent q for that of WFR.

6.3.11 Variation N.11 - EINO as a function of δ_{amb}, θ_{amb}, Mach, HEratio and WFR

The following formulation involves the simultaneous introduction of the ratios between FL and SL conditions of HEratio and WFR.

$$EINO_{FL} = k * EINO_{SL} \left(\frac{\delta^a_{amb}}{\theta^b_{amb}}\right)^c \left(\frac{\dot{m}_{HEratioFL}}{\dot{m}_{HEratioSL}}\right)^p \left(\frac{WFR_{FL}}{WFR_{SL}}\right)^q M^d \, e^H \quad (6.50)$$

The considerations made earlier regarding the optimized coefficients of the ratios between FL and SL conditions for the parameters HEratio and WFR remain valid. Therefore, a positive exponent p is expected for the FL/SL ratio of HEratio, and a negative exponent q for that of WFR.

6.3.12 Variation N.12 – EINO as a function of δ_{amb}, θ_{amb}, Mach, HEratio, WFR, FAR and PBratio

The final updated mathematical formulation, which integrates the combined ratios between FL and SL conditions of all previously introduced parameters, is presented below. By incorporating the maximum number of parameters, the estimation accuracy is anticipated to be optimized accordingly.

$$EINO_{FL} = k * EINO_{SL} \left(\frac{\delta^a_{amb}}{\theta^b_{amb}}\right)^c \left(\frac{\dot{m}_{HEratioFL}}{\dot{m}_{HEratioSL}}\right)^r \left(\frac{WFR_{FL}}{WFR_{SL}}\right)^s \left(\frac{FAR_{FL}}{FAR_{SL}}\right)^t \left(\frac{\dot{m}_{PBratioFL}}{\dot{m}_{PBratioSL}}\right)^u M^d \, e^H \quad (6.51)$$

The previously discussed considerations regarding the ratios between FL and SL conditions remain applicable. However, with the introduction of the maximum number of parameters, aimed at optimizing estimation accuracy, the probability of oscillation in the sign of the mathematically optimized exponents is maximized.

Chapter 7 - Results and Discussion

7.1 NO_x Emission Index from 0D Kinetic-Chemical Simulations

As outlined in Chapters 5.2 and 5.3 dedicated to the recalculation of propulsive and emissive databases, two sets of EINO can be evaluated based on the mass fractions resulting from two different combustion modelling approaches for the main combustion chamber performed using the two interfaces of the Cantera software. Specifically, the Matlab interface of Cantera integrated into the Matlab propulsion model allows for the evaluation of flame temperature, pressure, and mass fraction of the combustion gas mixture under chemical equilibrium conditions. Conversely, the Python interface of Cantera enables conducting 0D kinetic-chemical simulations of the combustion process, thereby deriving the same thermochemical parameters. However, in this case, these parameters are evaluated as a result of a succession of equilibrium states reached in the chamber over time, and thus are also representative of the kinetics of the combustion process. Starting from the mass fractions resulting from these two modelling approaches, it is possible to derive two distinct sets of EINO, whose reliability is directly influenced by the characteristics of the modelling that generated them. Additional considerations regarding the two modelling strategies, chemical equilibrium, and chemical kinetic simulations can be made based on the information provided in [34], [35], and [38]. Consider a closed chemical system under certain initial conditions of temperature and pressure, denoted by T and P, respectively. Since the system is closed, the quantities of elements present in the system remain constant. However, the quantities of species can vary due to chemical reactions. The closed chemical system reaches a state of chemical equilibrium when the rates of forward and reverse reactions among all possible species are balanced i.e., the net rates of reactions are zero. This equilibrium state corresponds to a minimum Gibbs energy state according to thermodynamics, independent of kinetic considerations. Therefore, the equilibrium problem can be formulated as a mathematical problem where the unknowns are the quantities of species that minimize the Gibbs energy of the system at the given temperature T, pressure P, and elemental quantities. The Gibbs energy minimization problem is a constrained optimization problem. The presence of phases containing multiple species and the intricate relationship between species activities and species quantities make the Gibbs energy minimization problem nonlinear and thus more challenging to solve. The linear equality constraints correspond to the mass-balance equations enforcing the closed-system constraint. The inequality constraints ensure that the equilibrium quantities of each species are non-negative. These constraints, coupled with the nonlinear behaviour of the Gibbs energy function, render the chemical equilibrium problem considerably complex. On the other hand, concerning chemical kinetic simulations, they represent the study of how the composition of a chemical system changes over time as a result of chemical reactions. Thus, chemical kinetic calculations are usually conducted to gain deeper insights into the behaviour of a chemical system, specifically how its state evolves over time, when the use of chemical equilibrium calculations alone is insufficient. The possibility of a more detailed transient description of a chemical system necessitates a greater understanding of the underlying chemical reaction

mechanisms involved. Additionally, more input data are required for modelling chemical kinetics than for modelling chemical equilibrium. In equilibrium reactions, only their equilibrium constants are needed to fully determine the chemical state of the system, whereas for reactions not in equilibrium, i.e., reactions controlled by kinetics, many more parameters are necessary to compute their rates, such as a rate constant at some reference temperature and activation energy, or other conditions. Initially, describing the combustion process based on the determination of the equilibrium state of a chemical reaction system can be considered accurate. Indeed, if it is assumed that the chemical reactions occur rapidly compared to other processes like diffusion, heat conduction, and flow, thermodynamics alone allows for the description of the system both globally and locally. However, in most cases, chemical reactions are characterized by time scales comparable to those of flow and molecular transport processes. Therefore, information about the rate of chemical reactions, i.e., chemical kinetics, is required. For this reason, kinetic EINO evaluations obtained through Cantera Python are utilized as a reference in the modification process of the FF and P3T3 methods. Table 7.1 reports both sets of EINO compared with those from the original emissive database. A discussion regarding the trends of the two sets of EINO from the updated database, depicted in Figure 7.1, is also provided. Starting from the comparison between the two sets of EINO, the motivations that prompted the selection of the kinetic EINO set as the reference for updating the estimation methods of NO_x emissions are highlighted.

Mach	**EINO original database**	**EINO updated Database**	
	EINO Cantera Python (kinetic-chemical simulations)	EINO Cantera Matlab (chemical equilibrium)	EINO Cantera Python (kinetic-chemical simulations)
0.1	1,80E+00	2,07E-02	1,93E+01
0.2	1,79E+00	2,03E-02	1,94E+01
0.3	1,79E+00	2,00E-02	1,94E+01
0.4	1,78E+00	1,98E-02	1,93E+01
0,5	1,79E+00	1,97E-02	1,92E+01
0,6	1,75E+00	1,95E-02	1,92E+01
0,7	1,75E+00	1,91E-02	1,92E+01
0,8	1,75E+00	1,87E-02	1,92E+01
0,9	7,12E-01	1,82E-02	1,93E+01
1	7,10E-01	1,81E-02	1,92E+01
1,1		1,77E-02	1,82E+01
1,2		1,73E-02	1,73E+01
1,3		1,71E-02	1,64E+01
1,4		1,68E-02	1,56E+01
1,5	5,37E-01	1,66E-02	1,48E+01
1,6		1,64E-02	1,41E+01
1,7		1,63E-02	1,34E+01
1,8		1,62E-02	1,28E+01
1,9		1,64E-02	1,21E+01
2	8,57E-01	1,68E-02	1,16E+01
2,1		1,76E-02	1,16E+01
2,2		1,85E-02	1,16E+01
2,3		1,95E-02	1,18E+01
2,4		2,06E-02	1,18E+01

2,5	4,38E-01	2,19E-02	1,19E+01
2,6		2,33E-02	1,21E+01
2,7		2,48E-02	1,22E+01
2,8		2,65E-02	1,23E+01
2,9		2,87E-02	1,27E+01
3	9,65E-01	3,09E-02	1,28E+01
3,1		3,36E-02	1,32E+01
3,2		3,65E-02	1,36E+01
3,3		3,97E-02	1,42E+01
3,4		4,33E-02	1,48E+01
3,5	1,64E+00	4,74E-02	1,57E+01
3,6		5,21E-02	1,67E+01
3,7		5,73E-02	1,79E+01
3,8		6,32E-02	1,95E+01
3,9		6,99E-02	2,13E+01
4	3,59E+00	7,77E-02	2,33E+01
4,1		8,48E-02	2,59E+01
4,2		9,29E-02	2,86E+01
4,3		1,02E-01	3,19E+01
4,4		1,13E-01	3,58E+01
4,5	7,79E+00	1,25E-01	4,03E+01
4,6		1,39E-01	4,51E+01
4,7		1,56E-01	5,10E+01
4,8		1,41E-01	4,69E+01
4,9		1,30E-01	4,34E+01
5	2,22E+01	1,11E-01	3,73E+01

Table 7.1 - EINO from original and updated emissive databases

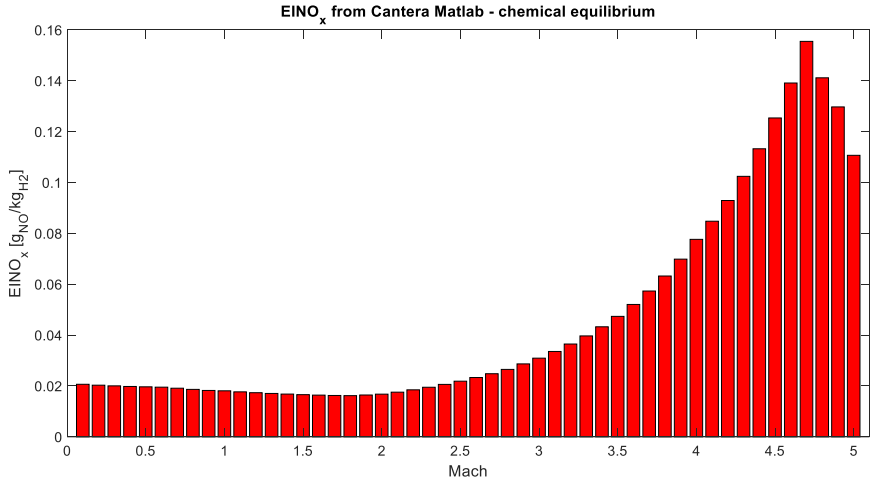

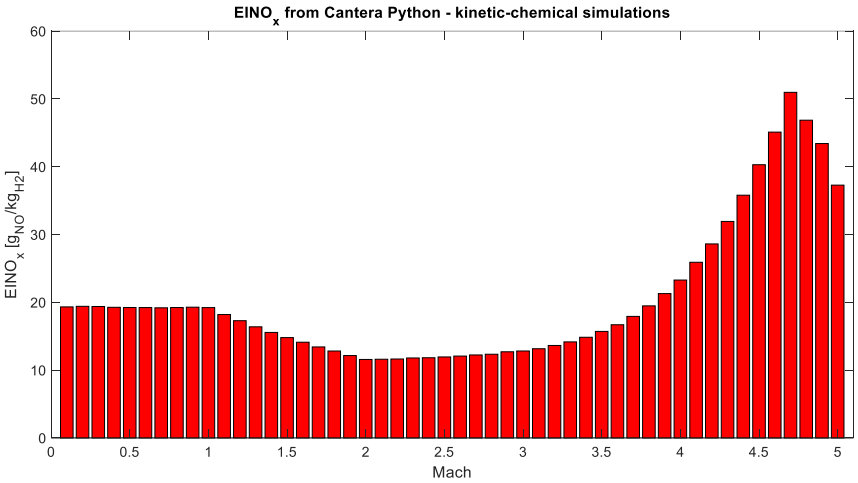

Figure 7.1 - Thermodynamic and kinetic EINO from the updated emissive database

The two sets of EINO depicted in Figure 7.1 exhibit both similarities and distinct differences. Both sets of EINO indeed display a trend that approximately mirrors that of the flame temperature with increasing Mach number: decreasing until Mach 2, increasing from Mach 2 to Mach 4.7, and finally decreasing between Mach 4.7 and Mach 5. This trend of the flame temperature results from the combined effect of the conditions of the mixture entering the main combustion chamber, particularly pressure (p_3), temperature (T_3), and the fraction of H_2O resulting from combustion in the preburner, as analysed previously in Chapter 5.4. Despite the common resemblance to the trend of the flame temperature, the two sets of EINO differ in magnitude and in the rate of growth and decline they exhibit as a function of Mach number. Regarding this latter point, the difference between the two sets of EINO lies in the ability of the two proposed modelling approaches, thermo-chemical and chemical-kinetic, to capture the role of H_2O in the combustion chamber. The thermodynamic EINO derives from mass fractions evaluated using the *equilibrate* function in Cantera via Matlab, corresponding to chemical equilibrium conditions in the chamber. The same *equilibrate* function is also used to calculate the flame temperature, explaining the perfect alignment between the profiles of thermodynamic EINO and flame temperature as a function of Mach. Therefore, it can be concluded that the trend of this set of EINO, like that of the flame temperature, is the result of the combined effect of T_3 and the H_2O mass fraction at the entrance of the main combustion chamber, given that p_3 uniformly increases with increasing Mach. In particular, as explained earlier, H_2O in the combustion chamber has three main effects: it reduces the temperature reached, causes oxygen deficiency, and reacts with other species present in the chamber. Both the thermoregulatory effect and the kinetic-chemical effects ideally lead to a decrease in NO_x produced during combustion. The *equilibrate* function in Cantera, which evaluates equilibrium conditions using an approach based on minimizing Gibbs free energy, can only capture the thermal effect of H_2O and not the kinetic-chemical effects. This limitation stems from the global nature of the evaluation of chemical equilibrium conditions performed with *equilibrate*, which does not consider the temporal evolution of the mixture during combustion, and thus does not account for the infinite intermediate equilibrium conditions reached. The kinetic-chemical effects of H_2O in the combustion chamber emerge from the trend of kinetic EINO, particularly from its rate of growth and decline as a function of Mach. It is observable that as Mach increases, the trend of kinetic EINO deviates from that of thermodynamic EINO, and consequently from that of the flame temperature. This deviation is a function of the profile of the H_2O mass fraction at the inlet to the main combustion chamber. Such profile is well represented by the parameter PBratio rather than by the WFR, which instead is also affected by variations in the H_2 mass fraction at the inlet of the chamber. Considering that the chemical-kinetic effects of H_2O in the combustion chamber cause a decrease in EINO produced with increasing H_2O, a brief analysis of the superposition of effects can be conducted. Please refer to the trends shown in Figure 7.2 for this analysis. In particular, for Mach numbers

lower than 1, the flame temperature and the thermodynamic EINO decrease, but so does the H_2O mass fraction at the inlet to the main combustion chamber, resulting in kinetic EINO remaining approximately constant as Mach increases. In the range from Mach 1 to Mach 2, the thermodynamic EINO and the flame temperature decrease slightly, while H_2O mass fraction at the inlet to the main combustion chamber increases until reaching its maximum value; consequently, the decrease in kinetic EINO is greater than that of thermodynamic EINO. Beyond Mach 2, the H_2O mass fraction at the inlet to the main combustion chamber decreases uniformly up to Mach 5, while the flame temperature, thermodynamic EINO, and kinetic EINO increase until Mach 4.7 and then decrease from Mach 4.7 to Mach 5, in accordance with T_3. What is interesting to note in this Mach range in the context of superposition of effects is the difference in growth rate between the two sets of EINO. The trend of thermodynamic EINO, in fact, after Mach 2, increases until it recovers, for a Mach condition of approximately 2.5, the value it assumed under subsonic conditions, and then exponentially increases until Mach 4.7 and then decreases. This trend perfectly mirrors that of the flame temperature, which, after reaching a minimum at Mach 2, recovers the value reached under subsonic conditions at a Mach condition of approximately 2.5, then exponentially increases, and finally decreases. In contrast, the trend of kinetic EINO is such that the values reached under subsonic conditions are recovered at a Mach condition of approximately 4. The Mach 4 condition corresponds to when the H_2O mass fraction at the inlet to the main combustion chamber, after decreasing from the maximum value reached at Mach 2, returns to the initial values recorded in subsonic conditions. Therefore, it can be concluded that the trend of kinetic EINO as Mach increases is a modulation of the flame temperature trend, and consequently of that of thermodynamic EINO, operated as a function of the PBratio trend i.e., the H_2O mass fraction at the inlet of the combustion chamber. This modulation is justified by the fact that chemical-kinetic simulation of the combustion process allows for the evaluation of the temporal evolution of the mixture composition in the chamber as a result of a succession of intermediate equilibrium states. Unlike the Gibbs free energy minimization approach, which only considers the initial state of the system and its thermochemical characteristics, the time-dependent simulation of the combustion chamber enables the analysis of the dynamics of the process and the reactions among the different chemical species, considering the instantaneous characteristics of the mixture and not just the initial ones. This enables the capture of the kinetic-chemical effects of the presence of H_2O in the combustion chamber, not just the thermoregulatory one, as highlighted by the analysis of the superposition of effects.

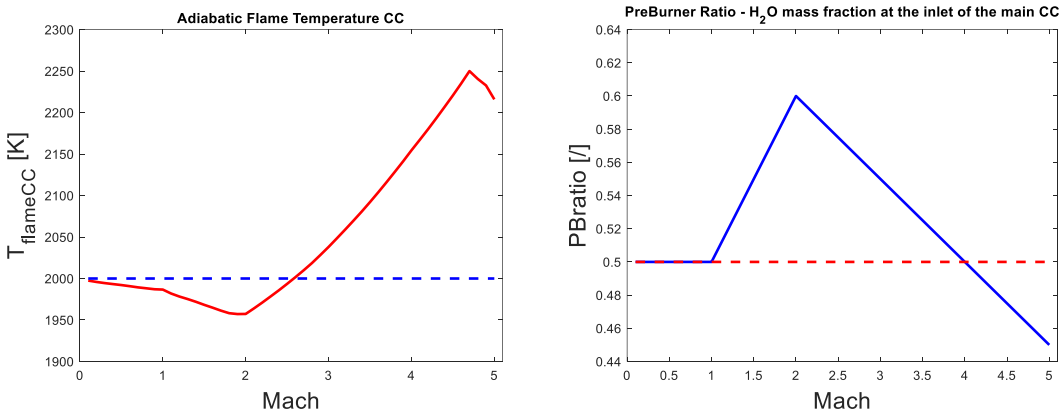

Figure 7.2 - useful parameters for the analysis of superposition of the effects

The second difference between the two sets of EINO concerns their orders of magnitude. It is conceivable that the underestimation of NO mass fractions evaluated with Cantera Matlab to those kinetically resulting from Cantera Python can be attributed, once again, to the presence of H_2O within the combustion chamber. Specifically, the discrepancy in the orders of magnitude of the two sets of EINO may originate from the

characteristics of the *z24_nox20* model in relation to the concept of chemical equilibrium. The general concept behind thermochemical equilibrium is that all spontaneous reactions evolve towards the direction that increases the overall entropy of the universe, encompassing both the system under consideration and the surrounding environment. When the system composition reaches a state in which the total entropy for the system and surroundings reaches a maximum, it becomes frozen, as movement in any direction in composition space results in a decrease in entropy, thus violating the second law and preventing spontaneous occurrence. Therefore, the chemical equilibrium state corresponds to this final state, which all spontaneously reacting systems ultimately achieve given sufficient time. There are various types of equilibrium problems, and the one proposed for the main CC modelling of SABRE can be outlined as follows. The system is treated as a fixed-volume, adiabatic box. In this setup, as reactions proceed, both the temperature and pressure inside the box change. Consequently, the final temperature and pressure are unknown and are determined by the solution of different sets of equations depending on the approach used to assess equilibrium. As previously mentioned, the Cantera *equilibrate* command evaluates chemical equilibrium conditions through a minimization process of Gibbs free energy. The equilibrium conditions evaluated in this way ideally correspond to an infinite time, such that all reactions can be considered to have reached completion. This condition of infinite time, besides being physically unattainable, can be misleading when considering the presence of H_2O in the combustion chamber. The kinetic scheme *z24_nox20* indeed contains a complex network of dissociation and recombination reactions involving species such as H_2O, OH, H_2, H_2O_2, HNO, N_2O, NO_2, and NO, which may result in a much lower mass fraction of NO produced at infinite time compared to that observed at finite time consistent with the actual residence times in the chamber. Therefore, the EINO calculated using the Cantera *equilibrate* command correspond to an ideally infinite time when all dissociation and recombination reactions associated with H_2O can result in an underestimation of NO mass fractions. These mass fractions are the result of purely mathematical modelling based solely on thermodynamic data and thus do not reflect the reality of what happens at finite and reasonable residence times in the chamber. In conclusion, EINO resulting from kinetic modelling should therefore be considered more reliable than those derived from modelling chemical equilibrium conditions, as they provide an accurate representation of the combustion chamber under a condition of non-global equilibrium, corresponding to an intermediate time. For evaluating the kinetic EINO, the simulation stop time is set at 2 seconds, which corresponds to a moment at which dissociation and recombination reactions associated with the presence of H_2O in the combustion chamber, leading to the underestimation of NO mass fractions, do not occur.

7.2 Novel formulations of P_3T_3 Method

In this section, the novel formulations of the P3T3 method derived in Chapter 6.2 are presented and applied to the SABRE case study. To streamline the discussion, all new formulations are described solely by the recalculated exponent coefficients, which have been optimized to best fit the EINO from the emissive database. Furthermore, a discussion regarding the chemical and physical justifications of the exponent coefficients is provided, referencing the more comprehensive formulation that includes all newly introduced ratios, which yields the most accurate emission index estimation. Finally, the EINO resulting from the original and the updated formulation of the P3T3 method are compared to the reference EINO from the emissive database in terms of relative and absolute errors. Please note that, lacking a validated standard reference for SABRE emissions, this final step does not validate the calculated EINO. However, it serves the purpose of verifying the effectiveness of the methodology employed for adapting the P3T3 method to the case study, measured in terms of the achieved estimation accuracy.

The optimized exponents obtained for the first 5 new formulations proposed are reported in Table 7.2, compared with the exponent coefficients of the original formulation of the P3T3 method. Analysing these first five formulations separately, which involve the addition of only one of the new ratios between flight level and sea level conditions, allows to identify which of the parameters considered has the best effect on the estimation of the EINO. In Figure 7.3, the estimated EINO using these new formulations are compared with the EINO from the emissive database, enabling the visualization of the prediction capability of these novel formulations. Similarly, this comparison is specialized for subsonic flight conditions in Figure 7.4 and for high-speed conditions in Figure 7.5. For the same purpose, Figure 7.6 and Figure 7.7 depict the relative and absolute errors of the EINO estimates obtained, always with respect to the EINO from the emissive database. To ensure continuity and facilitate comparison with the EINO from the original emissive database, all images refer to the originally studied Mach conditions, rather than all 50 conditions of the updated database.

	k	a	b	c	d	e	f
Original $EINO_{FL}$= f(p3)	1.0000	0.4	0	-	-	-	-
$EINO_{FL}$= f(p_3, FAR)	1.0000	3.2563	3.3281	-	-	-	-
$EINO_{FL}$= f(p_3, FAR, M)	0.9828	3.2396	3.4742	-0.1347	-	-	-
$EINO_{FL}$= f(p_3, FAR, M, $\dot{m}_{PBratio}$)	1.0000	0.6858	1.1216	-0.3701	-5.0476	-	-
$EINO_{FL}$= f(p_3, FAR, M, WFR)	1.0000	2.4806	1.1014	-0.3864	-	-2.3265	-
$EINO_{FL}$= f(p_3, FAR, M, $\dot{m}_{HEratio}$)	0.7843	1.7799	15.3641	-0.8562	-	-	3.5608

Table 7.2 - Exponent coefficients of the original and updated formulations of the P3T3 method

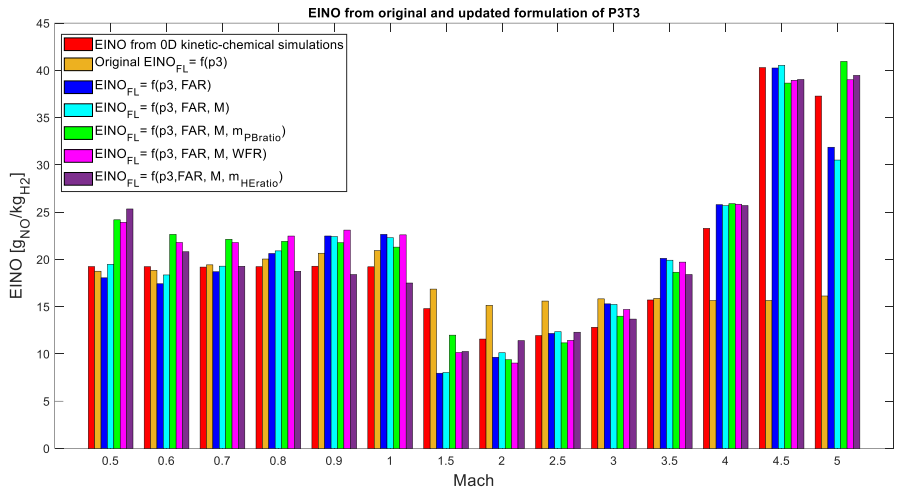

Figure 7.3 - Comparison between EINO reference, EINO from the original P3T3, and EINO from the updated P3T3 method

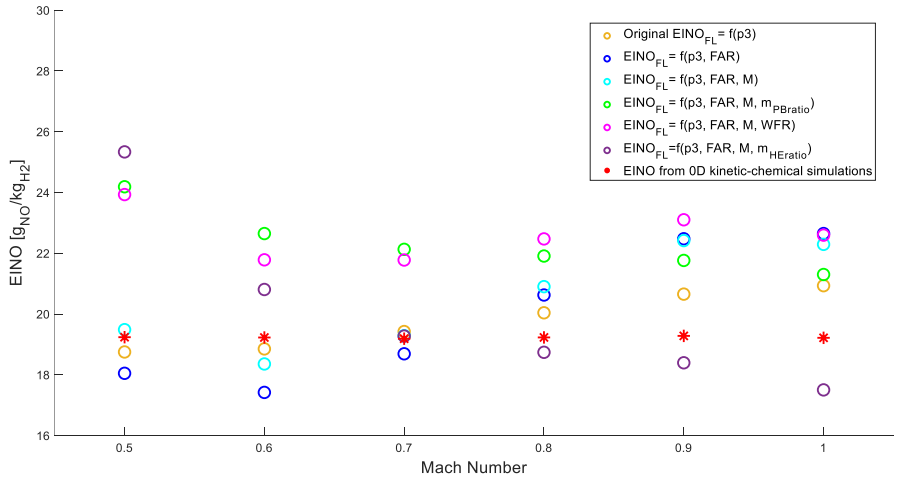

Figure 7.4 - Comparison between EINO reference, EINO from the original P3T3 and EINO from the updated P3T3 method at subsonic conditions

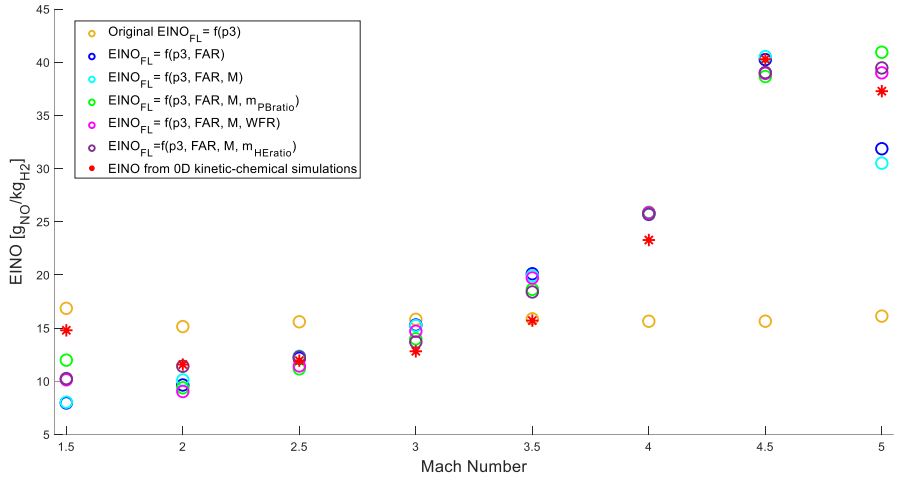

Figure 7.5 - Comparison between EINO reference, EINO from the original P3T3 and EINO from the updated P3T3 method at high-speed conditions

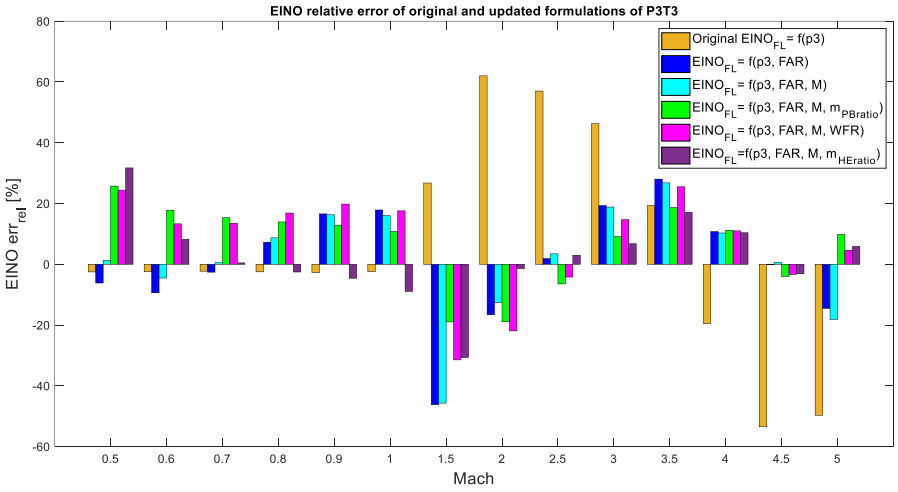

Figure 7.6 - Relative errors of the original P3T3 and new formulations of the P3T3 method

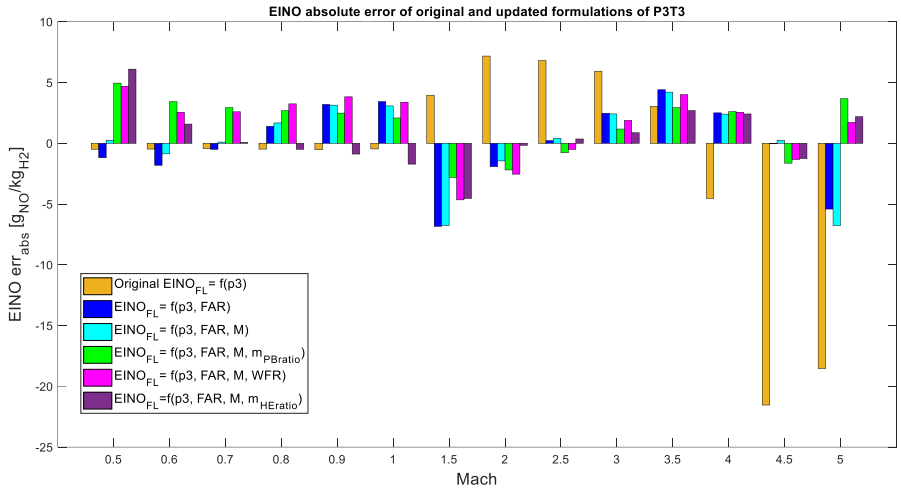

Figure 7.7 - Absolute errors of the original P3T3 and new formulations of the P3T3 method

It is possible to make some observations regarding the trends presented in the preceding figures. Concerning flight conditions with Mach numbers lower than 1, the original formulation of the P3T3 method generally provides the best estimation for the EINO. This outcome aligns with the inherently subsonic nature of the emission estimation performed by the original P3T3 formulation. However, the original formulation still exhibits minimal errors in the subsonic regime, which can be attributed to the application of the method to the hydrogen-fuelled case study rather than to an engine powered by traditional fuels. Beyond the Mach 1 condition, the original P3T3 formulation shows increasing errors with increasing Mach number. Regarding the new formulations, errors are significantly reduced, particularly with respect to the formulation including the ratio between FL and SL conditions of the HEratio parameter. Proceeding with the more comprehensive formulations derived in Chapter 6.2, they involve the introduction of two ratios between FL and SL conditions for the newly introduced parameters. Additionally, alongside these formulations, the one encompassing all the ratios of the new parameters introduced is also provided. As the number of new ratios introduced increases, there is a decrease in estimation errors, thereby resulting in an improvement in accuracy.

	k	**a**	**b**	**c**	**d**	**e**	**f**
$\mathbf{EINO_{FL}= f(p_3,FAR,M,\dot{m}_{PBratio},WFR)}$	1.0000	-3.3096	3.8024	0.0440	-18.8869	8.9923	-
$\mathbf{EINO_{FL}= f(p_3,FAR,M,\dot{m}_{PBratio},\dot{m}_{HEratio})}$	0.7869	-1.5831	-13.5152	-0.4824	-3.6352	-	-11.5123
$\mathbf{EINO_{FL}= f(p_3,FAR,M,WFR,\dot{m}_{HEratio})}$	1.0831	-3.5506	0.6250	-0.1016	-	-	4.8906
$\mathbf{EINO_{FL}= f(p_3,FAR,M,\dot{m}_{PBratio},WFR,\dot{m}_{HEratio})}$	1.0406	-3.5104	12.7935	0.0700	-19.5566	11.4036	2.1054

Table 7.3 - Exponent coefficients of the updated formulations of the P3T3 method

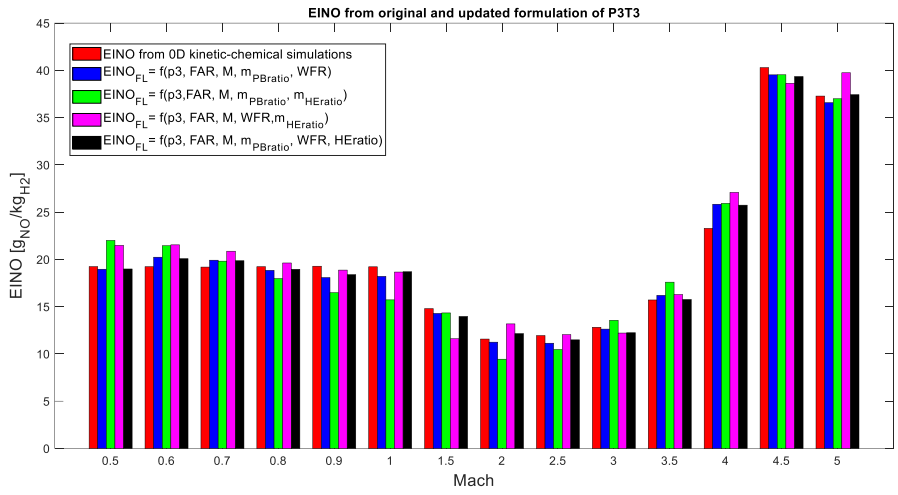

Figure 7.8 - Comparison between Eino reference and EINO from the updated P3T3

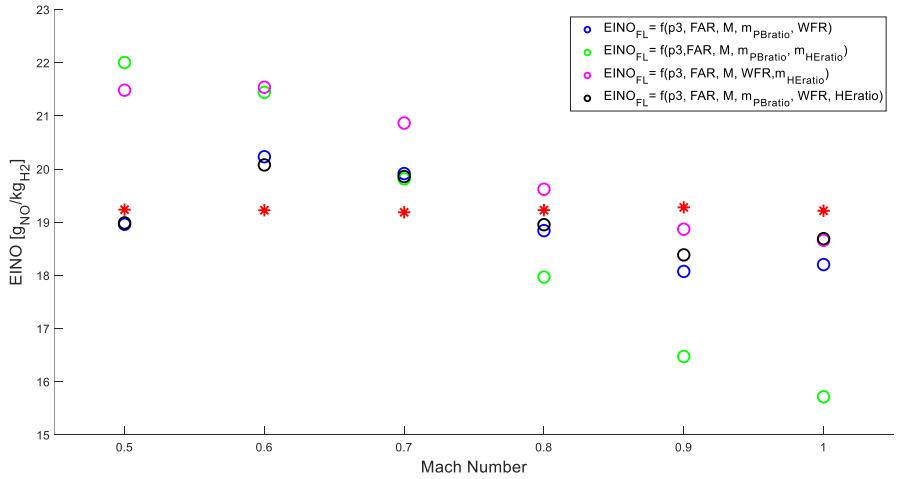

Figure 7.9 - Comparison between EINO reference and EINO from the updated P3T3 method at subsonic conditions

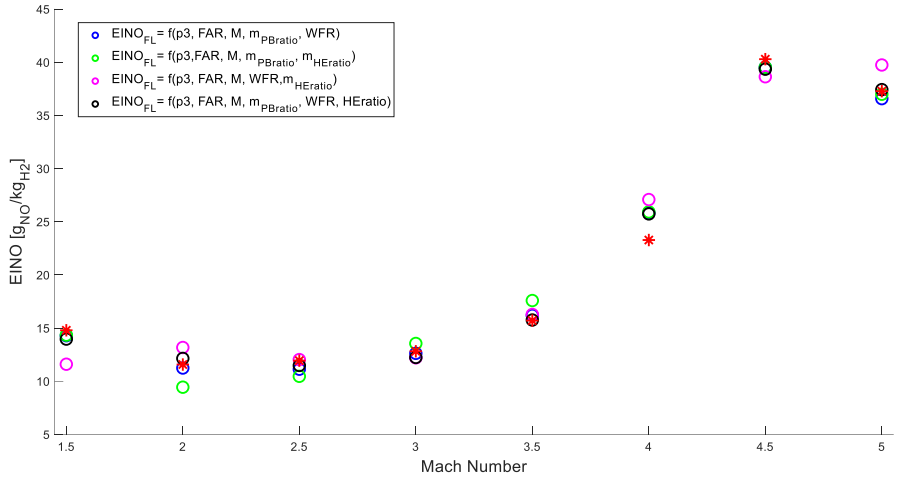

Figure 7.10 - Comparison between EINO reference and EINO from the updated P3T3 method at high-speed conditions

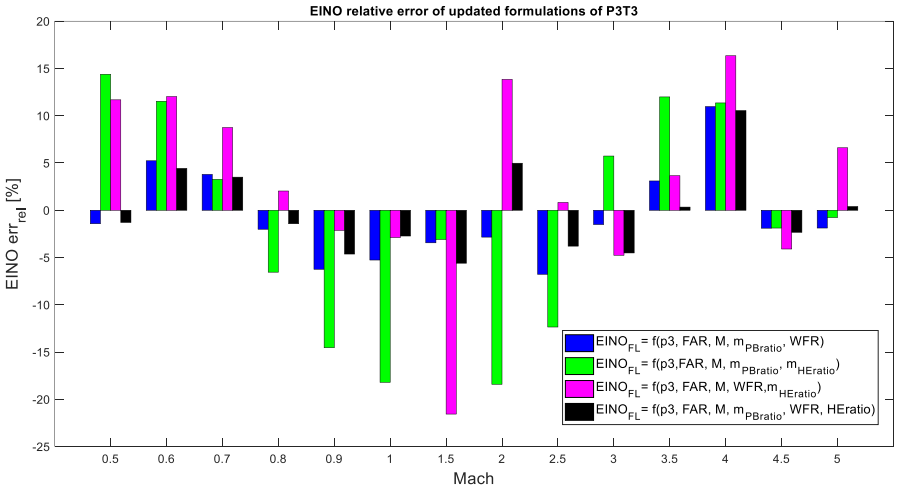

Figure 7.11 - Relative errors of the new formulations of the P3T3 method

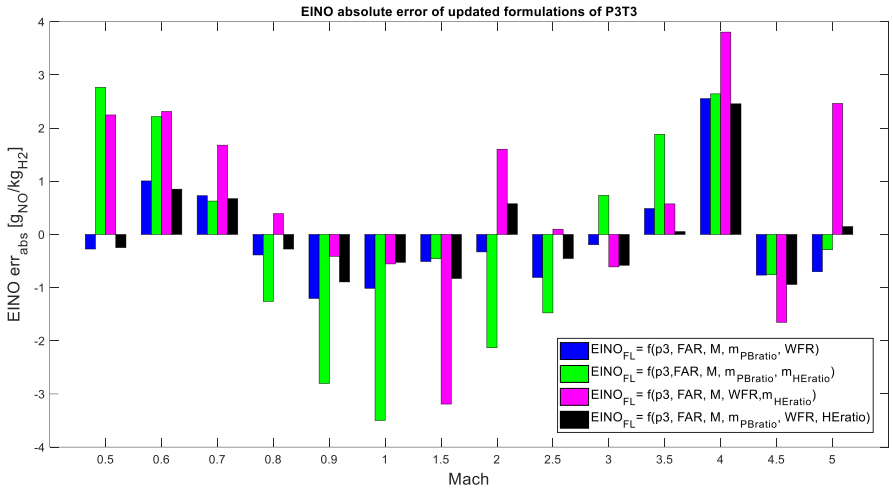

Figure 7.12 - Absolute errors of the new formulations of the P3T3 method

Overall, it is possible to observe significant variations in the optimized exponents' signs as the number of parameters and ratios introduced in the new formulations increases. This oscillating behaviour of the coefficient exponents may be due to the purely mathematical optimization performed in Matlab, which disregards the physics and chemistry of the processes and bases the recalculation of these coefficients solely on the input data. Since the ratios between FL and SL conditions exhibit markedly different trends with respect to Mach, it is normal to obtain different optimized exponents for different combinations of these ratios. Indeed, the calculator refers to a single set of EINO for determining the best fit for all the new mathematical formulations, which nonetheless present different ratio values that intervene. Considering the most comprehensive formulation, whose optimized coefficients are reported in the last row of Table 7.3, it is possible to derive some chemical-physical conclusions and justifications about the numerical values of these coefficients. Considering the p_3 pressure ratio between FL and SL conditions, the coefficient *a* results in negative values. The pressure ratio is less than one, decreasing with increasing Mach. As Mach increases, p_3 increases uniformly; however, the linear fit of p_3 in SL conditions expressed as a function of T_3 increases more rapidly, which, in turn, increases with Mach. Therefore, p_3 and the corresponding ratio between FL and SL conditions exhibit opposite behaviour with increasing Mach. Consequently, the effect of coefficient *a* on the p_3 pressure ratio results in an increasing mathematical contribution from this ratio to the increase in EINO as Mach increases. The increasing mathematical contribution of the pressure ratio with increasing Mach in the formulation for $EINO_{FL}$ has a physico-chemical justification. Indeed, an increase in the mixture's pressure p_3 entering the main combustion chamber translates to an increase in the pressure reached during combustion, leading to an increase in the flame temperature. An increase in the flame temperature leads to an increase in NO_x produced by the engine. Examining the FAR ratio term, the positive exponent value, along with the ratio between FL and SL conditions itself being greater than 1 and increasing with Mach, mathematically demonstrates that this ratio term positively contributes to the formulation for calculating EINO as Mach increases. However, this mathematical result contradicts physical expectations. As the Mach number increases, FAR rises, ideally leading to an increase in the hydrogen fraction in the combustion chamber. Since combustion occurs under conditions of FAR beyond stoichiometric, the flame temperature decreases as the hydrogen fraction increases, consequently reducing NO_x emissions, at least ideally. The increasing contribution of the FAR ratio, which appears in the formulation but not in all the studied formulations, may be due to the purely mathematical optimization performed in Matlab, which can result in sign oscillations for the optimized exponents as the number of introduced ratios in the formulations increases. Another justification for this unexpected contribution may be derived from considering the engine's overall FAR to construct the corresponding ratio. The engine's overall FAR is not representative

of the hydrogen fraction trend in the main combustion chamber due to the combustion in two stages characterized by a precise flow regulation law expressed by the PBratio. If the concept of FAR is specialized for the main combustion chamber by constructing the ratio between the mass fraction of H_2 and the mass fraction of O_2 at the chamber's inlet as shown in Figure 5.16 (*d*), it is evident that this recalculated fictitious FAR does not correspond to the uniformly increasing trend of the engine's overall FAR. As for the positive Mach coefficient resulting in the complete formulation, it is consistent with the physico-chemical expectation of increased NO_x production by the engine as speed increases. However, most of the new formulations are characterized by a negative Mach coefficient. This oscillation of the Mach exponent coefficient towards negative values can be justified by the lack of memory of the flow entering the combustion chamber concerning the inlet engine conditions. Indeed, this engine's unique configuration entails the external air flow being deeply cooled and compressed immediately after intake, completely losing memory of the flow concerning its upstream conditions, and thus its speed regime. Regarding the ratio between FL and SL conditions of the parameter PBratio, its negative exponent, coupled with the ratio itself being above one and its segmented trend as a function of Mach, faithfully mirrors that of the parameter PBratio, is in line with physical expectations. This configuration leads to a decreasing mathematical contribution in the formulation for EINO as Mach increases up to Mach 2, followed by a decreasing mathematical contribution up to Mach 5. An increase in the air flow to the preburner results in a greater segmentation of combustion, leading to a reduction in the temperature reached in the main combustion chamber and consequently a decrease in NO_x production. Conversely, the ratio between FL and SL conditions of the parameter WFR exhibits a completely different trend with increasing Mach compared to that of the WFR parameter that generated it. The ratio between FL and SL conditions of the WFR exhibits a value less than unity and decreases with increasing Mach. This configuration, coupled with a positive exponent coefficient, leads to a decreasing contribution of the ratio with increasing Mach. This behaviour aligns with physical expectations only for Mach conditions less than or equal to 2, while it lacks physical justification for Mach conditions greater than 2 due to the apparent independence between the trend of WFR and its corresponding ratio between FL and SL conditions, as a result of fitting SL conditions as a function of T_3. On the contrary, the positive exponent of the ratio between FL and SL conditions of the parameter HEratio, combined with the ratio itself being less than one and uniformly decreasing with Mach, aligns with physical expectations. An increase in the HEratio reflects a higher thermal load managed by the engine, thus leading to a higher temperature reached in the chamber and an increase in NO_x production. In this case as well, this configuration does not guarantee physical justification for all Mach conditions due to the apparent independence between the trend of HEratio and its corresponding ratio between FL and SL conditions, as a result of fitting SL conditions as a function of T_3.

7.3 Novel formulations of BFFM2

In this section, the same discussion of results proposed for the new formulations of the P3T3 method is conducted for the novel formulations of the FF method derived in Chapter 6.3. These formulations are presented and applied to the SABRE case study. A discussion is provided regarding the optimized exponent coefficients included in the most comprehensive formulation, which encompasses all the ratios of the newly introduced parameters. in addition, the exponent coefficients for all intermediate formulations are also reported, along with the results of their application to the case study. Since the Fuel Flow method utilizes non-proprietary engine parameters as input data, which are less specific compared to those provided by the P3T3 method, the accuracy of estimation provided by the new formulations of this method is consequently reduced compared to that provided by the new formulations of the P3T3 method. This becomes evident when comparing the errors of the new formulations of the FF method with respect to the reference EINO from the emissive database with the corresponding errors of the new formulations of the P3T3 method.

	k	a	b	c	d	i
Original $EINO_{FL}$= f(δ_{amb},θ_{amb})	1	1.02	3.3	0.5	-	-
$EINO_{FL}$= f(δ_{amb},θ_{amb},M)	0.9429	0.2669	2.3982	-2.3701	-0.0943	-
$EINO_{FL}$= f(δ_{amb},θ_{amb},M,FAR)	1.0000	0.2967	2.7304	-2.1717	-0.0607	0.4737
$EINO_{FL}$= f(δ_{amb},θ_{amb},M, $\dot{m}_{PBratio}$)	1.0000	0.2279	2.1673	-2.5784	-0.0577	-0.1391
$EINO_{FL}$= f(δ_{amb},θ_{amb},M,WFR)	1.0000	0.4038	3.8644	-1.5238	-0.0607	-0.1584
$EINO_{FL}$= f(δ_{amb},θ_{amb},M, $\dot{m}_{HEratio}$)	1.0000	0.3877	3.8545	-1.6205	-0.0791	0.1500

Table 7.4 - Exponent coefficients of the original and updated formulations of the FF method

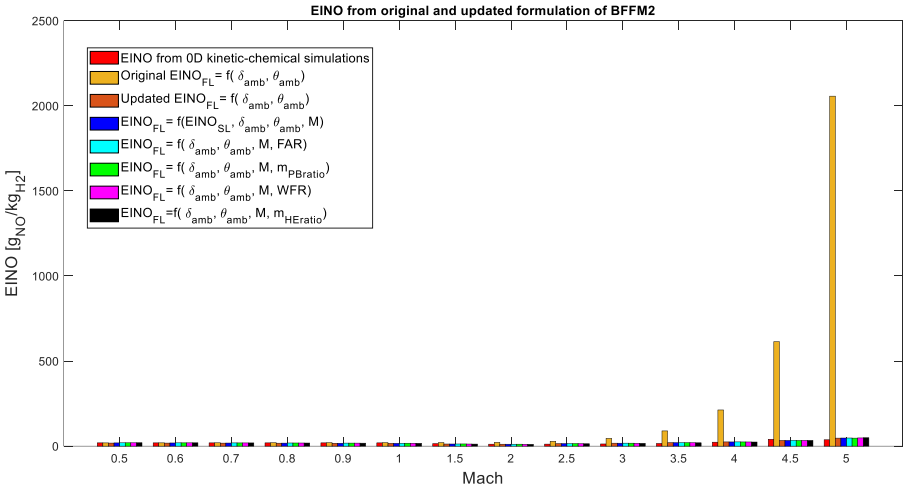

Figure 7.13 - Comparison between EINO reference, EINO from the original BFFM2, and EINO from the updated FF method

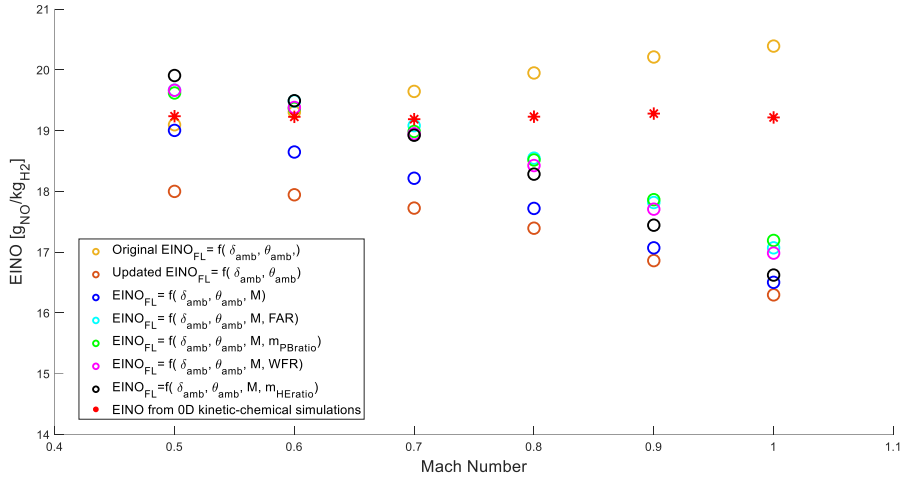

Figure 7.14 - Comparison between EINO reference, EINO from the original BFFM2, and EINO from the updated FF method at subsonic conditions

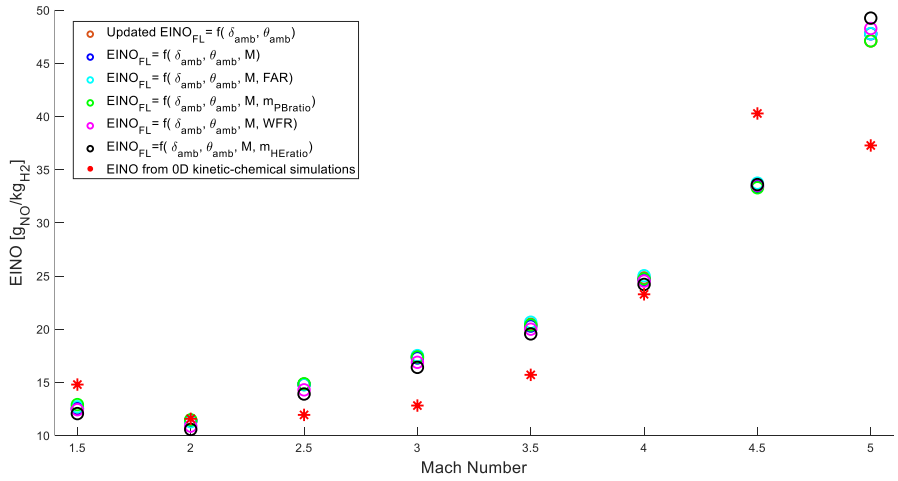

Figure 7.15 - Comparison between EINO reference and EINO from the updated FF method at high-speed conditions

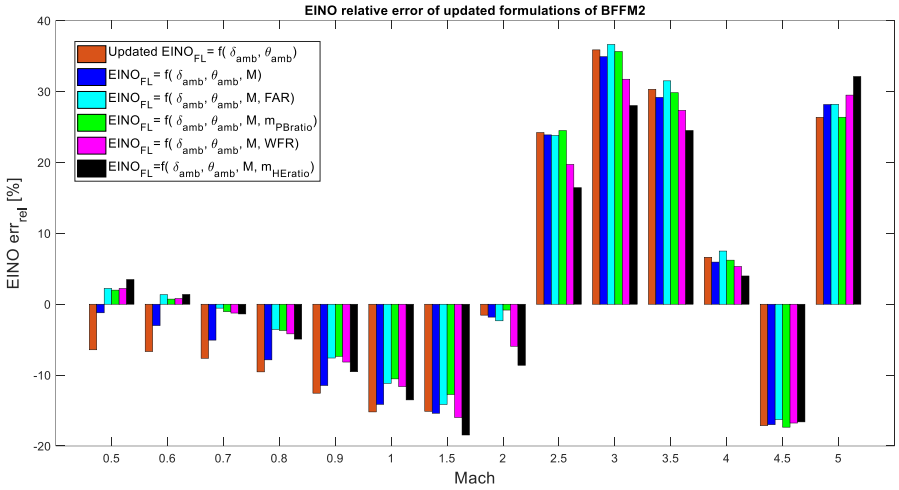

Figure 7.16 - Relative errors of the new formulations of the FF method

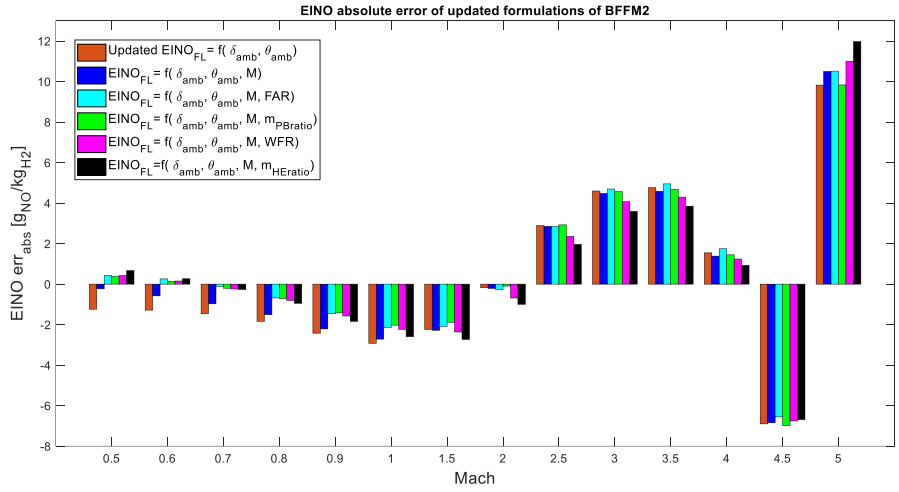

Figure 7.17 - Absolute errors of the new formulations of the FF method

It is possible to make some observations regarding the trends presented in the preceding images. Concerning flight conditions with Mach numbers lower than 1, the original formulation of the BFFM2 generally provides the best estimation for the EINO. This outcome, also obtained in the case of the P3T3 method in the previous section, aligns with the inherently subsonic nature of the emission estimation performed by the original BFFM2 formulation. However, even in this case, the original formulation still exhibits minimal errors in the subsonic regime, attributable to the application of the method to the hydrogen-fuelled case. Beyond the Mach 1 condition, the original BFFM2 formulation provides an EINO estimation that exponentially increases with increasing Mach number, leading to much larger estimation errors compared to those obtained with the original formulation of the P3T3. This error trend is consistent with the inherently more accurate nature of the estimation performed by the P3T3 method compared to the BFFM2. Regarding

the new formulations, errors are significantly reduced, particularly with respect to the formulation including the ratio between FL and SL conditions of the PBratio parameter. Proceeding with the more comprehensive formulations derived in Chapter 6.3, they involve the introduction of two ratios between FL and SL conditions for the newly introduced parameters. Additionally, alongside these formulations, the one encompassing all the ratios of the new parameters introduced is also provided. As the number of new ratios introduced increases, there is a decrease in estimation errors, thereby resulting in an improvement in accuracy.

	k	**a**	**b**	**c**	**d**	**p**	**q**
$EINO_{FL}$= f(δ_{amb},θ_{amb},M,$\dot{m}_{PBratio}$,FAR)	1.0000	0.3154	2.9912	-1.8822	-0.0516	-0.1174	0.0790
$EINO_{FL}$= f(δ_{amb},θ_{amb},M,$\dot{m}_{PBratio}$,WFR)	1.0000	0.3300	3.1430	-1.8198	-0.0624	-0.1384	-0.1646
$EINO_{FL}$= f(δ_{amb},θ_{amb},M,$\dot{m}_{PBratio}$,$\dot{m}_{HEratio}$)	1.0000	0.1117	0.7726	0.9867	-0.0435	-1.6224	1.5209
$EINO_{FL}$= f(δ_{amb},θ_{amb},M,FAR,$\dot{m}_{HEratio}$)	1.0000	0.3108	3.0193	-1.7935	-0.0464	0.0814	0.1035
$EINO_{FL}$= f(δ_{amb},θ_{amb},M,FAR,WFR)	1.0000	0.0399	0.7414	-2.7339	0.0473	0.6764	-0.8319
$EINO_{FL}$= f(δ_{amb},θ_{amb},M,$\dot{m}_{HEratio}$,WFR)	1.0000	0.5506	5.4750	-1.0988	-0.0938	0.1912	-0.2240

Table 7.5 - Exponent coefficients of the updated formulations of the FF method

$EINO_{FL}$= f(δ_{amb}, θ_{amb}, Mach, $\dot{m}_{HEratio}$, WFR, FAR, $\dot{m}_{PBratio}$,)

k	**a**	**b**	**c**	**d**	**r**	**s**	**t**	**u**
1.0000	0.2110	1.9797	-1.8745	-0.1714	0.4039	-0.9982	-0.0157	-0.8152

Table 7.6 - Exponent coefficients of the updated formulations of the FF method

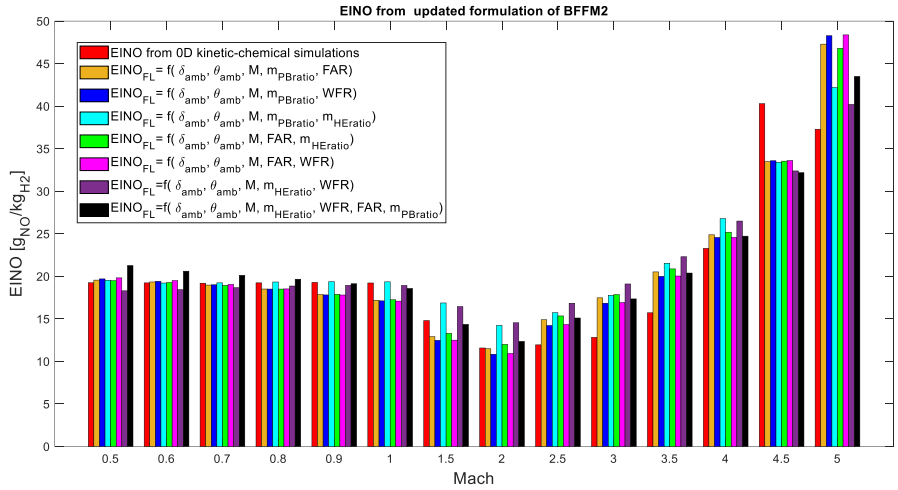

Figure 7.18 - Comparison between EINO reference, EINO from the original BFFM2, and EINO from the updated FF method

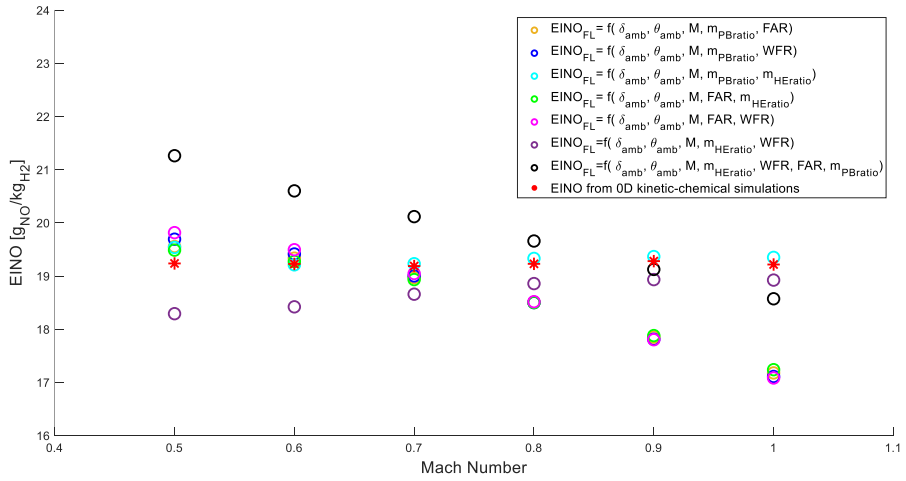

Figure 7.19 - Comparison between Eino reference and EINO from the updated FF method at subsonic conditions

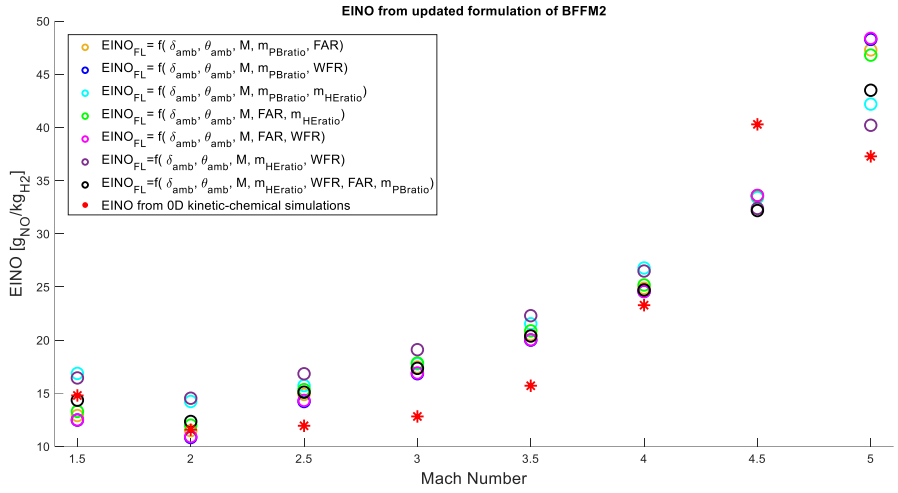

Figure 7.20 - Comparison between EINO reference and EINO from the updated FF method at high-speed conditions

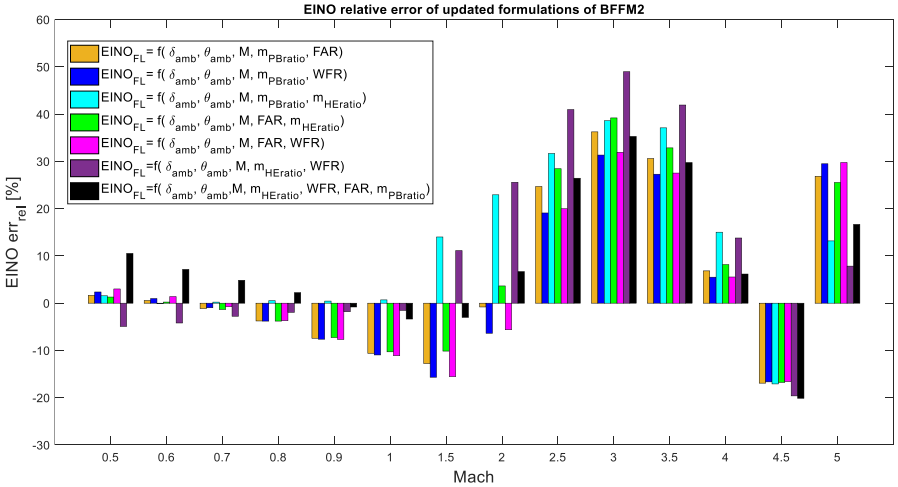

Figure 7.21 - Relative errors of the new formulations of the FF method

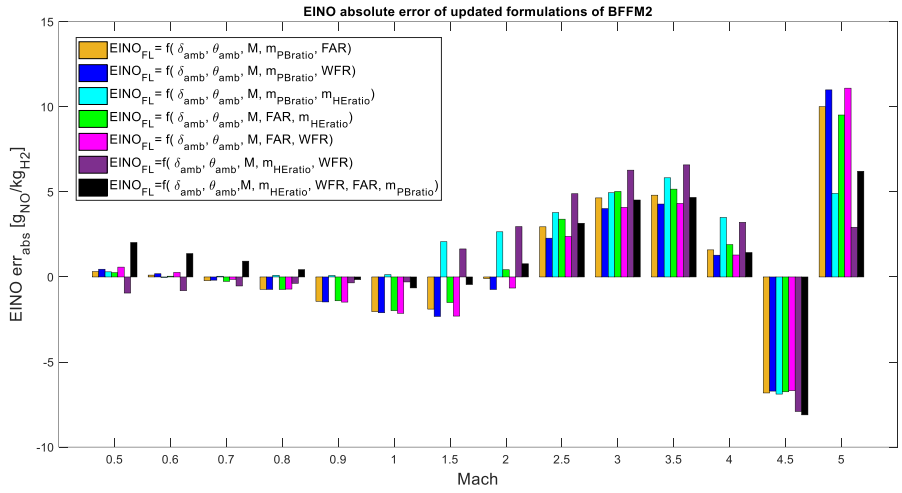

Figure 7.22 - Absolute errors of the new formulations of the P3T3 method

In contrast to the findings observed in the update of the P3T3 method, regarding the new formulations of the FF method, a nearly constant trend in the optimized exponents can be observed as the number of parameters and ratios introduced in the new formulations increases. With the addition of each new ratio, the optimized coefficients for the ratios evaluated in the previous formulation are validated by the absence of oscillation in the recalculated coefficients. Making this general observation on the recalculated exponent coefficients, it is possible to delve into the most comprehensive formulation to discuss the justifications about the numerical values of its optimized coefficients, whose values are reported in Table 7.6. Considering the ratios of temperature and pressure between ambient conditions and standard sea level (SL) conditions, it is necessary to consider the combined effect of the positive coefficients *a* and *b*, and the negative coefficient *c*. Specifically, the pressure ratio has a value less than one and decreases with increasing Mach. Therefore, the combined effect of coefficients a and c results in an increasing contribution from the pressure ratio to the increase in EINO as Mach increases. Similarly, the temperature ratio has a value less than one and decreases with increasing Mach. However, in this case, the combined effect of coefficients *b* and *c* results in a decreasing contribution from the temperature ratio to the increase in EINO as Mach increases. As Mach increases, the pressure and temperature at the engine inlet decrease according to the ISA standard, consequently reducing the respective ratios between FL and standard SL conditions. The increasing mathematical contribution of the pressure ratio with increasing Mach in the formulation for $EINO_{FL}$ is not in line with physical expectations. Indeed, a decrease in the pressure and temperature of the air entering the engine compared to standard SL conditions ideally translates to a decrease in temperature and pressure in the combustion chamber and therefore a decrease in the NO_x produced by the engine. However, in the case of the SABRE, its deeply precooled configuration results in the pressure and temperature conditions of the air entering the engine not being felt at the combustion chamber level. This justifies the unexpected contribution of the pressure ratio in the mathematical formulation, as well as the optimized negative coefficient of Mach that appears in almost all the formulations studied. Despite an expected increasing mathematical contribution of Mach with increasing speed in the updated formulations for EINO, such contribution instead decreases when the exponent d is less than 0. Additionally, regarding the FAR ratio term, the ratio between FL and SL conditions has a value below one and uniformly decreases with increasing Mach. This trend, combined with the negative exponent value *t*, mathematically demonstrates that this ratio term positively contributes to the formulation for calculating EINO as Mach increases. However, this mathematical result is not consistent with what is expected physically. Indeed, as the Mach number increases, the FAR increases, leading to an increase in the hydrogen fraction in the combustion chamber. Since combustion occurs under conditions of FAR beyond stoichiometric, the flame temperature decreases

as the hydrogen fraction increases, consequently reducing NO_x emissions, at least ideally. The increasing contribution of the FAR ratio, which appears in the most complete formulation but not in all the studied formulations, may be due to the purely mathematical optimization performed in Matlab, which can result in sign oscillations for the optimized exponents as the number of introduced ratios in the formulations increases. Another justification for this unexpected contribution lies in the opposite trends presented by the FAR and the corresponding ratio between FL and SL conditions as the Mach number increases. As Mach and FAR increase, the FAR ratio decreases. This inconsistency may therefore originate from a superposition of errors in the various estimated SL fits involved in the evaluation of this ratio. Additionally, the discussion made for this ratio in the context of the update of the P3T3 method remains valid: the FAR employed to construct the ratios refers to the overall engine and is therefore not specifically representative of the H_2 mass fraction entering the main CC. On the contrary, the positive exponent of the ratio between FL and SL conditions of the parameter HEratio, combined with the ratio itself being above one and uniformly increasing with Mach, aligns with physical expectations. An increase in the HEratio reflects a higher thermal load managed by the engine, thus leading to a higher temperature reached in the chamber and an increase in NO_x production. Moving on to the ratio between FL and SL conditions of the parameter PBratio, it has a value above one and a segmented trend as a function of Mach that faithfully mirrors that of the parameter PBratio that generated it. This trend, coupled with the negative exponent *u* reported in Table 7.6 for the ratio between FL and SL conditions of this parameter, is in line with physical expectations. An increase in the air flow to the preburner results in a greater distribution of combustion processes between the two stages present in the engine, PreBurner and main CC, leading to a reduction in the temperature reached in the main combustion chamber and consequently a decrease in NO_x production. The same reasoning applies to the ratio between FL and SL conditions of the parameter WFR, which exhibits a value above unity coupled with a negative exponent and demonstrates a segmented trend that faithfully mirrors that of the parameter PBratio. This configuration leads to a decreasing mathematical contribution in the formulation for EINO as Mach increases up to Mach 2, followed by a decreasing mathematical contribution up to Mach 5. This behaviour aligns with physical expectations and is attributed to the decrease in temperature reached in the chamber due to the presence of a significant fraction of water vapor in the incoming flow. Alongside the thermoregulatory effect, the kinetic-chemical effects of H_2O in the combustion chamber also contribute to the reduction of NO_x produced.

Chapter 8 - Conclusion

The present study introduces innovative analytical formulations aimed at estimating non-CO_2 emissions at the outset of the design process, with the goal to meet upcoming environmental requirements in the context of a growing demand for access to space. Specifically, to forecast nitrogen oxide emissions during conceptual design, two emission estimation methods, namely the BFFM2 and P3T3 methods, were selected from those available in literature due to their compatibility with the quantity and accuracy of available data in the conceptual design phase. These methods were originally devised for assessing the Emission Index of greenhouse gases and pollutants produced by engines powered by traditional fuels and used for subsonic flight. The original mathematical formulations of these methods were modified and adapted to (i) advanced air-breathing propulsion systems for high-speed flights and (ii) environmentally friendly fuels, such as hydrogen. The step-by-step approach used to derive these innovative analytical formulations customized for the Synergetic Air-Breathing Rocket Engine (SABRE) is outlined. For this purpose, a methodology for updating existing propulsive and emissive modelling of the SABRE engine is introduced. Currently, this innovative engine concept is still under study, making it particularly useful to generate increasingly accurate estimators for propulsive and emissive variables, given the absence of certified official databases. The accuracy of the data in the two updated databases, propulsive and emissive, is higher compared to that of the original databases derived from previous modelling efforts. Thanks to the Matlab interface of the Cantera kinetic-chemical simulation software, it was possible to propose an initial version of unified propulsive-emissive modelling of the engine, thereby increasing the results reliability. However, due to the still limited functionalities of Cantera Matlab, it is not yet possible to rely on the emissive results of the unified model; nevertheless, the generation of the two databases appears to be more coherent. Starting from a thorough study of the engine and hydrogen combustion chemistry, correlations between nitrogen oxides production and key parameters including the Mach number, Fuel-to-Air ratio (FAR), airflow rate into the PreBurner (PBratio), water flow rate into the main Combustion Chamber (WFR), and helium flow rate used for regeneratively managing the engine's thermal load (HEratio) were identified. These parameters were then appropriately integrated into the new formulations of the P3T3 and FF methods to adapt their application to the SABRE case study and, more generally, to aircraft with similar characteristics. The introduction of new factors to enhance the analytical formulations is based on the analysis of the engine architecture and the correlations between chemical and propulsion parameters with the formation of NO_x within the engine. This analysis aims to minimize emissions by reducing the temperature reached in the chamber, which proves to be the determining parameter in NO_x formation from hydrogen combustion in high-speed aviation propulsive systems. The innovative formulations derived for the FF and P3T3 methods adopt a methodology similar to the original ones, enabling the forecast of in-flight emissions based on emissions at sea-level conditions, corrected with the ratios between flight level and sea-level conditions of some chemical-propulsive parameters. However, the incorporation of new parameters into the analytical formulations alters the original methods application, necessitating the establishment of supplementary intermediate steps for calculation and interpolation. The original BFFM2 and P3T3 methods offer a single analytical formulation with adjustable parameters to effectively model various engine architectures. In

contrast, the proposed strategy of updating and adapting leads to multiple mathematical formulations tailored for the same engine architecture (SABRE). These diverse formulations generally exhibit an increasing level of accuracy across the entire Mach range as the number of introduced parameters increases. Having multiple formulations of the method characterized by varying errors, larger or smaller depending on Mach, allows for the selection of the estimation formulation based on the desired speed regime to be better modelled, thus rendering the methods application more flexible. The new formulations of the P3T3 method exhibit smaller estimation errors compared to the new formulations of the FF method. The rationale behind this difference in the obtained errors lies in the inherently more precise estimation performed with the P3T3 method compared to the FF method. The P3T3 method originally relies on proprietary engine data, such as temperature and pressure at the inlet of the combustion chamber and it is therefore likely to exhibit higher estimation accuracy compared to the FF method, which instead relies on data that are less representative of the engine operation but are more easily estimable or obtainable, such as environmental conditions and fuel flow profiles. Based on the satisfactory estimation error results obtained for both methods, it is possible to suppose that the proposed methodology can serve as a baseline for adapting analytical formulations of any estimation methods. Moreover, the updating methodology described has a general application, allowing it to be applied to other engines that exhibit characteristics similar to those of the SABRE. In particular, the integration approach of the two softwares used for propulsion and emission modeling, namely Matlab and Cantera, is particularly promising and can be applied to any type of engine. Finally, the developed analytical formulations can quantitatively support trade-off analysis during the propulsive architecture definition phase. Additionally, these new analytical estimation formulations can be valuable for reducing engine emissions even before they occur. In fact, integrating these simple formulations into emission minimization route optimization strategies can lead to emission reduction from the outset of the design process.

Bibliography

[1] United Nations Framework Convention on Climate Change (FCCC). Session and meeting reports. UN Climate Change Conference. United Arab Emirates, 30 November to 12 December 2023.

[2] Dallas, J.A., Raval, S.A., Gaitan, J.P., Saydam, S., & Dempster, A.G. (2020). The environmental impact of emissions from space launches: A comprehensive review. Journal of Cleaner Production, Vol. 255, 120209.

[3] ESA Space Debris Office. (2023). ESA'S ANNUAL SPACE ENVIRONMENT REPORT 2023.

[4] Larsson, J., Elofsson, A., Sterner, T., Åkerman, J. (2019). International and national climate policies for aviation: a review. Climate Policy, Vol. 19, No. 6, pp 787–799.

[5] Bicer, Y., Dincer, I. (2017). Life cycle evaluation of hydrogen and other potential fuels for aircrafts. International Journal of Hydrogen Energy, Vol. 42, Issue 16, pp 10722-10738.

[6] Pletzer, J., Hauglustaine, D., Cohen, Y., Jöckel, P., Grewe, V. (2022). The climate impact of hydrogen-powered hypersonic transport. Atmospheric Chemistry and Physics, Vol. 22, Issue 21, pp. 14323–14354.

[7] Ingenito, A. (2018). Impact of hydrogen fueled hypersonic airliners on the O3 layer depletion. International Journal of Hydrogen Energy, Vol. 43, Issue 50, pp 22694-22704.

[8] Zhang, J., Wuebbles, D., Kinnison, D., Baughcum, S.L. (2021). Stratospheric ozone and climate forcing sensitivity to cruise altitudes for fleets of potential supersonic transport aircraft. Journal of Geophysical Research Atmospheres, Vol. 126, Issue 16, No. e2021JD034971.

[9] Mahashabde, A., Wolfe, P., Ashok, A., Dorbian, C., He, Q., Fan, A., Lukachko, S., Mozdzanowska, A., Wollersheim, C., Barrett, S.R.H., Locke, M., Waitz, I.A. (2011). Assessing the environmental impacts of aircraft noise and emissions. Progress in Aerospace Sciences, Vol. 47, Issue 1, pp. 15-52.

[10] Tait, K.N., Khan, M.A.H., Bullock, S., Lowenberg, M.H., Shallcross, D.E. (2022). Aircraft emissions, their plume-scale effects, and the spatio-temporal sensitivity of the atmospheric response: a review. Aerospace, Vol. 9, No. 355.

[11] International Air Transport Association (IATA). (2022). Annual Review 2022. 78th Annual General Meeting and World Air Transport Summit. Doha, Qatar.

[12] International Civil Aviation Organization (ICAO). (2022). ICAO 2022 Environmental Report.

[13] Air Transportation Action Group (ATAG). (2021). Waypoint 2050 Project Report.

[14] Verstraete, D. (2013). Long range transport aircraft using hydrogen fuel. International Journal of Hydrogen Energy, Vol. 38, Issue 34, pp. 14824-14831.

[15] European Union Aviation Safety Agency (EASA). (2022). What are Sustainable Aviation Fuels (SAF) exactly? Sustainable Pilot Training Webinar.

[16] International Civil Aviation Organization (ICAO). (2018). Sustainable aviation fuels guide. Version 2.

[17] Undavalli, V., Olatunde, O.B.G., Boylu, R., Wei, C., Haeker, J., Hamilton, J., Khandelwal, B. (2023). Recent advancements in sustainable aviation fuels. Progress in Aerospace Sciences, Vol. 136, No. 100876.

[18] Soone, J. (2023). ReFuelEU Aviation initiative: Sustainable aviation fuels and the 'fit for 55' package. European Parliamentary Research Service.

[19] Lee, D.S., Fahey, D.W., Skowron, A., Allen M.R., Burkhardt, U., Chen, Q., Doherty, S.J., Freeman, S., Forster, P.M., Fuglestvedt, J., Gettelman, A., De Leon´, R.R., Lim, L.L., Lund, M.T., Millar, R.J., Owen, B., Pennerj, J.E., Pitari, G., Prather, M.J., Sausen, R., Wilcox, L.J. (2021). The contribution of global aviation to anthropogenic climate forcing for 2000 to 2018. Atmospheric Environment, Vol. 244, No. 117834.

[20] Saccone, G., Marini, M. (2024). Chemical Kinetic Analysis of High-Pressure Hydrogen Ignition and Combustion toward Green Aviation. Aerospace. Vol. 11, Issue 112.

[21] International Air Transport Association (IATA). (2020). FACT SHEET 7: Liquid hydrogen as a potential low- carbon fuel for aviation.

[22] Matthes, S., Lee, D.S., De Leon, R.R., Lim, L., Owen, B., Skowron, A., Thor, R.N., Terrenoire, E. (2022). Review: The Effects of Supersonic Aviation on Ozone and Climate. Aerospace, Vol. 9, Issue 41. https://doi.org/10.3390/aerospace9010041.

[23] Warnatz, J., Maas, U., Dibble, R.W. (2006). Combustion - Physical and Chemical Fundamentals, Modeling and Simulation, Experiments, Pollutant Formation. Springer Berlin, Heidelberg. https://doi.org/10.1007/978-3-540-45363-5.

[24] Zhang, Y., Mathieu, O., Petersen, E.L., Bourque, G., & Curran, H.J. (2017). Assessing the predictions of a NOx kinetic mechanism on recent hydrogen and syngas experimental data. Combustion and Flame, Vol. 182, pp. 122-141.

[25] Reaction Engines Limited. (2014). SKYLON User's Manual. Doc. No. - SKY-REL-MA-0001, Revision 2.

[26] Fernandez-Villace, V. (2013). Simulation, design and analysis of air-breathing combined-cycle engines for high speed propulsion. Doctoral Thesis. Universidad Politécnica de Madrid, Madrid.

[27] Grimaldi G. (2021). Development of a conceptual design tool to predict performance and pollutant and GHG emissions of high-speed vehicles using liquid hydrogen. Master's Degree Thesis. Politecnico di Torino, Torino.

[28] Moino S. (2021). Methodology and tools for propulsive performance characterization of high-speed aircraft in conceptual design. Master's Degree Thesis. Politecnico di Torino, Torino.

[29] Fusaro, R., Saccone, G., Viola, N. (2024). NOx emissions estimation methodology for air-breathing reusable access to space vehicle in conceptual design. Acta Astronautica. Vol. 216, pp. 304-317.

[30] Zettervall, N., & Fureby, C. (2018). A Computational Study of Ramjet, Scramjet and Dual-mode Ramjet Combustion in Combustor with a Cavity Flameholder.

[31] Chandrasekaran, N., Guha, A., (2012). Study of Prediction Methods for NOx Emission from Turbofan Engines. J. Propuls. Power, Vol. 28, pp. 170–180.

[32] DuBois, D., Paynter, G.C. (2006). 'Fuel Flow Method2' for Estimating Aircraft Emissions. SAE Trans, Vol. 115, pp. 1–14.

[33] Villette, S., Adam, D., Alexiou, A., Aretakis, N., Mathioudakis, K. (2024). A Simplified Chemical Reactor Network Approach for Aeroengine Combustion Chamber Modeling and Preliminary Design. Aerospace. Vol. 11, Issue 22. https://doi.org/10.3390/aerospace11010022.

[34] Camberos, J.A, Moubry, J.G. (2001). Chemical Equilibrium Analysis with the Method of Element Potentials. AIAA Papers: 39th AIAA Aerospace Sciences Meeting, Reno, NV.

[35] Felden, A. (2015). CANTERA Tutorials: A series of tutorials to get started with the python interface of Cantera version 2.1.1. Centre Européen de Recherche et de Formation Avancée en Calcul Scientifique (CERFACS).

[36] Landman, M.J., Derksen, M.A.F., Kok, J.B.W. (2006). Effect of combustion air dilution by water vapor or nitrogen on nox emission in a premixed turbulent natural gas flame: an experimental study, Combustion Science and Technology, Vol. 178, Issue 4, pp. 623-634. DOI: 10.1080/00102200500241214.

[37] Vandel, A., Chica Cano, J.P., de Persis, S., Cabot, G. (2022). Study of the influence of water vapour and carbon dioxide dilution on pollutants emitted by swirled methane/oxygen-enriched air flames. Experimental Thermal and Fluid Science. Volume 130, 110483, ISSN 0894-1777, https://doi.org/10.1016/j.expthermflusci.2021.110483.

[38] Naoumov, V.I., Krioukov, V.G., Abdullin, A.L., Demin, A. V. (2019). “Approaches to Combustion Simulation: Patterns, Models, and Main Equations,” in Chemical Kinetics in Combustion and Reactive Flows: Modeling Tools and Applications, Cambridge: Cambridge University Press, pp. 3–40.